A Quark Rearrangement and Annihilation Model for $\bar{N}N$ Interaction at Low Energies

Masahiro Maruyama

Department of Applied Mathematics,
Faculty of Engineering Science,
Osaka University, Toyonaka 560, JAPAN

Abstract

A quark rearrangement and annihilation model is proposed to describe the $\bar{N}N$ annihilation into mesons and the $\bar{N}N$ scattering at low energies of $T_{lab} \lesssim 300$ MeV. For the $\bar{N}N$ annihilation we consider quark rearrangement process into three mesons and one $\bar{q}q$-pair annihilation process into two mesons, where the mesons are the SU(6) s- and p-wave ones.

By the use of the meson and the nucleon wave functions based on a non-relativistic quark potential model, amplitudes for the two processes are derived and meson branching ratios are estimated at rest ($T_{lab} = 0$ MeV) and in flight ($T_{lab} > 0$ MeV). The result is in good agreement with data except for some channels. We find that the quark rearrangement process dominates in the annihilation from initial $\bar{N}N$ S states, while it is comparable with the quark annihilation process in the annihilation from other states.

We also present microscopic $\bar{N}N$ optical potentials based on the annihilation amplitudes. The potentials have separable forms dependent on energies and the states with the range of $0.4 \sim 0.6$ fm. By taking account of the one-boson-exchange contribution, too, to the $\bar{N}N$ interaction, several observables of the $\bar{P}P$ scattering are calculated. We find that they are qualitatively well described by the potentials with modification by a phenomenological repulsion at short distances.

Contents

A list of errata

p.4	ℓ.2	an useful ----> a useful
p.6	ℓ.1	Frui ----> Furui
p.15	ℓ.11	give ----> gives
p.24	ℓ.15∿ℓ.17	Later it ••• of $\bar{N}N$.
		----> Later we will Fourier-transform it and get an expression for optical potential of $\bar{N}N$ system.
p.27	ℓ.15	(3-29)) ----> (3-29)
p.30	ℓ.4	$Y^{*}_{0}(\hat{X})$ ----> $Y^{*}_{00}(\hat{X})$
p.42	ℓ.17	the one by the ----> the one obtained by the
p.46	ℓ.19	except for ----> except that
	ℓ.20	channels smaller ----> channels are smaller
	ℓ.20	The wrong fit ----> The poor fit
p.49	ℓ.6	and contribution ----> and the contribution
p.51	ℓ.25	The contributions ----> The predictions
p.52	ℓ.5	The contributions from P → ss are
		----> The existence of the process P → ss is
	ℓ.9	The contributions from D → ps are
		----> The existence of the process D → ps are
p.54	ℓ.5	would slightly alter. ----> would be modified.
p.58	ℓ.10	intial ----> initial
p.61	ℓ.7 ∿ℓ.8	The energy of the real part having
		----> The energy at which the real part is
p.63	ℓ.7	fits. ----> discrepancies
p.68	ℓ.7	all in the energy range
		----> in the whole energy range
p.70	ℓ.9	are required. ----> are accumulated.

§ 1 Introduction

The study of the $\bar{N}N$ interaction bears considerable significance to both particle and nuclear physics. In spite of many attempts, little has been understood about mechanism of the $\bar{N}N$ annihilation. Besides, only very scarcely or poorly determined experimental data are available at present. However, in a last few years interest on the annihilation processes has been aroused both theoretically and experimentally.

On the experimental side, a new facility for antiproton physics at low energies with intense beams of antiprotons came into operation at LEAR (Low Energy Antiproton Ring) in CERN at the beginning of 1983[1]. The LEAR is expected to produce abundant information about low energy antiproton physics and change drastically the present situation in which precise data are scarce in comparison with the ones for nucleon-nucleon scattering.

Annihilation into mesons embodies the most characteristic feature of the $\bar{N}N$ interaction. Couplings with meson states are so strong that the annihilation cross section amounts to more than a half of the $\bar{N}N$ total cross section. The $\bar{N}N$ annihilation is very unique, compared with other hadron reactions, in that it enables us to observe quark dynamics directly. It is important in order to study the quark interactions, since it contains much information about the mechanism of quark confinement. However, the $\bar{N}N$ dynamics is difficult to treat, since the $\bar{N}N$ system is very complicated

with a large number of quarks and antiquarks confined by the boundaries both sides of whom have different vacuum phases. The fundamental theory of the strong interactions, QCD, cannot be used with the present computation technique. Therefore, at the present stage it is necessary to establish some phenomenological models which are able to describe experimental data for the $\bar{N}N$ scattering as much as possible.

Historically, many investigations have been performed by various approaches since the work of Ball and Chew[2]. Local[3~8] or separable[9~11] potentials or boundary conditions[12,13] have been introduced to represent the effect of the annihilation phenomenologically. There the real part of the $\bar{N}N$ potential is obtained by the G-parity transformation of the NN OBEP (One Boson Exchange Potential). It is more realistic to study the $\bar{N}N$ system coupled to effective annihilation channels with mesons[14~17]. However, experimental information about branching ratios of the final state mesons has not been taken into consideration in these works. They attempted to reproduce only the cross sections in the $\bar{N}N$ channel. They could not reliably predict the energy and state dependences of the annihilation channels and the spatial form of the annihilation potentials. Nor have they developed the analysis about the mechanism of the $\bar{N}N$ annihilation.

In the present situation, we ought to assume some sort of phenomenological quark dynamics for the couplings from the nucleon-antinucleon system to the meson systems. In 1966,

Rubinstein and Stern[18] proposed a naive idea to describe the $\bar{N}N$ annihilation processes. The $\bar{N}N$ annihilation is assumed to occur dominantly from quark rearrangement processes. They, however, could not reproduce the observed branching ratios of the final mesons. In 1967, Harte et al.[19] attempted to improve the quark rearrangement model introducing the $\bar{N}N$ initial state interactions. Although several attractive features were observed, the model could not be regarded as a phenomenological one for the $\bar{N}N$ annihilation as it was.

In 1981, we proposed a new version of the quark rearrangement model[20] for the $\bar{N}N$ annihilation at rest (T_{lab}= 0 MeV). We introduced meson-dependent couplings and the effect of the initial state interactions as adjustable parameters. The feature of the observed branching ratios was well reproduced. Our model raised many questions at the same time. What physical meanings do the couplings newly introduced represent ? Can the model be extended to the $\bar{N}N$ annihilation in flight (T_{lab}> 0 MeV) or below the $\bar{N}N$ threshold (T_{lab}< 0 MeV) ? For that purpose it is necessary to derive the relation to the optical potential for the $\bar{N}N$ system. How should we treat the experimental fact that there exist two meson annihilations and p-wave meson productions ?

In the model the quark dynamics is represented by the overlap of spin-isospin wave functions of the initial nucleon-antinucleon and the final mesons and also by the multiplication of the coupling constants which are adjustable parameters. To answer the above questions we must clarify the

space-time structure of the quark reactions. The quark potential model[21,22] provides an useful and practical approach to treat it. The bag model[23] is not suitable for the treatment of hadron reactions at present, since the bag boundaries, which represent the quark confinement, are deformed in the reaction process. Of course, the quark potential model has similar problems. However, the prospect for the problems seems good as the system is described only by quarks as the effect of the boudaries is effectively represented by the potentials.

In 1982, we proposed a quark rearrangement model with spatial overlap functions[24,25] for the three meson annihilation processes. In this model the spatial part of nucleon and meson wave functions is taken into account and the amplitudes for the $\bar{N}N$ annihilation into three mesons are assumed to be given by the overlap of the spatial wave functions instead of the multiplication of the coupling constants. This work offers a physical explanation of the adjustable parameters and has the following favorable properties. It is easy to get the annihilation amplitudes at rest and in flight and also optical potentials for the $\bar{N}N$ system. Furthermore, p-wave mesons are naturally introduced into the model. It is possible to deal with two meson annihilation processes if we make a reasonable assumption on the quark diagrams for them and the interaction of the $\bar{q}q$ pair annihilation.

The purpose of this paper is to investigate the $\bar{N}N$

annihilations both into three mesons and into two mesons at rest (T_{lab}= 0 MeV) and in flight (T_{lab}= 50 $\sim$ 300 MeV). We also derive the optical potentials for the $\bar{N}N$ system from the annihilation amplitudes and compare the elastic and the inelastic cross sections and the angular distributions of the $\bar{P}P$ elastic and the charge-exchange scatterings. We take account of p-wave mesons in addition to s-wave mesons. It is assumed that one $\bar{q}q$ pair annihilation processes dominate the two meson annihilation and the $\bar{q}q$ pair annihilates from the $^3s_1$ state. The meson and the nucleon wave functions are derived, based on the non-relativistic quark model while kinematics of the final state mesons is relativistic. Widths of mesons are represented by mass distribution functions which play an important role for heavy meson productions. Using the wave functions of hadrons by Isgur and Karl[21,22], we derive expressions for the amplitudes of the $\bar{N}N$ annihilation into mesons and estimate the meson branching ratios and their energy dependences. And we also obtain the optical potentials with separable forms dependent on energies and their states. This property gives remarkably different feature of the $\bar{N}N$ scattering from the conventional local and energy-independent potentials.

The $\bar{N}N$ scattering due to the quark rearrangement model have also been studied by Green et al.[26,27]. However, since their potential is not based on the observed meson branching ratios and they treat the kinematics of mesons in the intermediate states non-relativistically, the energy and state

dependence of the optical potentials is less realistic. Frui et al.[28] have given the meson branching ratios at rest energy by the bag model. In their treatment it is not easy to derive the optical potentials or extend the model to the case of other energies.

The contents of this paper are as follows. In § 2 the original quark rearrangement model with effective coupling constants at rest energy is reviewed. The earlier works are also reviewed briefly and the problems in their models are pointed out. The quark rearrangement and annihilation model with spatial overlap function is presented in § 3, where the annihilations processes including p-wave mesons is considered. We give the amplitudes for the three and two meson annihilations and explicit expressions of the optical potentials. The case of the $^3p_0$ $\bar{q}q$ annihilation into two mesoms is also investigated. Section 4 is devoted to show the result of numerical calculations for branching ratios at T_{lab}= 0 $\sim$ 300 MeV. We also offer a physical interpretation for the coupling constants introduced in section 2.

In § 5 we discuss the characteristic feature of the optical potentials and the $\bar{N}N$ scattering by our model. Several observables are compared with experimental data. Finally, section 6 contains summary of our result and remarks for our model.

§ 2 A quark rearrangement model with effective coupling constants

In this section we review the works earlier than ours and our original version of the quark rearrangement model. Assuming that the quark rearrangement processes shown in fig. 1a dominate the antinucleon-nucleon ($\bar{N}$-N) annihilation into mesons, Rubinstein and Stern[18] attempted to understand meson branching ratios. They estimated the probability of an initial $\bar{N}N$ state with isospin I and spin S annihilating into a final three meson (α, β, γ) state by

$$P(IS,\alpha\beta\gamma;E_{CM}) = V(\alpha\beta\gamma,E_{CM})\ C(IS,\alpha\beta\gamma), \tag{2-1}$$

where $C(IS,\alpha\beta\gamma)$ is the overlap squared of the SU(6) spin-isospin wave functions of the initial $\bar{N}N$ state and the final three meson (α,β,γ) state, and $V(\alpha\beta\gamma,E_{CM})$ is the phase space volume of the final three meson state with center-of-mass energy E_{CM}. The phase space volume is given in the center-of-mass frame by

$$V(\alpha\beta\gamma,E_{CM}) = \int \frac{d^3p_1}{E_1}\frac{d^3p_2}{E_2}\frac{d^3p_3}{E_3}\ \delta^3(\vec{p}_1+\vec{p}_2+\vec{p}_3)\ \delta(E_1+E_2+E_3-E_{CM}), \tag{2-2}$$

where $\vec{p}_i$ and E_i are the momentum and the energy of the meson i, respectively. The followings are assumed in this model.

i) The three quarks (q) in the nucleon and the three antiquarks ($\bar{q}$) in the antinucleon ($\bar{N}$) rearrange themselves into three quark-antiquark pairs, or three mesons, without exchanging spins, isospins and strangenesses among the quarks.

ii) Relative angular momenta between q and q are zero, so that the mesons (α,β,γ in fig. 1a) in the final state are restricted to π, η, η', ω and ρ, where ω is in the ideal mixing, that is, it does not involve strange quarks.

iii) All the relative angular momenta between the nucleon and the antinucleon as well as between the mesons are zero.

Their model could not, however, reproduce experimental data even at rest. In particular, the decay branching ratios of the three meson channels with two or three heavy mesons (ρ or ω) were underestimated. The discrepancies between the predictions and the experimental data amounted to an order of magnitude in the channels with high pion multiplicities.

Harte et al.[19] regarded the annihilation rates in each of the four initial $\bar{N}N$ states with spin S and isospin I as adjustable parameters and tried to improve the discrepancies. But the deviations of the predictions from the experimental data were still large mainly because of the underestimation of the three meson channels with two or three heavy mesons as it was in the model by Rubinstein and Stern[18] (Table I). Hence we find it neccessary to enhance the channels by some mechanisms or to take account of other diagrams.

These models, however, have several attractive features. The annihilation rates into strange mesons or ϕ mesons are predicted to be zero, which should be compared with the small experimental values of strange meson production rates[29] and the ratio $\sigma(\phi\pi^+\pi^-)/\sigma(\omega\pi^+\pi^-) \sim 1/100$ [30]. Although the predicted branching ratios of $\bar{P}P \to \omega^\circ\pi^+\pi^-$, $\rho^\circ\pi^+\pi^-$ are too

large, the ratio between the two channels is consistent with data. Furthermore, as suggested by Fields [31,32], the quark rearrangement process (fig. 1a) can give an explanation for coherence of the $\rho^0\pi^+\pi^-$ and the $\omega\pi^+\pi^-$ final states in the $\bar{P}P$ annihilation. This fact is considered to mean suppression of the processes with $\bar{q}q$ pair annihilations (figs. 1b and 1c). At rest energy the fraction of the two meson annihilation is known to be about 10 $\sim$ 20 % of the total annihilation and in particular only 0.3% in the $\pi^+\pi^-$ channel experimentally[33], which implies that the three or more meson annihilation processes are dominant at this energy.

Let us consider the couplings for a $\bar{q}q$ pair to combine into a meson as parameters. They should depend on quark dynamics. Assuming that they can be described by effective constants g_α dependent only on kinds of mesons α, we have proposed a model possible to fit the branching ratios of the $\bar{P}P$ annihilation at rest. The model is as follows. The probabilities with which an initial $\bar{N}N$ system with isospin I and spin S annihilates into the three meson (α, β and γ) states (fig. 1a) at rest (T_{lab}= 0 MeV) are written by

$$P(IS,\alpha\beta\gamma) = b(IS)\ \tilde{V}(\alpha\beta\gamma,E_{CM}=2M_N)\ C(IS,\alpha\beta\gamma)\ g_\alpha g_\beta g_\gamma. \qquad (2\text{-}3)$$

Here $C(IS,\alpha\beta\gamma)$ represents the overlap squared of the SU(6) spin-isospin components of the wave functions of the initial $\bar{N}N$ state and the final three meson (α, β and γ) state (Table II). $\tilde{V}(\alpha\beta\gamma,E_{CM})$ is the phase space volume of the α, β and γ meson state at the center-of-mass energy of E_{CM}. It is written

instead of eq. (2-2) as follows:

$$\tilde{V}(\alpha\beta\gamma,E_{CM}) = \int dm_1 dm_2 dm_3 \; f_\alpha(m_1) f_\beta(m_2) f_\gamma(m_3) \times \int \frac{d^3p_1}{E_1} \frac{d^3p_2}{E_2} \frac{d^3p_3}{E_3} \; \delta^3(\vec{p}_1+\vec{p}_2+\vec{p}_3) \; \delta(E_1+E_2+E_3-E_{CM}). \tag{2-4}$$

Here we introduce the mass distribution by using the function $f_\alpha(m)$. $f_\pi(m)$ and $f_\eta(m)$ are given by

$$f_\pi(m) = \delta(m - m_\pi) \tag{2-5}$$

and

$$f_\eta(m) = \delta(m - m_\eta), \tag{2-6}$$

where m_{π°= 135.0 MeV, $m_{\pi^\pm}$= 139.6 MeV and m_η= 548.8 MeV. $f_\rho(m)$ and $f_\omega(m)$ are determined by fitting the experimental mass distributions[34,35] (figs. 2a and 2b):

$$f_\rho(m) = \left(\frac{1200-m}{1200-m_\rho}\right) C_\rho \left|\tfrac{1}{2}\Gamma_\rho/(m-m_\rho+\tfrac{1}{2}i\Gamma_\rho)+a_1+ia_2\right|^2, \quad \text{for } 600 \leq m \leq 1200 \text{ MeV}$$

$$= \left(\frac{1200-m}{1200-m_\rho}\right) C_\rho\{a_3(m-279.2)^2+a_4(m-279.2)\}, \quad \text{for } 279.2 \leq m \leq 600 \text{ MeV} \tag{2-7}$$

with

$$m_\rho = 776 \text{ MeV}, \qquad \Gamma_\rho = 155 \text{ MeV},$$
$$a_1 = 0.18, \qquad a_2 = -0.48,$$
$$A_3 = 5.65\times10^{-6} \text{ MeV}^{-2}, \qquad a_4 = 111.75\times10^{-6} \text{ MeV}^{-2}, \tag{2-8}$$

and

$$f_\omega(m) = \left(\frac{1200-m}{1200-m_\omega}\right) C_\omega \left|\tfrac{1}{2}\Gamma_\omega/(m-m_\omega+\tfrac{1}{2}i\Gamma_\omega)+a_1'+ia_2'\right|^2,$$
$$\text{for } 700 \leqq m \leqq 1200 \text{ MeV}$$

$$= \left(\frac{1200-m}{1200-m_\omega}\right) C_\omega\{a_3'(m-418.8)^2+a_4'(m-418.8)\},$$
$$\text{for } 418.8 \leqq m \leqq 700 \text{ MeV} \qquad (2\text{-}9)$$

with

$$m_\omega = 783.2 \text{ MeV}, \quad \Gamma_\omega = 30 \text{ MeV},$$
$$a_1' = 0.04, \quad a_2' = 0.175,$$
$$a_3' = 0.52\times10^{-6} \text{ MeV}^{-2}, \quad a_4' = -8.22\times10^{-6} \text{ MeV}^{-2}. \qquad (2\text{-}10)$$

Here they are normalized as

$$\int_{279.2}^{1200} dm\, f_\rho(m) = 1, \qquad (2\text{-}11)$$

and

$$\int_{418.8}^{1200} dm\, f_\omega(m) = 1. \qquad (2\text{-}12)$$

The numerical calculation of the phase space volume is carried out in Appendix A.

In eq. (2-3) we take the adjustable parameters, b(I,S) and g_α, and the mass distribution function, $f_\alpha(m)$, into our model. (See eq. (2-1).) The spin-isospin dependent parameters b(I,S) denote the effect of the initial $\bar{N}N$ state interaction and the meson dependent parameters g_α the couplings for a $\bar{q}q$ pair to combine into a meson. The mass distributions of mesons have an important role to produce three heavy mesons such as $\rho\rho\rho$, since the sum of the masses is much larger than the energy of

the $\bar{N}N$ threshold. The earlier works predicted the very small branching ratio for the 6-prong ($3\pi^+3\pi^-m\pi^\circ$) annihilation in comparison with our model due to the neglect of the mass distributions[19].

The branching ratio of each observed multi-meson channel $\{m\pi^+m\pi^-n\pi^\circ\}$ is given by

$$\frac{\sigma(\bar{N}N \to m\pi^+m\pi^-n\pi^\circ)}{\sigma(\bar{N}N \to \text{Total})} = \sum_I \sum_S \sum_{(\alpha,\beta,\gamma)} R(\alpha\beta\gamma \to m\pi^+m\pi^-n\pi^\circ) \times (2S+1)\, P(IS,\alpha\beta\gamma), \qquad (2\text{-}13)$$

where the summation (α,β,γ) means all combinations of α, β and γ mesons which decay into the observed set of pions. $R(\alpha\beta\gamma \to m\pi^+m\pi^-n\pi^\circ)$ is calculated by decay branching ratios of η, ρ and ω shown in Table III. Therefore, for example, in the case of

$$m = 2 \text{ and } n = 1, \qquad (2\text{-}14)$$

we should take (α,β,γ) all available charge states of (η,π,π), (ω,π,π), (ρ,ρ,π), etc.

Experimental data of the $\bar{P}P$ annihilation at rest (T_{lab}= 0 MeV) into various multi-pion channels[29,33,36∿45] are shown in Table Ia ∿ Ic. In Table Ia we remove the contribution from the two meson annihilation which is estimated to occupy about 10 ∿ 20 % of the total annihilation[33]. Fitting the predictions to the data with asterisks (*) in Table Ia fixes the adjustable parameters as

$$b(0,1)/b(0,0) = 0.41 \pm 0.1,$$

$$b(1,1)/b(0,0) = 0.40 \pm 0.1,$$

$$b(1,0)/b(0,0) = 0.34 \pm 0.1, \qquad (2\text{-}15)$$

and

$$g_\eta/g_\pi = 7.4 \pm 1,$$
$$g_\rho/g_\pi = 16.6 \pm 1,$$
$$g_\omega/g_\pi = 12.6 \pm 2. \qquad (2\text{-}16)$$

Comparisons of our results with the experimental data and those of Harte et al. are shown in Table Ia. Satisfactory agreement between the data and the predictions is obtained in our model. Table II shows the contribution of each three meson channel to the total annihilation. In these comparisons we find that owing to the large values of g_ρ/g_π and g_ω/g_π in eq. (2-16) the three meson channels with two or three heavy mesons are enhanced and the agreement with data are obtained. As shown in Table IV the quark rearrangement model also predicts the branching ratios of the antiproton-neutron ($\bar{P}$-n) annihilation at rest[46] by using the same values of parameters as the ones determined in $\bar{P}P$ annihilation process. Here the effect of a spectator particle (proton) is assumed to be unimportant in the antiproton-deuteron ($\bar{P}$-D) annihilation process. We get agreements between the data and the predictions as well as in the $\bar{P}P$ case.

It is important that the values of g_α given in eq. (2-16) are approximately in order of the masses of the mesons in addition to the fact of g_ρ/g_π and g_ω/g_π having large values. The parameters g_α represent the effect of the SU(6) symmetry breaking. The properties of g_α will be clarified in the next

section. There we will get a picture that the g_α reflect the differences of the overlap of the spatial components of the meson wave functions and the nucleon wave functions due to the mass differences of the mesons[24,25].

We find that b(0,0) is rather larger than other b(I,S). This enhancement of the I=0 and S=0 $\bar{N}N$ state could be explained in terms of the initial $\bar{N}N$ state interactions. The $\bar{P}P$ annihilation at rest into mesons proceeds with several states: (i) from $\bar{P}P$ scattering states at very low energies ($T_{lab} \sim 0$ MeV), (ii) from $\bar{P}P$ atomic bound states (protoniums) and (iii) from $\bar{P}P$ nuclear bound states (baryoniums). The contribution of the third process to the annihilation is small, since the photons or the pions emitted in the transition process from an atomic bound state to a nuclear bound state is in fact known to have much less intensity than that of the photons by the decays of π° produced totally in the $\bar{P}P$ annihilation[47]. Theoretically, the ratio of the radiative width by the transition to nuclear bound states vs. the total width of an atomic state is predicted to be less than 1/10[48].

It is probable that the state of target protons determines which of the $\bar{P}P$ annihilation, (i) or (ii), is the main process. However, in either case there is a good reason for the enhancement of the I=0, S=0 state. The one-pion-exchange potential (OPEP)

$$V(r) = -g_\pi^2 \frac{\mu^2}{12M_N^2} \vec{\tau}_1 \cdot \vec{\tau}_2 \{ \vec{\sigma}_1 \cdot \vec{\sigma}_2 + S_{12}\left(\frac{3}{(\mu r)^2} + \frac{3}{\mu r} + 1\right)\} \frac{e^{-\mu r}}{r} \qquad (2\text{-}17)$$

is known to produce a strong long-range attraction in the I=0, S=0 state. Therefore the $\bar{P}P$ wave function in the scattering at very low energies or of atomic bound states with the I=0 and the S=0 is pulled more into the short-distance region where the annihilation occurs. As pointed out by Desai[49], the oscillation time between the I=0 and the I=1 states by Coulomb interaction is one or two orders of magnitude shorter than the time in which the annihilation proceeds. Thus the enhancement in the I=0, S=0 atomic states is possible. Accordingly, we find the enhancement of b(0,0) reasonable.

Our version of quark rearrangement models give an explanation of the branching ratios of the $\bar{N}N$ annihilation at rest as seen in the above discussions. Next let us consider the $\bar{P}P$ annihilation in flight (T_{lab}= 50 $\sim$ 300 MeV). Table V shows that the P, D and F wave annihilation of the proton and the antiproton as well as the S wave one are necessary to take in when we consider the scattering problems in the energy range of T_{lab}= 100 $\sim$ 300 MeV[4]. This means that in flight case it is not sufficient to evaluate the meson branching ratios only by the S wave annihilation amplitudes. The extention of our model to higher partial waves is not, however, straightforward in the present form. As the non-vanishing angular momentum of the $\bar{P}P$ couples to the angular momenta and the spins of the mesons in the final state, we further have to introduce spin and momentum dependent couplings. Secondly p-wave SU(6) mesons, ε, D, f, H, δ, A_1, A_2 and B should be taken in the model in addition to the s-wave mesons, π, η, ρ and ω, since

experiments have pointed out that cotribution from the p-wave mesons to the total annihilation is by no means small[50,51]. Furthermore, the two meson annihilation processes must be taken into account in order to reproduce experimental branching ratios[50,51]. The two meson annihilation proceeds through the annihilation of at least one $\bar{q}q$ pair, so that the interaction of the quark-antiquark anihilation should be considered. It is not easy to include the quark dynamics in the present framework. In the next section we propose a model in which we can explain the properties of the parameters g_α and perform the above extension straightforwardly.

§ 3 A quark rearrangement and annihilation model

In this section we construct an extended quark rearrangement model by introducing spatial components of wave functions[24,25] and $\bar{q}q$ pair annihilation interaction. The two processes of the quark reactions, the quark rearrangement into three mesons (fig. 1a) and the one $\bar{q}q$ pair annihilation into two mesons (fig. 3) are taken into account. Here we assume a perturbative picture that the processes with fewer number of $\bar{q}q$ pairs annihilating or creating give more contribution to the annihilation cross section.

The model is set up as follows[52,53].

(i) The annihilation from the S, P and D states of the $\bar{N}N$ is taken into account. An optical model calculation[4] has pointed out that contribution from the S, P and D waves to the total annihilation cross section amounts to 85% or more at $T_{lab} \lesssim 300$ MeV (See Table V).

(ii) In addition to the s-wave mesons, π, η, ρ and ω, the p-wave mesons, ε, D, f, H, δ, A_1, A_2 and B, are taken in the final states. The masses, the widths and the decay branching ratios of the p-wave mesons which we use are shown in Table VI[60]. Here it should be pointed out that the decay branching ratios have large uncertainties for some mesons. The number of the p-wave mesons is restricted to zero or one in the final state. Because they are rather heavier than the s-wave mesons the contribution from the states with two or more p-wave mesons is small due to the small phase space volume occupied.

(iii) Spin-flips of quarks in the quark rearrangement process

are assumed not to occur as was in the preceding model. We also assume that the momentum dependence of the quark-quark interactions is small and the branching ratios of the meson channels are given by the ones calculated by neglecting the momentum dependence.

(iv) For the two meson annihilation shown in fig. 3 we assume that the $\bar{q}q$ annihilation occurs from the $^3s_1$ $\bar{q}q$ state. This assumption means that a $\bar{q}q$ pair annihilates into a vector boson state carrying spin 1, odd parity and odd G-parity. Therefore it is accompanied by spin-flip and parity-flip of another quark or antiquark.

It is not obvious how the $\bar{q}q$ annihilation interaction should be described. The $\bar{q}q$ annihilation may be followed by the emission of many gluons. For the description of this process there exists the pair creation model[54], or the $^3p_0$ model, to explain certain meson decays and meson-baryon vertices. There a $\bar{q}q$ pair annihilates or creates with the $^3p_0$ state, that is, the $\bar{q}q$ pair have the same quantum numbers as the vacuum. However, this is not the only possibility for the $\bar{q}q$ annihilation. We will discuss the $\bar{q}q$ annihilation interaction later in detail in the case of the $\bar{N}N$ annihilation.

Let us denote the initial $\bar{N}N$ S, P and D states as S, P and D, and an s-wave meson and a p-wave meson as s and p, respectively. For the initial S states the final meson states allowed in our model are the ones of three s-wave mesons, two s-wave mesons, and one p- and one s-wave mesons, where we use the abbreviations of S → sss, S → ss and S → ps for them

hereafter.

For the initial P states the three processes of P → ssp, P → ss and P → ps are considered. We remark that the process P → sss is forbidden by parity and G-parity conservation in the case of the quark interactions without spin-flip.

For the initial D states the process D → ps is considered. The amplitude of D → ss turns out to be considerably small as we estimate the process in our model. Although the process D → sss has small amplitude, we take account of the process D → sss, too. The contribution from this process will turn out to be necessary in several three meson channels.

The possible origins of the process D → sss are as follows. The momentum-dependent $\bar{q}q$ interactions would cause the direct D → sss annihilation, in which case the latter half of the assumption (iii) must be discarded. In order to consider the case we must assume the form , for example, of one-gluon-exchange potential. Secondly, the tensor forces between the nucleon and the antinucleon by exchanging bosons give rise to mixing of the S and D states with S=1 and J=1. The tensor forces are very strong due to the coherence of the exchanging pion and ρ meson in the $\bar{N}N$ case contrary to the NN case. Therefore, the $\bar{N}N$ in the D states can annihilate into three mesons, sss, by way of the S states within our framework. We need to solve the scattering problems to estimate this contribution. Thirdly, as suggested by Green et al.[26,27], the tensor components of the $\bar{N}N$-$\bar{N}\Delta$, $N\bar{\Delta}$ and $\bar{\Delta}\Delta$ potentials incorporate the annihilation from the $\bar{N}N$ D states through the

processes $\bar{N}N(D) \to N\bar{\Delta}$, $\bar{N}\Delta$, $\bar{\Delta}\Delta(S) \to$ mesons (fig. 4). Namely the initial $\bar{N}N$ D states make transition to the $N\bar{\Delta}$, $\bar{N}\Delta$ and $\bar{\Delta}\Delta$ S states by the pion or ρ meson exchange and then annihilate into mesons in the S states. This effect works also in the initial $\bar{N}N$ S and P states. Since in the D states the annihilation amplitudes predicted are smaller than in the S and P states, the processes would give larger contribution in the D states. The three s-wave mason annihilation is dominant in the S states. Therefore, we consider them only in the $D \to sss$ process for simplicity, although the $N\bar{\Delta}$, $\bar{N}\Delta$ and $\bar{\Delta}\Delta$ annihilation processes should be taken into account in all $\bar{N}N$ states. Assuming that the branching ratios from $D \to sss$ can be simulated by the ones from $S \to sss$, we treat two cases in the D states:

Case A: $D \to sss$ simulated by $S \to sss$, and $D \to ps$,

Case B: $D \to ps$ only.

The amplitude of the quark rearrangement process from an initial $\bar{N}N$ state with isospin I, I_z and total angular momentum J, J_z to a final state with three mesons, α, β and γ (fig. 1a), is given by

$$T_3(\alpha\beta\gamma,\vec{p}_1\vec{p}_2\vec{p}_3;II_zJJ_zLS,\vec{P}_N\vec{P}_{\bar{N}})$$

$$= \int d^3q_1' \cdots d^3q_6' \; d^3q_1 \cdots d^3q_6$$

$$\times \Psi^{\dagger}_{\alpha\beta\gamma}(II_zJJ_z,\vec{q}_1' \cdots \vec{q}_6',\vec{p}_1\vec{p}_2\vec{p}_3) \; O_3 \; \Psi_{\bar{N}N}(II_zJJ_zLS,\vec{q}_1 \cdots \vec{q}_6,\vec{P}_N\vec{P}_{\bar{N}}). \tag{3-1}$$

Here $\vec{P}_N$ ($\vec{P}_{\bar{N}}$) and $\vec{p}_i$ (i=1,2,3) are the momenta of the initial nucleon (antinucleon) and the final mesons respectively, and $\vec{q}_i$

and $\vec{q}_i'$ (i=1,$\cdots$,6) the quark momenta of the initial and the final states. $\Psi_{\bar{N}N}$ and $\Psi_{\alpha\beta\gamma}$ denote the spin-isospin and the spatial components of the initial and the final wave functions, respectively. The operator O_3 is constructed by assuming no momentum transfers and no spin-isospin flips among quarks and antiquarks:

$$O_3 = \lambda \prod_{i=1}^{6} \delta^3(\vec{q}_i' - \vec{q}_i) \tag{3-2}$$

with an adjustable parameter λ.

The amplitude for the annihilation into the final state with two mesons, α and β (fig. 3), is given by

$$\begin{aligned} & T_2(\alpha\beta, \vec{p}_1\vec{p}_2; II_zJJ_zLS, \vec{P}_N\vec{P}_{\bar{N}}) \\ &= \int d^3q_1' d^3q_2' d^3q_4' d^3q_5'\ d^3q_1 \cdots d^3q_6 \\ &\times \Psi^{\dagger}_{\alpha\beta}(II_zJJ_z, \vec{q}_1'\vec{q}_2'\vec{q}_4'\vec{q}_5', \vec{p}_1\vec{p}_2)\ O_2\ \Psi_{\bar{N}N}(II_zJJ_zLS, \vec{q}_1\cdots\vec{q}_6, \vec{P}_N\vec{P}_{\bar{N}}), \end{aligned} \tag{3-3}$$

where the operator O_2, describing the $\bar{q}q$ annihilation interaction, is defined in the case of fig. 3 by

$$\begin{aligned} O_2 = \lambda' & \ \delta^3(\vec{q}_4' - \vec{q}_4)\ \delta^3(\vec{q}_5' - \vec{q}_5) \\ & \times \{\ \delta^3(\vec{q}_1 + \vec{q}_3 + \vec{q}_6 - \vec{q}_1')\ \delta^3(\vec{q}_2' - \vec{q}_2)\ i\ \vec{\sigma}_{36} \cdot (\vec{\sigma}_1 \times (\vec{q}_1' - \vec{q}_1)) \\ & + \delta^3(\vec{q}_2 + \vec{q}_3 + \vec{q}_6 - \vec{q}_2')\ \delta^3(\vec{q}_1' - \vec{q}_1)\ i\ \vec{\sigma}_{36} \cdot (\vec{\sigma}_2 \times (\vec{q}_2' - \vec{q}_2))\}. \end{aligned} \tag{3-4}$$

Here λ' is another parameter which describes the strength of the two meson annihilation and $\vec{\sigma}_{36}$ is the Pauli matrix associated with the pair annihilation of the third quark and

the sixth quark. The form of O_2 is determined by the assumption (iii) of the $\bar{q}q$ annihilation from the $^3s_1$ state and the neglect of other momentum dependence. For the estimation in the case of the $^3p_0$ annihilation we use as O_2

$$O_2 = \tilde{\lambda}\, \delta^3(\vec{q}_4'-\vec{q}_4)\ \delta^3(\vec{q}_5'-\vec{q}_5)\ \vec{\sigma}_{36}\cdot(\vec{q}_3-\vec{q}_6)$$
$$\times \{\delta^3(\vec{q}_2'-\vec{q}_2)\ \delta^3(\vec{q}_1+\vec{q}_3+\vec{q}_6-\vec{q}_1') + \delta^3(\vec{q}_1'-\vec{q}_1)\ \delta^3(\vec{q}_2+\vec{q}_3+\vec{q}_6-\vec{q}_2')\}, \tag{3-5}$$

where we have also investigated the case replacing $\delta^3(\vec{q}_i+\vec{q}_3+\vec{q}_6-\vec{q}_i')$ by $\delta^3(\vec{q}_i'-\vec{q}_i)\ \delta^3(\vec{q}_3+\vec{q}_6)$, but the qualitative feature has been unchanged.

The spin-isospin component is derived within the framework of the SU(6) spin-isospin symmetry. Let us describe an α-meson state by the relative angular momentum ℓ^α, μ^α between a quark and an antiquark in the meson, the spin s^α, s_z^α, the total spin j^α, m^α, and the isospin i^α, i_z^α. We define

$$\phi_{j^\alpha m^\alpha \ell^\alpha s^\alpha i^\alpha i_z^\alpha}(\vec{q}) = \sum_{\mu^\alpha, s_z^\alpha} (\ell^\alpha \mu^\alpha s^\alpha s_z^\alpha | j^\alpha m^\alpha)\ Y_{\ell^\alpha \mu^\alpha}(\hat{q})\ f_\alpha(q)$$
$$\times \chi_{s^\alpha s_z^\alpha i^\alpha i_z^\alpha}. \tag{3-6}$$

Here $Y_{\ell^\alpha \mu^\alpha}(\hat{q})$ is a spherical harmonics, and $\chi_{s^\alpha s_z^\alpha i^\alpha i_z^\alpha}$ and $f_\alpha(q)$ are the SU(6) spin-isospin and the radial components of the α meson wave function. $\Psi_{\alpha\beta\gamma}(II_zJJ_z,\vec{q}_1\cdots\vec{q}_6,\vec{p}_1\vec{p}_2\vec{p}_3)$ and $\Psi_{\alpha\beta}(II_zJJ_z,\vec{q}_1\vec{q}_2\vec{q}_4\vec{q}_5,\vec{p}_1\vec{p}_2)$ are given by

$$\Psi_{\alpha\beta\gamma}(II_zJJ_z,\vec{q}_1\cdots\vec{q}_6,\vec{p}_1\vec{p}_2\vec{p}_3)$$
$$\propto \delta^3(\vec{q}_1+\cdots+\vec{q}_6-\vec{p}_1-\vec{p}_2-\vec{p}_3) \sum_{\{\Omega_3\}} (i^\alpha i_z^\alpha i^\beta i_z^\beta | i^{\alpha\beta} i_z^{\alpha\beta})$$

$$\times (i^{\alpha\beta} i_z^{\alpha\beta} i^{\gamma} i_z^{\gamma} | II_z)\ (j^{\alpha} m^{\alpha} j^{\beta} m^{\beta} | j^{\alpha\beta} m^{\alpha\beta})\ (j^{\alpha\beta} m^{\alpha\beta} j^{\gamma} m^{\gamma} | j^{\alpha\beta\gamma} m^{\alpha\beta\gamma})$$

$$\times (L_1 M_1 L_2 M_2 | L_{12} M_{12})\ (j^{\alpha\beta\gamma} m^{\alpha\beta\gamma} L_{12} M_{12} | JJ_z)$$

$$\times Y^*_{L_1 M_1}\left(\tfrac{1}{2}(\vec{p}_1 - \vec{p}_2)\right)\ Y_{L_1 M_1}\left(\tfrac{1}{2}(\vec{q}_1 + \vec{q}_4 - \vec{q}_2 - \vec{q}_5)\right)$$

$$\times \frac{1}{\frac{1}{4}|\vec{p}_1 - \vec{p}_2|^2}\ \delta\left(\tfrac{1}{2}|\vec{p}_1 - \vec{p}_2| - \tfrac{1}{2}|\vec{q}_1 + \vec{q}_4 - \vec{q}_2 - \vec{q}_5|\right)$$

$$\times Y^*_{L_2 M_2}\left(\tfrac{1}{3}(2\vec{p}_3 - \vec{p}_1 - \vec{p}_2)\right)\ Y_{L_2 M_2}\left(\tfrac{2}{3}(\vec{q}_3 + \vec{q}_6) - \tfrac{1}{3}(\vec{q}_1 + \vec{q}_2 + \vec{q}_4 + \vec{q}_5)\right)$$

$$\times \frac{1}{\frac{1}{9}|2\vec{p}_3 - \vec{p}_1 - \vec{p}_2|^2}\ \delta\left(\tfrac{1}{3}|2\vec{p}_3 - \vec{p}_1 - \vec{p}_2| - \tfrac{1}{3}|2(\vec{q}_3 + \vec{q}_6) - \vec{q}_1 - \vec{q}_2 - \vec{q}_4 - \vec{q}_5|\right)$$

$$\times \phi_{j^{\alpha} m^{\alpha} \ell^{\alpha} s^{\alpha} i^{\alpha} i_z^{\alpha}}(\vec{q}_1 - \vec{q}_4)\, \phi_{j^{\beta} m^{\beta} \ell^{\beta} s^{\beta} i^{\beta} i_z^{\beta}}(\vec{q}_2 - \vec{q}_5)\, \phi_{j^{\gamma} m^{\gamma} \ell^{\gamma} s^{\gamma} i^{\gamma} i_z^{\gamma}}(\vec{q}_3 - \vec{q}_6) \tag{3-7}$$

in which

$$\{\Omega_3\} = \{i_z^{\alpha}\ i_z^{\beta}\ i_z^{\gamma}\ i^{\alpha\beta}\ i_z^{\alpha\beta}\ m^{\alpha}\ m^{\beta}\ m^{\gamma}$$

$$j^{\alpha\beta}\ m^{\alpha\beta}\ j^{\alpha\beta\gamma}\ m^{\alpha\beta\gamma}\ L_1\ M_1\ L_2\ M_2\ L_{12}\ M_{12}\}, \tag{3-8}$$

and

$$\Psi_{\alpha\beta}(II_z JJ_z, \vec{q}_1 \vec{q}_2 \vec{q}_4 \vec{q}_5, \vec{p}_1 \vec{p}_2)$$

$$\propto \delta^3(\vec{q}_1 + \vec{q}_2 + \vec{q}_4 + \vec{q}_5 - \vec{p}_1 - \vec{p}_2) \sum_{\{\Omega_2\}} (i^{\alpha} i_z^{\alpha} i^{\beta} i_z^{\beta} | i^{\alpha\beta} i_z^{\alpha b})$$

$$\times (i^{\alpha\beta} i_z^{\alpha\beta} i^{\gamma} i_z^{\gamma} | II_z)\ (j^{\alpha} m^{\alpha} j^{\beta} m^{\beta} | j^{\alpha\beta} m^{\alpha\beta})\ (j^{\alpha\beta} m^{\alpha\beta} LM | JJ_z)$$

$$\times Y^*_{LM}\left(\tfrac{1}{2}(\vec{p}_1 - \vec{p}_2)\right)\ Y_{LM}\left(\tfrac{1}{2}(\vec{q}_1 + \vec{q}_4 - \vec{q}_2 - \vec{q}_5)\right)$$

$$\times \frac{1}{\frac{1}{4}|\vec{p}_1-\vec{p}_2|^2}\,\delta\left(\frac{1}{2}|\vec{p}_1-\vec{p}_2|-\frac{1}{2}|\vec{q}_1+\vec{q}_4-\vec{q}_2-\vec{q}_5|\right)$$

$$\times \phi_{j^{\alpha}m^{\alpha}\ell^{\alpha}s^{\alpha}i^{\alpha}i_z^{\alpha}}(\vec{q}_1-\vec{q}_4)\;\phi_{j^{\beta}m^{\beta}\ell^{\beta}s^{\beta}i^{\beta}i_z^{\beta}}(\vec{q}_2-\vec{q}_5) \qquad (3\text{-}9)$$

in which

$$\{\Omega_2\} = \{i_z^{\alpha}\;i_z^{\beta}\;i_z^{\gamma}\;i^{\alpha\beta}\;i_z^{\alpha\beta}\;m^{\alpha}\;m^{\beta}\;j^{\alpha\beta}\;m^{\alpha\beta}\;L\;M\}. \qquad (3\text{-}10)$$

For the initial state

$$\Psi_{\bar{N}N}(II_zJJ_zLS,\vec{q}_1\cdots\vec{q}_6,\vec{P}_N\vec{P}_{\bar{N}})$$

$$\propto \delta^3(\vec{q}_1+\cdots+\vec{q}_6-\vec{P}_N-\vec{P}_{\bar{N}})\sum_{S_z,M}(SS_zLM|JJ_z)$$

$$\times Y^*_{LM}\left(\frac{1}{2}(\vec{P}_N-\vec{P}_{\bar{N}})\right)\,Y_{LM}\left(\frac{1}{2}(\vec{q}_1+\vec{q}_2+\vec{q}_3-\vec{q}_4-\vec{q}_5-\vec{q}_6)\right)$$

$$\times \frac{1}{\frac{1}{4}|\vec{P}_N-\vec{P}_{\bar{N}}|^2}\;\delta\left(\frac{1}{2}|\vec{P}_N-\vec{P}_N|-\frac{1}{2}|\vec{q}_1+\vec{q}_2+\vec{q}_3-\vec{q}_4-\vec{q}_5-\vec{q}_6|\right)$$

$$\times \chi_{SS_zII_z}\;f_N(\vec{q}_1\vec{q}_2\vec{q}_3)\;f_{\bar{N}}(\vec{q}_4\vec{q}_5\vec{q}_6), \qquad (3\text{-}11)$$

where $\chi_{SS_zII_z}$ is the SU(6) spin-isospin wave function and $f_N(\vec{q}_1\vec{q}_2\vec{q}_3)$ is the spatial component of the internal quark wave function of the nucleon. In the above expression we take the spatial wave function between the nucleon and the antinucleon to be a plane wave with momentum $\frac{1}{2}(\vec{P}_N-\vec{P}_{\bar{N}})$. Later it will be Fourier-transformed to get the expression available to arbitrary wave functions of $\bar{N}N$.

We use the spatial component wave functions, $f_N(\vec{q}_1\vec{q}_2\vec{q}_3)$ and $f_{\bar{N}}(\vec{q}_4\vec{q}_5\vec{q}_6)$, given by Isgur and Karl[21] for the nucleon and

the antinucleon. Their model is based on the Hamiltonian with a harmonic oscillator confinement potential and a one-gluon-exchange potential:

$$H = \sum_{i=1}^{3} (m_i + \frac{p_i^2}{2m_i}) + \sum_{i<j} V^{ij} + \sum_{i<j} H_{hyp}^{ij} \qquad (3\text{-}12)$$

where

$$V^{ij} = \frac{\lambda^i}{2} \cdot \frac{\lambda^j}{2} \frac{1}{2} \kappa \{ |\vec{r}_1 - \vec{r}_2|^2 + |\vec{r}_2 - \vec{r}_3|^2 + |\vec{r}_3 - \vec{r}_1|^2 \}, \qquad (3\text{-}13)$$

and

$$H_{hyp}^{ij} = \frac{2\alpha_s}{3m_i m_j} \{ \frac{8\pi}{3} \vec{s}_i \cdot \vec{s}_j \delta^3(\vec{r}_{ij}) + \frac{1}{r_{ij}^3} (\frac{3\vec{s}_i \cdot \vec{r}_{ij} \; \vec{s}_j \cdot \vec{r}_{ij}}{r_{ij}^2} - \vec{s}_i \cdot \vec{s}_j) \}. \qquad (3\text{-}14)$$

In eq. (3-12) H_{hyp}^{ij} is treated as perturbation. Here m_i, r_i, p_i, s_i and $\frac{\lambda^i}{2}$ are the mass, the position, the momentum, the spin and the color matrix of the quark i, respectively, and

$$\vec{r}_{ij} = \vec{r}_i - \vec{r}_j. \qquad (3\text{-}15)$$

The zeroth-order wave function of a nucleon is

$$\psi_N = \frac{8D_N^3}{\pi^{3/2}} \exp\{-2D_N^2(\vec{\rho}^2 + \vec{\lambda}^2)\}, \qquad (3\text{-}16)$$

where

$$\vec{\rho} = \frac{1}{\sqrt{2}} (\vec{r}_1 - \vec{r}_2),$$

$$\vec{\lambda} = \frac{1}{\sqrt{6}} (\vec{r}_1 + \vec{r}_2 - 2\vec{r}_3), \qquad (3\text{-}17)$$

and

$$D_N = \frac{1}{2}(3m_q \kappa)^{1/4}. \qquad (3\text{-}18)$$

Adopting the values for parameters;

$$m_q = 330 \text{ MeV},$$
$$\kappa = 1.38 \text{ fm}^{-3},$$
$$\alpha_s = 1.62, \tag{3-19}$$

they have got the proton charge radius

$$\sqrt{\langle r_P^2 \rangle} = \frac{1}{2D_N} = 0.62 \text{ fm}, \tag{3-20}$$

and the mass difference between a nucleon and a $\Delta(1232)$ arising from the spin-spin interaction in H_{hyp}^{ij}:

$$M_\Delta - M_N = \frac{32\alpha_s D_N^3}{3\sqrt{2\pi} m_q} = 260 \text{ MeV}. \tag{3-21}$$

We use as the nucleon wave function the Fourier transform of eq. (3-16)

$$f_N(\vec{q}_1\vec{q}_2\vec{q}_3) = D_N^{-3} \exp\{-(\vec{q}_1-\vec{q}_2)^2/(16D_N^2) - (\vec{q}_1+\vec{q}_2-2\vec{q}_3)^2/(48D_N^2)\}. \tag{3-22}$$

In the same method we construct the wave function for the mesons with the Hamiltonian

$$H_m = \sum_{i=1}^{2} (m_i + \frac{p_i^2}{2m_i}) + \frac{\lambda^1}{2}\cdot\frac{\lambda^2}{2} \frac{1}{2}\kappa(\vec{r}_1-\vec{r}_2)^2$$
$$+ \frac{2\alpha_s}{3m_1m_2} \{\frac{8\pi}{3}\vec{s}_1\cdot\vec{s}_2\delta^3(\vec{r}_{12}) + \frac{1}{r_{12}^3}(\frac{3\vec{s}_1\cdot\vec{r}_{12}\ \vec{s}_2\cdot\vec{r}_{12}}{r_{12}^2} - \vec{s}_1\cdot\vec{s}_2)\}, \tag{3-23}$$

where the last term is also treated as perturbation. The unperturbed meson wave function is given by

$$\psi_s = \frac{(2D_s)^{3/2}}{\pi^{3/4}} \exp\{-D_s^2(\vec{r}_1-\vec{r}_2)^2\}, \tag{3-24}$$

in which

$$D_s = \frac{1}{2}(4\kappa m_q)^{1/4} = 0.87 \text{ fm}^{-1} \tag{3-25}$$

for the s-wave mesons except pion. This wave function gives the mass difference between a vector meson and a pseudoscalar meson by perturbation as

$$m(s=1)-m(s=0) = \frac{128}{9\sqrt{2}} \frac{\alpha_s D_s^3}{m_q^2\sqrt{\pi}} = 430 \text{ MeV} \tag{3-26}$$

and the root-mean-square radius as

$$\sqrt{\langle r_s^2 \rangle} = \frac{\sqrt{3}}{4D_\alpha} = 0.50 \text{ fm}. \tag{3-27}$$

Taking into account that the mass difference in eq. (3-26) is considerably smaller than the observed values in the isovector case:

$$m_\rho - m_\pi = 640 \text{ MeV}, \tag{3-28}$$

we should consider the property of pion as a Goldstone boson. (Experimentally the pion radius is in the range[55] of

$$\sqrt{\langle r_\pi^2 \rangle} = 0.5 \sim 0.8 \text{ fm}. \tag{3-29)}$$

We modify the pion wave function as

$$\psi_\pi = \frac{(2D_\pi)^{3/2}}{\pi^{3/4}} \exp\{-D_\pi^2(\vec{r}_1-\vec{r}_2)^2\}, \tag{3-30}$$

with

$$D_\pi = (1.0 \sim 2.3) \times D_s. \tag{3-31}$$

As shown in section 4 (Table VII), by fitting experimental data

we will obtain the best fit with the values

$$r_p \equiv \sqrt{\langle r_p^2 \rangle} = 0.62 \text{ fm (the case of Isugar and Karl)},$$
$$D_\pi = 2.3\ D_s. \qquad (3\text{-}32)$$

Once r_p and D_π are determined, the result does not depend sensitively on m_q. Therefore we will use the above values of parameters in the following discussions.

We summarize the meson wave functions in momentum space:

$$Y_{00}(\hat{q}) f_s(q) = D_s^{-3/2}\ Y_{00}(\hat{q})\ \exp\{-q^2/(16D_s^2)\ \} \qquad (3\text{-}33)$$

with $D_s = 0.87$ fm^{-1} for the s-wave mesons except pion,

$$Y_{00}(\hat{q}) f_\pi(q) = D_\pi^{-3/2}\ Y_{00}(\hat{q})\ \exp\{-q^2/(16D_\pi^2)\ \} \qquad (3\text{-}34)$$

with $D_\pi = 1.32$ fm^{-1} for the pion and

$$Y_{1\nu}(\hat{q}) f_p(q) = D_p^{-3/2}\ Y_{1\nu}(\hat{q})\ 1/\sqrt{12D_p^2}\ \ q\cdot\exp\{-q^2/(16D_p^2)\} \qquad (3\text{-}35)$$

with $D_p = 1.13$ fm^{-1} [22] for the p-wave mesons.

Substituting the wave functions, eqs. (3-7) and (3-9), into the expressions in eqs. (3-1) and (3-3), we get the amplitudes $T_K(F_K,\{\vec{p}_i\},II_zJJ_zLS,\vec{P}_N\vec{P}_{\bar{N}})$ (K=2,3) in which $F_3=\{\alpha,\beta,\gamma\}$ and $F_2=\{\alpha,\beta\}$. The center-of-mass momentum of the total system is removed by

$$T_K(F_K,\{\vec{p}_i\},II_zJJ_zLS,\vec{P}_N\vec{P}_{\bar{N}})$$
$$= \delta^3\Big(\sum_{i=1}^{K}\vec{p}_i - \vec{P}_N - \vec{P}_{\bar{N}}\Big)\ \overline{T}_K(F_K,\{\vec{p}_i\},II_zJJ_zLS,\tfrac{1}{2}(\vec{P}_N-\vec{P}_{\bar{N}})). \qquad (3\text{-}36)$$

Then $\overline{T}_K$ is Fourier-transformed as

$$\tilde{T}_K(F_K,\{\vec{p}_i\},II_zJJ_zLS,\vec{X}) = \int d^3P'\ e^{-i\vec{P}'\vec{X}}\ \overline{T}_K(F_K,\{\vec{p}_i\},II_zJJ_zLS,\vec{P}'). \tag{3-37}$$

By using the amplitudes $\tilde{T}_K$ we can compose optical potentials in the $\overline{NN}$ channel. Approximating the meson wave functions by plane waves in the intermediate states, we get the optical potentials in the center-of-mass frame,

$$\begin{aligned} &V_{opt}(E_{CM},\vec{X},\vec{X}',\alpha\beta\gamma,II_zJJ_zLS) \\ &= \int dm_1dm_2dm_3 f_\alpha(m_1)f_\beta(m_2)f_\gamma(m_3)\int \frac{d^3p_1}{E_1}\frac{d^3p_2}{E_2}\frac{d^3p_3}{E_3}\,\delta^3(\vec{p}_1+\vec{p}_2+\vec{p}_3) \\ &\quad\times \tilde{T}_3^{\dagger}(\alpha\beta\gamma,\vec{p}_1\vec{p}_2\vec{p}_3,II_zJJ_zLS,\vec{X})\ \frac{1}{E_{CM}-E_1-E_2-E_3+i\varepsilon} \\ &\quad\times \tilde{T}_3(\alpha\beta\gamma,\vec{p}_1\vec{p}_2\vec{p}_3,II_zJJ_zLS,\vec{X}') \end{aligned} \tag{3-38}$$

for the three meson intermediate states and

$$\begin{aligned} &V_{opt}(E_{CM},\vec{X},\vec{X}',\alpha\beta,II_zJJ_zLS) \\ &= \int dm_1dm_2 f_\alpha(m_1)f_\beta(m_2)\int \frac{d^3p_1}{E_1}\frac{d^3p_2}{E_2}\,\delta^3(\vec{p}_1+\vec{p}_2) \\ &\quad\times \tilde{T}_2^{\dagger}(\alpha\beta,\vec{p}_1\vec{p}_2,II_zJJ_zLS,\vec{X})\ \frac{1}{E_{CM}-E_1-E_2+i\varepsilon} \\ &\quad\times \tilde{T}_2(\alpha\beta,\vec{p}_1\vec{p}_2,II_zJJ_zLS,\vec{X}') \end{aligned} \tag{3-39}$$

for the two meson intermediate states. The potentials are obtained to be nonlocal, and energy- and state-dependent. The

explicit expressions are as follows.

(i) $S \to sss$ $(L=0,\ K=3)$

$$
\begin{aligned}
&V_{opt}(E_{CM},\vec{X},\vec{X}',\alpha\beta\gamma,II_zJJ_zL=0\ S) \\
&\quad = Y^*_{\gamma|0}(\hat{X})\ V_0(X,X_o)\ |S,J_z\rangle\langle S,J_z|\ Y_{00}(\hat{X}')\ V_0(X',X_o) \\
&\qquad \times \lambda^{2N_3}\ C(II_zJJ_zL=0\ S=J,\alpha\beta\gamma)\ (D_\alpha D_\beta D_\gamma)^{-3}\ D_N^{-12} \\
&\qquad \times G_0(D_\alpha,D_\beta,D_\gamma,D_N)^2 \int dm_1 dm_2 dm_3 f_\alpha(m_1) f_\beta(m_2) f_\gamma(m_3) \\
&\qquad \times \int \frac{d^3p_1}{E_1}\frac{d^3p_2}{E_2}\frac{d^3p_3}{E_3}\,\delta^3(\vec{p}_1+\vec{p}_2+\vec{p}_3)\,\frac{1}{E_{CM}-E_1-E_2-E_3+i\varepsilon} \\
&\qquad\quad \times \exp\{-(\vec{p}_1-\vec{p}_2)^2/(16D_N^2)-3(\vec{p}_1+\vec{p}_2)^2/(16D_N^2)\} \\
&\quad = Y^*_{00}(\hat{X})\ V_0(X,X_o)\ |S,J_z\rangle\langle S,J_z|\ Y_{00}(\hat{X}')\ V_0(X',X_o) \\
&\qquad\quad \times \lambda^2\ I^{S\to sss}(E_{CM},II_zJLS,\alpha\beta\gamma),
\end{aligned}
\tag{3-40}
$$

where $C(II_zJJ_zL=0\ S=J,\alpha\beta\gamma)$ is the overlap of the SU(6) spin-isospin wave functions, which is the same as $C(IS,\alpha\beta\gamma)$ given in eq. (2-1) (See Table II and IXa∿d.). The operator $|S,S_z\rangle\langle S,S_z|$ denotes the projection on the spin state. The form factor of the separable potential has a Gaussian form corresponding to Gaussian forms of the hadron internal wave functions:

$$
V_0(X,X_o) = \frac{2}{\pi X_o^3}\exp\{-(X/X_o)^2\},
\tag{3-41}
$$

where

$$
X_o^2 = 1/D_\alpha^2+2/(3D_N^2)-A_3(1/D_\alpha^2+1/D_N^2)^2
$$

$$-B_3\{1/D_\alpha^2+1/D_N^2-A_3(1/D_\alpha^2+1/D_N^2)^2\}^2, \tag{3-42}$$

$$A_3 = 1/(1/D_\alpha^2+1/D_\beta^2+2/D_N^2), \tag{3-43}$$

$$B_3 = 1/\{1/D_\alpha^2+1/D_\beta^2+2/D_N^2-A_3(1/D_\alpha^2+1/D_N^2)^2\}. \tag{3-44}$$

In eq. (3-40) N_3 ia a numerical constant independent of parameters in the three meson channels, and $G_0(D_\alpha,D_\beta,D_\gamma,D_N)$ is given by

$$G_0(D_\alpha,D_\beta,D_\gamma,D_N) = (A_3B_3)^{3/2}. \tag{3-45}$$

By using the values of the parameters in eqs. (3-19) and (3-33)∿(3-35), the range of the potential is

$$\begin{aligned} X_o &= 0.66 \text{ fm } (0.75 \text{ fm}) \quad \text{for } n=0, \\ &= 0.58 \text{ fm } (0.64 \text{ fm}) \quad \text{for } n=1, \\ &= 0.51 \text{ fm } (0.53 \text{ fm}) \quad \text{for } n=2, \\ &= 0.44 \text{ fm } (0.43 \text{ fm}) \quad \text{for } n=3, \end{aligned} \tag{3-46}$$

where n is the number of pions in the final state and the values in the parentheses are the ranges in the case of r_p= 0.7 fm.

(ii) P → ssp (L=1, K=3, γ(a p-wave meson))

$$\begin{aligned} &V_{opt}(E_{CM},\vec{X},\vec{X}',\alpha\beta\gamma,II_zJJ_zL=1\ S) \\ &= \sum_{L_zL_z'} (1L_zSJ_z-L_z|JJ_z)\ (1L_z'SJ_z-L_z'|JJ_z) \\ &\quad \times Y^*_{1L_z}(\hat{X})\ V_1(X,X_o)\ |S,J_z-L_z\rangle\langle S,J_z-L_z'|\ Y_{1L_z'}(\hat{X}')\ V_1(X',X_o) \end{aligned}$$

$$\times \lambda^{2N_3}\, C(II_zJJ_zL{=}1\ S,\alpha\beta\gamma)\ (D_\alpha D_\beta D_\gamma)^{-3}\ D_N^{-12}$$

$$\times G_1(D_\alpha,D_\beta,D_\gamma,D_N)^2 \int dm_1 dm_2 dm_3 f_\alpha(m_1) f_\beta(m_2) f_\gamma(m_3)$$

$$\times \int \frac{d^3p_1}{E_1}\frac{d^3p_2}{E_2}\frac{d^3p_3}{E_3}\,\delta^3(\vec{p}_1+\vec{p}_2+\vec{p}_3)\,\frac{1}{E_{CM}-E_1-E_2-E_3+i\varepsilon}$$

$$\times \exp\{-(\vec{p}_1-\vec{p}_2)^2/(16D_N^2)-3(\vec{p}_1+\vec{p}_2)^2/(16D_N^2)\}$$

$$= \sum_{L_zL_z'} (1L_zSJ_z{-}L_z|JJ_z)\ (1L_z'SJ_z{-}L_z'|JJ_z)$$

$$\times Y^*_{1L_z}(\hat{X})\ V_1(X,X_o)\ |S,J_z{-}L_z\rangle\langle S,J_z{-}L_z'|\ Y_{1L_z'}(\hat{X}')\ V_1(X',X_o)$$

$$\times \lambda^2\ I^{P\to ssp}(E_{CM},II_zJLS,\alpha\beta\gamma), \qquad (3\text{-}47)$$

where $C(II_zJJ_zL{=}1\ S,\alpha\beta\gamma)$ is given in Table Xa~h. The form factor becomes in the case of the $\bar{N}N$ P wave

$$V_1(X,X_o) = \frac{2}{\pi X_o^3}\left(\frac{X}{X_o}\right)\exp\{-(X/X_o)^2\}, \qquad (3\text{-}48)$$

where X_o is given in eq. (3-42). $G_1(D_\alpha,D_\beta,D_\gamma,D_N)$ is given by

$$G_1(D_\alpha,D_\beta,D_\gamma,D_N) = 2B_3/(\sqrt{3}D_\gamma X_o)\ \{1/D_\alpha^2+1/D_N^2-A_3(1/D_\alpha^2+1/D_N^2)^2\}. \qquad (3\text{-}49)$$

The range is

$$\begin{aligned} X_o &= 0.61\ \text{fm}\ (0.67\ \text{fm}) \quad \text{for } n=0,\\ &= 0.53\ \text{fm}\ (0.56\ \text{fm}) \quad \text{for } n=1,\\ &= 0.46\ \text{fm}\ (0.46\ \text{fm}) \quad \text{for } n=2, \end{aligned} \qquad (3\text{-}50)$$

where n is the number of pions. As the radius of the p-wave meson is smaller than that of the s-wave meson (eqs. (3-33) and

(3-35)), the values of X_o in eq. (3-50) are smaller than those in eq. (3-46).

(iii) S → ss (L=0, K=2)

$$V_{opt}(E_{CM},\vec{X},\vec{X}',\alpha\beta,II_zJJ_zL=0\ S)$$

$$= Y^*_{00}(\hat{X})\ V_0(X,X_o)\ |S,J_z\rangle\langle S,J_z|\ Y_{00}(\hat{X}')\ V_0(X',X_o)$$

$$\times \lambda'^2 N_2\ (D_\alpha D_\beta)^{-3}\ D_N^{-12}$$

$$\times \int dm_1 dm_2 f_\alpha(m_1) f_\beta(m_2) \int_0^\infty \frac{dp_1 p_1^2}{E_1 E_2}\ \frac{1}{E_{CM}-E_1-E_2+i\varepsilon}$$

$$\times \sum_i N_i(S\to ss)\ \{F\ Q_i^{(1)}(S\to ss)\ d\ p_1 \exp(-ap_1^2)$$

$$-F' Q_i^{(2)}(S\to ss)\ d' p_1 \exp(-a' p_1^2)\}^2$$

$$= Y^*_{00}(\hat{X})\ V_0(X,X_o)\ |S,J_z\rangle\langle S,J_z|\ Y_{00}(\hat{X}')\ V_0(X',X_o)$$

$$\times \lambda^2\ I^{S\to ss}(E_{CM},II_zJLS,\alpha\beta), \qquad (3\text{-}51)$$

where $N_i(S\to ss)$, $Q_i^{(1)}(S\to ss)$ and $Q_i^{(2)}(S\to ss)$ are coefficients determined by the momentum dependent interaction, O_2 (eq. (3-4)), and the wave functions of the initial and the final states, and given in Table XIa∿d. Here F is given by

$$F = (A_2 B_2 E_2)^{3/2}, \qquad (3\text{-}52)$$

where

$$A_2 = D_N^2, \qquad (3\text{-}53)$$

$$B_2 = 1/(1/D_\alpha^2 + 1/D_N^2), \qquad (3\text{-}54)$$

$$E_2 = 1/\{1/D_\beta^2+2/D_N^2-(A_2+B_2)/(2D_N^2)^2\}, \quad (3\text{-}55)$$

and

$$a = 1/(16D_\alpha^2)+1/(16D_\beta^2)+1/(4D_N^2)-B_2(1/D_\alpha^2+1/D_N^2)^2/16$$
$$-E_2\{1/D_\beta^2+1/D_N^2+B_2(1/D_\alpha^2+1/D_N^2)/(2D_N^2)\}^2/16, \quad (3\text{-}56)$$

$$d = B_2(1/D_\alpha^2+1/D_N^2)/2$$
$$+(B_2-A_2)E_2\{1/D_\beta^2+1/D_N^2+B_2(1/D_\alpha^2+1/D_N^2)/(2D_N^2)\}/(4D_N^2), \quad (3\text{-}57)$$

and primes (F', a', b' and d') mean that D_α is replaced by D_β and vice versa in the definition of F, a, b and d. In eq. (3-51) X_o is given in the two meson annihilation by

$$X_o^2 = 2(b+b'), \quad (3\text{-}58)$$

where

$$b = 1/(16D_N^2)-(A_2+B_2)/(4D_N^2)^2-E_2\{1/D_N^2-(A_2+B_2)/(2D_N^2)^2\}^2/4, \quad (3\text{-}59)$$

The range is

$$X_o = 0.44 \text{ fm } (0.50 \text{ fm}) \quad \text{for } n=0,$$
$$= 0.39 \text{ fm } (0.42 \text{ fm}) \quad \text{for } n=1,$$
$$= 0.33 \text{ fm } (0.33 \text{ fm}) \quad \text{for } n=2, \quad (3\text{-}60)$$

where n is the number of pions in the final state and the values in the parentheses are the ranges in the case of r_P= 0.7 fm.

(iv) $S \to ps$ ($L=0$, $K=2$, α(a p-wave meson))

$$V_{opt}(E_{CM},\vec{X},\vec{X}',\alpha\beta,II_zJJ_zL=0\ S)$$

$$= Y_{00}^{*}(\hat{X})\ V_0(X,X_o)\ |S,J_z\rangle\langle S,J_z|\ Y_{00}(\hat{X}')\ V_0(X',X_o)$$

$$\times \lambda'^2 N_2\ (D_\alpha D_\beta)^{-3}\ D_N^{-12}\ /\ (12D_\alpha^2)$$

$$\times \int dm_1 dm_2 f_\alpha(m_1) f_\beta(m_2) \int_0^\infty \frac{dp_1 p_1^2}{E_1 E_2}\ \frac{1}{E_{CM}-E_1-E_2+i\varepsilon}$$

$$\times \sum_i N_i(S\to ps)\ \{F\ Q_i^{(1)}(S\to ps)\ (12B_2+6E_2gf+dhp_1^2)\ \exp(-ap_1^2)$$

$$+F'Q_i^{(2)}(S\to ps)\ (12E_2'g-d'wp_1^2)\ \exp(-a'p_1^2)\}^2$$

$$= Y_{00}^{*}(\hat{X})\ V_0(X,X_o)\ |S,J_z\rangle\langle S,J_z|\ Y_{00}(\hat{X}')\ V_0(X',X_o)$$

$$\times \lambda^2\ I^{S\to ps}(E_{CM},II_zJLS,\alpha\beta), \qquad (3\text{-}61)$$

where $N_i(S\to ps)$, $Q_i^{(1)}(S\to ps)$ and $Q_i^{(2)}(S\to ps)$ are given in Table XIIa∿d and

$$g = (A_2-B_2)/(2D_N^2), \qquad (3\text{-}62)$$

$$f = -B_2/D_N^2, \qquad (3\text{-}63)$$

$$h = B_2(1/D_\alpha^2+1/D_N^2)-1$$

$$+B_2E_2\{1/D_\beta^2+1/D_N^2+B_2(1/D_\alpha^2+1/D_N^2)/(2D_N^2)\}/(2D_N^2) \qquad (3\text{-}64)$$

and

$$w = E_2'\{1/D_\alpha^2+1/D_N^2+B_2'(1/D_\beta^2+1/D_N^2)/(2D_N^2)\}. \qquad (3\text{-}65)$$

In deriving eq. (3-61), we have neglected certain small

components (Appendix B). The range is

$$X_o = 0.41 \text{ fm } (0.44 \text{ fm}) \quad \text{for } n=0,$$
$$= 0.35 \text{ fm } (0.35 \text{ fm}) \quad \text{for } n=1, \tag{3-66}$$

where n is the number of pions.

(v) $P \to ss$ (L=1, K=2)

$$V_{opt}(E_{CM},\vec{X},\vec{X}',\alpha\beta,II_zJJ_zL{=}1\ S)$$

$$= \sum_{L_zL_z'} (1L_zSJ_z{-}L_z|JJ_z)\ (1L_z'SJ_z{-}L_z'|JJ_z)$$

$$\times Y^*_{1L_z}(\hat{X})\ V_1(X,X_o)\ |S,J_z{-}L_z\rangle\langle S,J_z{-}L_z'|\ Y_{1L_z'}(\hat{X}')\ V_1(X',X_o)$$

$$\times \lambda'^2 N_2\ (D_\alpha D_\beta)^{-3}\ D_N^{-12}$$

$$\times \int dm_1 dm_2 f_\alpha(m_1) f_\beta(m_2) \int_0^\infty \frac{dp_1 p_1^2}{E_1 E_2}\ \frac{1}{E_{CM}-E_1-E_2+i\varepsilon}$$

$$\times \sum_i N_i(P\to ss)\ \{F\ Q_i^{(1)}(P\to ss)\ (\tfrac{1}{3}cdp_1^2+e)/b^{1/2}$$

$$\times \exp(-ap_1^2)$$

$$+F'Q_i^{(2)}(P\to ss)\ (\tfrac{1}{3}c'd'p_1^2+e')/b'^{1/2}$$

$$\times \exp(-a'p_1^2)\}^2$$

$$= \sum_{L_zL_z'} (1L_zSJ_z{-}L_z|JJ_z)\ (1L_z'SJ_z{-}L_z'|JJ_z)$$

$$\times Y^*_{1L_z}(\hat{X})\ V_1(X,X_o)\ |S,J_z{-}L_z\rangle\langle S,J_z{-}L_z'|\ Y_{1L_z'}(\hat{X}')\ V_1(X',X_o)$$

$$\times \lambda^2\ I^{P\to ss}(E_{CM},II_zJLS,\alpha\beta), \tag{3-67}$$

where $N_i(P\to ss)$, $Q_i^{(1)}(P\to ss)$ and $Q_i^{(2)}(P\to ss)$ are given in Table XIIIa∿h and

$$c = B_2(1/D_\alpha^2+1/D_N^2)/(8D_N^2)$$
$$-E_2(1/D_\beta^2+1/D_N^2+B_2(1/D_\alpha^2+1/D_N^2)/(2D_N^2))$$
$$\times (1/D_N^2-(A_2+B_2)/(2D_N^2)^2)/4, \qquad (3\text{-}68)$$

$$e = (A_2-B_2)\{-1/(2D_N^2)+E_2(1/D_N^2-(A_2+B_2)/(2D_N^2)^2)/(2D_N^2)\}. \qquad (3\text{-}69)$$

In the derivation of eq. (3-67) we use the approximation

$$|cp_1P_N| \ll 1, \qquad (3\text{-}70)$$

where numerically

$$c \sim -0.03 \text{ fm}^2,$$
$$P_N \lesssim 2 \text{ fm}^{-1},$$
$$p_1 \lesssim 5 \text{ fm}^{-1}. \qquad (3\text{-}71)$$

The range is

$$X_o = 0.44 \text{ fm } (0.50 \text{ fm}) \quad \text{for } n=0,$$
$$= 0.39 \text{ fm } (0.42 \text{ fm}) \quad \text{for } n=1, \qquad (3\text{-}72)$$

where n is the number of pions.

(vi) $P \to ps$ ($L=1$, $K=2$, α(a p-wave meson))

$$V_{opt}(E_{CM},\vec{X},\vec{X}',\alpha\beta,II_zJJ_zL=1\ S)$$
$$= \sum_{L_zL_z'} (1L_zSJ_z-L_z|JJ_z)\ (1L_z'SJ_z-L_z'|JJ_z)$$

$$\times Y^{*}_{1L_z}(\hat{X})\ V_1(X,X_o)\ |S,J_z-L_z\rangle\langle S,J_z-L'_z|\ Y_{1L'_z}(\hat{X}')\ V_1(X',X_o)$$

$$\times \lambda'^2 N_2\ (D_\alpha D_\beta)^{-3}\ D_N^{-12}\ /\ (12D_\alpha^2)$$

$$\times \int dm_1 dm_2 f_\alpha(m_1) f_\beta(m_2) \int_0^\infty \frac{dp_1 p_1^2}{E_1 E_2}\ \frac{1}{E_{CM}-E_1-E_2+i\varepsilon}$$

$$\times \sum_i N_i(P\to ps)\ \{F\ Q_i^{(1)}(P\to ps)\ d\ j\ p_1 \exp(-ap_1^2)$$

$$-F' Q_i^{(2)}(P\to ps)\ d'z\ p_1 \exp(-a' p_1^2)\}^2$$

$$= \sum_{L_z L'_z} (1L_z SJ_z-L_z|JJ_z)\ (1L'_z SJ_z-L'_z|JJ_z)$$

$$\times Y^{*}_{1L_z}(\hat{X})\ V_1(X,X_o)\ |S,J_z-L_z\rangle\langle S,J_z-L'_z|\ Y_{1L'_z}(\hat{X}')\ V_1(X',X_o)$$

$$\times \lambda^2\ I^{P\to ps}(E_{CM}, II_z JLS, \alpha\beta), \qquad (3\text{-}73)$$

where $N_i(P\to ps)$, $Q_i^{(1)}(P\to ps)$ and $Q_i^{(2)}(P\to ps)$ are given in Table XIVa∿h and

$$j = B_2/D_N^2 - B_2 E_2 (1/D_N^2 - (A_2+B_2)/(2D_N^2)^2)/D_N^2, \qquad (3\text{-}74)$$

and

$$z = 2E'_2 (1/D_N^2 - (A'_2+B'_2)/(2D_N^2)^2). \qquad (3\text{-}75)$$

In eq. (3-73) we neglect small components as well as in eq. (3-61). The range is

$$X_o = 0.41 \text{ fm } (0.44 \text{ fm}) \quad \text{for } n=0,$$
$$= 0.35 \text{ fm } (0.35 \text{ fm}) \quad \text{for } n=1, \qquad (3\text{-}76)$$

where n is the number of pions.

(vii) $D \to ps$ ($L=2$, $K=2$, α(a p-wave meson))

$$
\begin{aligned}
&V_{opt}(E_{CM},\vec{X},\vec{X}',\alpha\beta,II_zJJ_zL{=}2\ S) \\
&= \sum_{L_zL_z'} (2L_zSJ_z{-}L_z|JJ_z)\ (2L_z'SJ_z{-}L_z'|JJ_z) \\
&\quad \times Y^*_{2L_z}(\hat{X})\ V_2(X,X_o)\ |S,J_z{-}L_z\rangle\langle S,J_z{-}L_z|\ Y_{2L_z'}(\hat{X}')\ V_2(X',X_o) \\
&\quad \times \lambda'^2 N_2\ (D_\alpha D_\beta)^{-3}\ D_N^{-12}\ /\ (12D_\alpha^2) \\
&\quad \times \int dm_1 dm_2 f_\alpha(m_1) f_\beta(m_2) \int_0^\infty \frac{dp_1 p_1^2}{E_1E_2}\ \frac{1}{E_{CM}-E_1-E_2+i\varepsilon} \\
&\quad \times \frac{2}{9} \sum_i N_i(D\to ps)\ \{F\ Q_i^{(1)}(D\to ps)\ ((eh+dj)cp_1^2+3ej)/b \\
&\qquad\qquad \times \exp(-ap_1^2) \\
&\qquad -F'Q_i^{(2)}(D\to ps)\ ((-e'w+d'z)c'p_1^2+3e'z)/b' \\
&\qquad\qquad \times \exp(-a'p_1^2)\}^2 \\
&= \sum_{L_zL_z'} (2L_zSJ_z{-}L_z|JJ_z)\ (2L_z'SJ_z{-}L_z'|JJ_z) \\
&\quad \times Y^*_{2L_z}(\hat{X})\ V_2(X,X_o)\ |S,J_z{-}L_z\rangle\langle S,J_z{-}L_z'|\ Y_{2L_z'}(\hat{X}')\ V_2(X',X_o) \\
&\qquad \times \lambda^2\ I^{D\to ps}(E_{CM},II_zJLS,\alpha\beta), \qquad (3\text{-}77)
\end{aligned}
$$

where $N_i(D\to ps)$, $Q_i^{(1)}(D\to ps)$ and $Q_i^{(2)}(D\to ps)$ are given in Table XVa~h and the form factor is

$$V_2(X,X_o) = \frac{2}{\pi X_o^3}\left(\frac{X}{X_o}\right)^2 \exp\{-(X/X_o)^2\}. \qquad (3\text{-}78)$$

The range is

$$X_o = 0.41 \text{ fm } (0.44 \text{ fm}) \quad \text{for } n=0,$$
$$= 0.35 \text{ fm } (0.35 \text{ fm}) \quad \text{for } n=1, \tag{3-79}$$

where n is the number of pions.

Using these potentials, we can estimate the partial annihilation cross sections from the $\bar{N}N$ state with isospin I and angular momentum $^{3S+1}L_J$ to the final state F_K of α, β and γ mesons, or α and β mesons. We obtain the cross sections as

$$\sigma_3(F_3,I,^{2S+1}L_J,E_{CM}) = b(I,^{2S+1}L_J,E_{CM}) \times \text{Im } I^{L\to\alpha\beta\gamma}(E_{CM},II_zJLS,\alpha\beta\gamma) \tag{3-80}$$

for three meson annihilations and

$$\sigma_2(F_2,I,^{2S+1}L_J,E_{CM}) = b(I,^{2S+1}L_J,E_{CM}) \times \text{Im } I^{L\to\alpha\beta}(E_{CM},II_zJLS,\alpha\beta) \tag{3-81}$$

for two meson annihilations. The effect of the initial $\bar{N}N$ interaction, $b(I,^{2S+1}L_J,E_{CM})$, is given by the form factor $V_L(X,X_o)$ and the relative wave function of the nucleon and the antinucleon. It is separated from the part dependent on intermediate mesons due to the separable form of the optical potentials. In order to estimate $b(I,^{2S+1}L_J,E_{CM})$ exactly, we must solve the scattering problems by using the optical potentials. However, since the contribution of those many

annihilation cross sections of the $\bar{N}N$ partial waves would amount almost to their optical limits, and there are ambiguities about the annihilation cross sections due to the ambiguities of the short range part of the OBEP, we may determine them approximately as follows. The annihilation cross section of the Lth partial wave is given by

$$\sigma(L,E_{CM}) = \sum_{ISJ} \{\sum_{F_3} \sigma_3(F_3,I,{}^{2S+1}L_J,E_{CM}) + \sum_{F_2} \sigma_2(F_2,I,{}^{2S+1}L_J,E_{CM})\} \tag{3-82}$$

and in the potential model also given by

$$\sigma(L,E_{CM}) = \frac{\pi}{8k_{CM}^2} \sum_{ISJ} (2J+1) \{1-|\eta(I,{}^{2S+1}L_J,E_{CM})|^2\} \tag{3-83}$$

with inelasticity $|\eta(I,{}^{2S+1}L_J,E_{CM})|$. An optical model calculation with a phenomenological annihilation potential by Ueda[4] has estimated the values $8k_{CM}^2/\pi\ \sigma(L,E_{CM})$ shown in Table V. Fitting $\sigma(L,E_{CM})$ in eq. (3-82) to the values in Table V we get the values of $b(I,{}^{2S+1}L_J,E_{CM})$ with the assumption of

$$b(L,E_{CM}) = b(I,{}^{2S+1}L_J,E_{CM}) \tag{3-84}$$

where the dependence on isospin and total angular momentum is neglected. Then the probability of an observed particle channel $\{m\pi^+m\pi^-n\pi^\circ\}$ is given by

$$\sigma(\bar{N}N\to\{m\pi^+m\pi^-n\pi^\circ\},E_{CM}) = \sum_{IJLS} \sum_{K} \sum_{F_K} R(F_K\to\{m\pi^+m\pi^-n\pi^\circ\}) \times \sigma_K(F_K,I,{}^{2S+1}L_J,E_{CM}), \tag{3-85}$$

where $R(F_K\to\{m\pi^+m\pi^-n\pi^\circ\})$ is the decay branching ratios with which F_K decays into $m\pi^+m\pi^-n\pi^\circ$ (See eq. (2-13)).

§ 4 Numerical results on $\bar{N}N$ annihilation and comparison with data

In this section we show the results of numerical calculations for the branching ratios of various meson channels and comparison with experimental data and give a physical interpretation for the parameters g_α defined in section 2.

Let us determine the values of the parameters. Our model contains five parameters: the strength of the three meson annihilation interaction λ in eq. (3-2), that of the two meson annihilation interaction λ' in eq. (3-4), the proton charge radius r_p in eq. (3-20), the range of the pion wave function D_π in eq. (3-31) and the range of the p-wave meson wave function D_p in eq. (3-35). In order to determine the overall strength of the potential it is necessary to construct the optical potentials and to solve the $\bar{N}N$ scattering problem. In this section the sum of the partial annihilation cross sections with the same angular momenta L is approximated by the one by the optical model calculation[4] when the relative branching ratios of various meson channels are estimated. Therefore, only the ratio λ'/λ is adjustable in this section. Their absolute value and the deviations from the exact calculation will be discussed in the next section where the partial cross sections in the $\bar{N}N$ scattering will be calculated by using the optical potentials due to our model.

In the first place we consider the $\bar{N}N$ annihilation at rest ($E_{CM} = 2M_N$, $T_{lab} = 0$ MeV) and determine the values of the parameters. At this energy it is assumed as has been done in

section 2 that the $\bar{N}N$ annihilation occurs dominantly from the $\bar{N}N$ S (L=0) states. Table VII shows the result of

$$\text{Im } I^{S\to sss}(E_{CM}=2M_N, II_zJ\ L=0\ S,\alpha\beta\gamma)$$
$$= -\sigma_3(F_3, I, {}^{2S+1}L=0_J,\ E_{CM}=2M_N)/b(I, {}^{2S+1}L=0_J, E_{CM}=2M_N), \quad (4\text{-}1)$$

normalized with the $\bar{P}P \to \rho^\circ\pi^\circ\pi^\circ$ channel for several values of r_P and D_π/D_s (The present version is referred as model II hereafter.). There we also give a comparison with the ones of the preceding version given in section 2 which is referred as model I hereafter. The result of model II is in good agreement with that of model I except for several channels with three heavy mesons. To see this more clearly let us calculate the effective values g_α^{eff} in model II for g_α in model I by comparing $-I_m\ I^{S\to sss}(E_{CM}=2M_N, II_zJ\ L=0\ S,\alpha\beta\gamma)$ with $P(IS,\alpha\beta\gamma)/b(I,S)$ in eq. (2-3):

$$-\text{Im } I^{S\to sss}(E_{CM}=2M_N, II_zJ\ L=0\ S,\alpha\beta\gamma)$$
$$= \left(\frac{g_\alpha^{eff}}{g_\alpha}\right)\left(\frac{g_\beta^{eff}}{g_\beta}\right)\left(\frac{g_\gamma^{eff}}{g_\gamma}\right)\frac{P(IS,\alpha\beta\gamma)}{b(I,S)}\ . \quad (4\text{-}2)$$

The result of g_α^{eff} is given in Table VIII in the case of r_P= 0.62 fm and D_π/D_s = 2.3. Here the predicted values for the four channels $\eta\pi\pi$, $\rho\pi\pi$, $\omega\pi\pi$ and $\rho\rho\pi$ are used to determine g_π^{eff}, g_η^{eff}, g_ρ^{eff} and g_ω^{eff}. Using those values of g_α^{eff} and comparing with the result in model I, we estimate the deviations ν for other channels by

$$-\text{Im } I^{S\to sss}(E_{CM}=2M_N, II_zJ\ L=0\ S,\alpha\beta\gamma)$$
$$= \nu^3\left(\frac{g_\alpha^{eff}}{g_\alpha}\right)\left(\frac{g_\beta^{eff}}{g_\beta}\right)\left(\frac{g_\gamma^{eff}}{g_\gamma}\right)\frac{P(IS,\alpha\beta\gamma)}{b(I,S)}\ . \quad (4\text{-}3)$$

The result is

$$\nu \sim 1 \qquad (4\text{-}4)$$

in most channels except in a few ones in which three mesons are all heavy (Table VIII). This means that the characteristic feature of the coupling constants g_α introduced in model I originates from the properties of the spatial components of the wave functions. We get the following physical interpretation. The larger the sum of the masses of the final state mesons is, the smaller phase space the final state occupies. Then the momenta of the quarks in the mesons are smaller. This corresponds to that the smaller momentum components of the quark wave functions of the initial nucleon and antinucleon mainly contribute to the annihilation amplitudes. Noting that the quark wave functions, having the Gaussian forms shown in eq. (3-22), are decreasing with momentum, we find that the channels with many heavy mesons are enhanced and thus g_α for heavy mesons become large.

Table VII indicates that a set of parameters r_p= 0.62 fm and D_π/D_s= 2.3, where r_p= 0.62 fm is the value of Isgur-Karl Model[21], is preferable and the result is not so much dependent on the values of parameters. Furthermore, we also check that once r_p and D_π/D_s are determined the result does not depend sensitively on other parameters such as m_q and κ in eq. (3-19).

In the next place we determine the ratio λ'/λ. The experimental data for the branching ratios of two meson annihilations at rest tells us that the two meson annihilations

occupy about 10 ∿ 20 % of the total one (Table I). Calculating $\sigma_3(F_3,I,^{2S+1}L=0_J,E_{CM}=2M_N)$ in eq. (3-80) for S → sss and $\sigma_2(F_2,I,^{2S+1}L=0_J,E_{CM}=2M_N)$ in eq. (3-81) for S → ss, ps in the $\bar{N}N$ L=0 states and using the above experimental information, we can determine the ratio λ'/λ such that

$$\frac{\sum_{ISJ}\ \sum_{\text{observed } F_2}\sigma_2(F_2,I,^{2S+1}L=0_J,E_{CM}=2M_N)}{\sum_{ISJ}\{\sum_{F_2}\sigma_2(F_2,I,^{2S+1}L=0_J,E_{CM}=2M_N)+\sum_{F_3}\sigma_3(F_3,I,^{2S+1}L=0_J,E_{CM}=2M_N)\}}$$

$$= 0.1 \sim 0.2. \qquad (4\text{-}5)$$

Here we have to pay attention to ε° p-wave meson. The ε° meson has the large width (200 ∿ 600 MeV) and the large branching ratio (∿ 60 %) for the decay $\varepsilon^\circ \to \pi^+\pi^-$. Therefore, for example, the $\omega^\circ\varepsilon^\circ$ channel is difficult to be separated from $\omega^\circ\pi^+\pi^-$, since it is observed as the channel $\omega^\circ\pi^+\pi^-$ experimentally. Taking account of this we readjust the parameters and obtain another set as

$$r_p = 0.7 \text{ fm}, \qquad (4\text{-}6)$$

$$D_p = 1.13 \text{ Fm}^{-1}, \qquad (4\text{-}7)$$

and

$$D_\pi/D_s = 3.0 \ (r_\pi = 0.33 \text{ fm}). \qquad (4\text{-}8)$$

Now we get all the values of parameters in model II but the absolute value of λ. In order to compare the predictions with data for observed multipion channels $\{m\pi^+m\pi^-n\pi^\circ\}$ it is necessary to estimate $b(I,^{2S+1}L=0_J,E_{CM}=2M_N)$ given in eq.

(3-81). For this purpose we have to know what states a nucleon and an antinucleon are in before annihilation, that is, the process that an antinucleon is captured by a nucleon. It should be estimated by using the annihilation amplitudes (T_3 in eq. (3-1) and T_2 in eq. (3-3)) and Coulomb and nuclear forces between the nucleon and the antinucleon. However, the process, which would depend on the state of targets, is not exactly known at present. Here, we regard $b(I,{}^{2S+1}L=0_J,E_{CM}=2M_N)$ as parameters as has been done in section 2. Fitting the predictions with data given in Table I we obtain the values

$$b(0,{}^3S_1,E_{CM}=2M_N)/b(0,{}^1S_0,E_{CM}=2M_N) = 0.80,$$

$$b(1,{}^3S_1,E_{CM}=2M_N)/b(0,{}^1S_0,E_{CM}=2M_N) = 0.86,$$

$$b(1,{}^1S_0,E_{CM}=2M_N)/b(0,{}^1S_0,E_{CM}=2M_N) = 0.68. \qquad (4\text{-}9)$$

The result for $\sigma(\bar{N}N\to\{m\pi^+m\pi^-n\pi^\circ\},E_{CM}=2M_N)$ in eq. (3-84) and $\sigma_2(F_2,I,{}^{2S+1}L=0_J,E_{CM}=2M_N)$ in eq. (3-81) are shown in Table XVI and Table XVII, respectively. The fit to data is satisfactory both in three meson annihilations and in two meson annihilations except for the predictions of the $3\pi^+3\pi^-m\pi^\circ$ ($m\geqq 0$) and $\pi^+\pi^-$ channels smaller than data (Table XVI). The wrong fit in the former channels comes from underestimations of the three meson annihilations into three heavy mesons such as $\bar{N}N \to \rho\rho\rho$, $\omega\rho\rho$, $\omega\omega\eta$, $\omega\omega\rho$ and $\omega\omega\omega$ in Table II. However, since in these three heavy meson channels the sum of the masses of the three mesons is above the $\bar{N}N$ threshold $E_{CM}= 2M_N$, the widths of

ρ and ω mesons are essential to nonvanishing contributions of the channels. Thus the partial cross sections become sensitive to the shapes of the mass distribution functions $f_\alpha(m)$ of ρ and ω shown in figs. 2a and 2b, in particular, the ones in the small mass region below their peaks. Therefore there are ambiguities in the predictions for the three heavy meson channels.

In Table XVII the predictions for the two meson annihilation channels are found in agreement with data. This justifies that the $\bar{q}q$ interaction, describing the annihilation from the $^3s_1$ $\bar{q}q$ state and being defined by O_2 in eq. (3-4), is appropriate for the $\bar{q}q$ annihilation and the two meson annihilation processes are mainly described by one $\bar{q}q$ annihilation diagrams (fig. 1b). We have also investigated another case for O_2 describing the annihilation from the $^3p_0$ $\bar{q}q$ state which is given by eq. (3-5). With this interaction a two meson annihilation occurs from an initial P (L=1) state. The result is shown in Table XVII. We find that the predictions for the annihilations into two heavy mesons (ρρ, ρω, ρω) are too large in comparison with other channels and it is unfavorable for reproducing overall data. It is neccessary to take account of some other diagrams for the two meson annihilation in order to describe the $\bar{q}q$ annihilation only from the $^3p_0$ $\bar{q}q$ state. It is, however, possible that $\bar{q}q$ pair annihilations and creations from several $\bar{q}q$ states coexist. We, keeping this in mind, restrict the $\bar{q}q$ annihilation interaction to the annihilation from the $^3s_1$ $\bar{q}q$ state and make

sure whether or not it is possible to reproduce data for the two meson annihilations.

Once the ratio λ'/λ and other parameters r_P, D_π and D_p are fixed, we can estimate the amplitudes for the initial P and D states as well as the S states at any energies. As mentioned at the end of section 3, $b(I,{}^{2S+1}L_J,E_{CM})$ at T_{lab}= 100 $\sim$ 300 MeV are determined by requiring that the L-dependence of the annihilation cross section is equal to those of an optical model calculation[4] with the assumption $b(I,{}^{2S+1}L_J,E_{CM}) = b(L,E_{CM})$ given in eq. (3-84). Now we can predict the partial cross sections of various decay channels $\sigma_3(F_3,I,{}^{2S+1}L_J,E_{CM})$ in eq. (3-80), $\sigma_2(F_2,I,{}^{2S+1}L_J,E_{CM})$ in eq. (3-81) and $\sigma(\{m\pi^+m\pi^-n\pi^\circ\},E_{CM})$ in eq. (3-85).

As mentioned in section 3, we consider two cases in the D states:

Case A: D $\rightarrow$ sss simulated by S $\rightarrow$ sss and D $\rightarrow$ ps,

Case B: D $\rightarrow$ ps only.

The branching ratios from D $\rightarrow$ sss are assumed to be similar to the ones from S $\rightarrow$ sss. In case A the normalization of the amplitude of D $\rightarrow$ sss is determined by fitting overall the partial cross sections of $\bar{P}P \rightarrow$ sss at T_{lab}= 100 $\sim$ 300 MeV.

The partial cross sections of $\{n\pi^+n\pi^-m\pi^\circ\}$ channels in the energy range of T_{lab}= 50 $\sim$ 300 MeV are shown in figs. 5a $\sim$ 5h[51,56,57] and the fractions, $\rho\pi$ and $f^\circ\pi^\circ$ in $\sigma(\pi^+\pi^-\pi^\circ)$, the ones, $\rho^\circ\pi^+\pi^-$, $f^\circ\pi^+\pi^-$, $\rho^\circ\rho^\circ$, $\rho^\circ f^\circ$ and $A_2^\pm\pi^\mp$ in $\sigma(2\pi^+2\pi^-)$ and the ones, $\omega^\circ\pi^+\pi^-$, $\rho^\circ\rho^\pm\pi^\mp$, $\rho^\pm\pi^\mp\pi^+\pi^-$, $\omega^\circ\rho^\circ$, $\omega^\circ f^\circ$ and $A_2^\circ\pi^+\pi^-$ in $\sigma(2\pi^+2\pi^-\pi^\circ)$, are given in figs. 6a $\sim$ 6c[29,36,51,57$\sim$59),

respectively, as functions of incident momentum. We find that the result is in agreement with data except for several partial cross sections. The fits to the various branching ratios give us the picture that the quark rearrangement and annihilation model is valid for describing the $\bar{N}N$ annihilation process.

The observed branching ratios and contribution from each partial wave ($L \to \alpha\beta\gamma$, $L \to \alpha\beta$) at T_{lab}= 100 and 300 MeV are given in Tables XVIII and XIX, respectively. We note here that the quark rearrangement processes appear to dominate (80 $\sim$ 90 %) at rest (T_{lab}= 0 MeV), which means the dominance of three meson annihilation in the $\bar{N}N$ S states, while at T_{lab}= 100 $\sim$ 300 MeV the contribution from them (45%) is comparable with those of the $\bar{q}q$ annihilation processes (54 $\sim$ 42 %), where particularly the processes $\bar{N}N \to ps$ have large contribution (45 $\sim$ 39 %).

$\sum_{\alpha\beta\gamma} I^{L\to\alpha\beta\gamma}(E_{CM}, II_z JLS, \alpha\beta\gamma)$ in eqs. (3-40) and (3-47), and $\sum_{\alpha\beta} I^{L\to\alpha\beta}(E_{CM}, II_z JLS, \alpha\beta)$ in eqs. (3-51), (3-61), (3-67), (3-73) and (3-77) at T_{lab}= 100 and 300 MeV are given in Tables IX $\sim$ XV and shown in figs. 7 $\sim$ 13, respectively. Observing the imaginary parts of $\sum_{\alpha\beta\gamma} I^{L\to\alpha\beta\gamma}(E_{CM}, II_z JLS, \alpha\beta\gamma)$ and $\sum_{\alpha\beta} I^{L\to\alpha\beta}(E_{CM}, II_z JLS, \alpha\beta)$ in figs. 7 $\sim$ 13 we find that the processes $\bar{P}P \to$ sss, ssp, ps represent flat or increasing energy dependences and the processes $\bar{P}P \to$ ss decreasing energy dependences in this energy range. This is because in the former case the thresholds of many channels of them are near or just above the $\bar{N}N$ threshold. Below the $\bar{N}N$ threshold the two

s-wave meson channels or the three meson channels with light mesons occupy large portion of the decay branching ratios.

When we compare the predicted fractions with data we should keep it in mind that it is not easy to divide the final state $\{m\pi^+m\pi^-\pi^\circ\}$ into each fraction both theoretically and experimentally. On the experimental side, the final state interactions among produced mesons make the peaks of mesons in the invariant mass distribution unclear. In addition the separation of the peaks from background becomes ambiguous due to large widths of mesons such as ρ, H, ε, B, A_1 and A_2 (Table VI). On the theoretical side, it is not clear for the same reason what channels should be included in calculating a fraction. For example, as pointed out in the above discussion the two meson channels $\varepsilon^\circ\rho^\circ$ and $\varepsilon^\circ\omega^\circ$ ought to be observed as the fraction $\rho^\circ\pi^+\pi^-$ or $\rho^\circ f^\circ$ in $2\pi^+2\pi^-$ and the one $\omega^\circ\pi^+\pi^-$ or $\omega^\circ f^\circ$ in $2\pi^+2\pi^-\pi^\circ$ respectively. This is because the width of ε° meson is so large (200 $\sim$ 600 MeV[60]) and the mass of ε° meson is so close to that of f° meson that it is not easy to discriminate two mesons $\pi^+\pi^-$ or p-wave meson f° from ε°. As shown in Tables XVIII and XIX we include these contributions which amount to $\sim$ 30 % in $\sigma(\rho^\circ\pi^+\pi^-)$, $\sigma(\rho^\circ f^\circ)$, $\sigma(\omega^\circ\pi^+\pi^-)$ and $\sigma(\omega^\circ f^\circ)$. Similarly, the channel $A_1\rho$ contributes to the $\rho\pi\pi\pi$ channel since A_1 meson decays into 3π (Table VI). The predictions of fractions should be carefully compared with data.

Let us investigate each channel in more detail. In case B the predicted values for $\sigma(\omega^\circ\pi^+\pi^-)$, $\sigma(\rho^\circ\rho^\pm\pi^\mp)$ and $\sigma(\rho^\pm\pi^\mp\pi^+\pi^-)$

are $\sim$ 1/2 of data and decrease with momentum rapidly, because contributions to these channels come only from S $\rightarrow$ sss and the occupation rate of the S state annihilation in the total annihilation decreases with momentum as seen in table V (22.9% at T_{lab}= 100 MeV and 12.7% at T_{lab}= 300 MeV). This indicates that the predicted values for $\sigma(\omega^{\circ}\pi^{+}\pi^{-})$, $\sigma(\rho^{\circ}\rho^{\pm}\pi^{\mp})$ and $\sigma(\rho^{\pm}\pi^{\mp}\pi^{+}\pi^{-})$ with only the process S $\rightarrow$ sss are not enough. The flat or increasing energy dependences of these fractions give an evidence for the existence of the contributions from the initial D states. The existence is supported by the reasons mentioned in the beginning of section 3: possible momentum dependent $\bar{q}q$ interactions, mixing of the $\bar{N}N$ S and D states by tensor forces between N and $\bar{N}$, and the $\bar{N}\Delta$, $N\bar{\Delta}$, $\Delta\bar{\Delta}$ annihilations. In case A we take in the process D $\rightarrow$ sss. The normalization of the D $\rightarrow$ sss, whose branching ratios are simulated by those of S $\rightarrow$ sss, is a new parameter. It is determined so as to reproduce the partial cross sections of $\bar{P}P$ $\rightarrow$ sss at T_{lab}= 100 $\sim$ 300 MeV. Then we obtain

$$\sigma(D \rightarrow sss)/\{\sigma(D \rightarrow sss)+\sigma(D \rightarrow ps)\} = 0.6. \qquad (4\text{-}10)$$

Since the portion of the annihilation from the $\bar{N}N$ D states in the total annihilation increases with momentum, the predicted values for $\sigma(\omega^{\circ}\pi^{+}\pi^{-})$, $\sigma(\rho^{\circ}\rho^{\pm}\pi^{\mp})$ and $\sigma(\rho^{\pm}\pi^{\mp}\pi^{+}\pi^{-})$ are enhanced with energy and their energy dependences are improved as seen in fig. 6c.

The contributions from P $\rightarrow$ ssp are well tested in the partial cross sections, $\sigma(f^{\circ}\pi^{+}\pi^{-})$ and $\sigma(A_2^{\circ}\pi^{+}\pi^{-})$ (#5c and #6f in

Table XVIII and figs. 6b and 6c, respectively). They show flat energy dependences due to the annihilation from the initial P states. Our model is also consistent with the fact that $\sigma(f\rho\pi)$ and $\sigma(A_2^{\pm}\pi^{\mp}\pi^{\circ})$ are very small experimentally.

The contributions from $P \to ss$ are justified by the fit in $\sigma(\omega^{\circ}\rho^{\circ})$ (#6d in Table XVIII and fig. 6c). Its slightly decreasing energy dependence is consistent with the annihilation from the initial P states.

The contributions from $D \to ps$ are also justified by the good fits and the energy dependences in $\sigma(\rho^{\circ}f^{\circ})$ and $\sigma(\omega^{\circ}f^{\circ})$ (#5d and #6e in Table XVIII and figs. 6b and 6c, respectively). Their increasing energy dependences indicate that main contributions of them come from the initial D states. (The portion of the D state annihilation in the total one increases with energy from 22 % at T_{lab}= 100 MeV to 39 % at 300 MeV.) Furthermore the fractions of both channels in case B are predicted too large. This fact supports that case A is adequate for the description of the D state annihilation processes.

We overestimate the channels with one p-wave meson and one pion such as $f^{\circ}\pi^{\circ}$, $A_2^{\pm}\pi^{\mp}$ and $B^{\pm}\pi^{\mp}$. The large predictions for these channels are due to good overlap of the spatial and the spin-isospin wave functions and the large available phase volumes. In fig. 6a the fraction of the $f^{\circ}\pi^{\circ}$ channel amounts to 30 $\sim$ 40 % in comparison with data $\sim$ 5 %. However, as seen in fig. 5b this difference is mainly due to the underestimation of $\sigma(\pi^{+}\pi^{-}\pi^{\circ})$. We should note in Table XVIII that for the

branching ratio of $f^\circ\pi^\circ$ in the total annihilation the predicted value 0.5 % is close to the experimental value 0.2 $\sim$ 0.5 %. Espigat et al.[59] estimate that the fraction of $B^{\pm}\pi^{\mp}$ in $\sigma(2\pi^+2\pi^-\pi^\circ)$ is very small ($\sim$ 0 %), while as shown in Table XVII the predicted branching ratio is 5 $\sim$ 6 % of the total annihilation at T_{lab}= 100 MeV. If B meson decays mainly into $\omega\pi$, the fraction in $\sigma(2\pi^+2\pi^-\pi^\circ)$ amounts to $\sim$ 20 %, and thus B meson must be observed contrary to the experiment.

Finally we mention the process S $\rightarrow$ ss. The predictions of $\sigma(\pi^+\pi^-)$, $\sigma(\rho\pi)$ and $\sigma(\rho^\circ\rho^\circ)$ are too small (#2, 3a and 5b in Table XVIII and figs. 5a and 5b, respectively). However, the fractions are only a few percent of the total annihilation. By use of duality argument for πN scattering, the processes of $\bar{N}N \rightarrow \pi\pi$, $\rho\pi$ and $\rho\rho$ via the exchange of N or Δ (fig. 14) are known to be important. Therefore we may interpret the disagreement as being due to the neglect of the processes such as two $\bar{q}q$ pairs annihilate and two mesons are created (fig.1c).

Below the $\bar{N}N$ threshold the branching ratios show different feature. As seen in figs. 7 $\sim$ 13 the imaginary potentials of $\bar{P}P \rightarrow$ ss become considerably large and the ones of $\bar{P}P \rightarrow$ 3 mesons become small in comparison with the ones above the $\bar{N}N$ threshold. In other words, the quark annihilation processes give larger contribution. Furthermore, fig. 19 shows that the channels with more pions occupy larger parts of the potentials below the $\bar{N}N$ threshold. Therefore, decay channels of a $\bar{N}N$ nuclear bound state with large binding energy, if it exists, will have large contribution from three meson channels with

many pions and two s-wave meson channels.

We should comment on $b(I,{}^{2S+1}L_J,E_{CM})$. It is assumed that $b(I,{}^{2S+1}L_J,E_{CM})$ do not depend on S, I and J for fixed L. In fact, they depend on them and the predictions for branching ratios would slightly alter. For example, if the I=0 $^3P_2$ channel is suppressed, the fraction of $A_2^{\pm}\pi^{\mp}$ will become small (Table XIVa). In order to estimate $b(I,{}^{2S+1}L_J,E_{CM})$ exactly, we must solve the scattering problems by using the optical potentials due to the annihilation. This problem will be discussed in the next section.

The result mentioned above points out that the feature of the $\bar{N}N$ annihilation into mesons can be explained by the quark rearrangement and annihilation model, although a minor modification with $\sim$ 10% of the total annihilation is necessary to consider by taking in other contributions in addition to the ones from the processes assumed in our model. Possible origins are the followings.

(i) Final state interactions among mesons would alter the production rates of mesons. For example, if a specific two meson interaction has one or more resonances in an available energy range and in a certain state, the partial cross section of the two meson channel producing in the state will be enhanced.

(ii) We have considered two meson annihilations by the $\bar{q}q$-pair annihilation only from the $^3s_1$ $\bar{q}q$ state. Although the predictions in the case of only the $^3p_0$ $\bar{q}q$ annihilation are not in agreement with data (Table XVII), we cannot exclude the

possibility of coexistence of the $\bar{q}q$ annihilations from several $\bar{q}q$ states. The relative weights of two heavy meson channels are larger in ^3p_o case than in $^3s_1$ case as seen in Table XVII. Thus inclusion of the $^3p_0$ case is expected to cure the overestimations of $f^\circ\pi^\circ$, $B^\pm\pi^\mp$ and $A_2^\pm\pi^\mp$ channels to a certain extent.

(iii) In addition to (ii) we should investigate the possibility of contributions from other diagrams such as fig. 1c. Although some attempts have been made[31,32,61,62], we could not reach a convincing conclusion about this at the present stage. Since the data for partial cross sections and angular distributions of $\bar{P}P \to \pi^+\pi^-$, K^+K^- at available low energies have recently been presented[63] and some experiments related to this problem are expected at the LEAR facility, the analyses of their amplitudes will be developed in the near future.

(iv) In case A we add only the process $D \to sss$ in all D states. As shown in section 3 we have considered that this is due to the momentum dependent part of the $\bar{q}q$ interactions, tensor forces in the OBEP and the $\bar{N}\Delta$, $N\bar{\Delta}$, $\Delta\bar{\Delta}$ annihilation. Therefore, we should take account of the effect by these origins in the processes $S \to sss$, ss, ps, $P \to ssp$, ss, ps and $D \to sss$, ss, ps, in particular, by the $\bar{N}\Delta$, $N\bar{\Delta}$, $\Delta\bar{\Delta}$ annihilation (fig. 4). Moreover, each contribution should have its own dependence for the initial $\bar{N}N$ state $^{2I+1,2S+1}L_J$. For example, the process $\bar{N}N(L=2) \to \bar{N}\Delta$, $N\bar{\Delta}(L=0) \to$ mesons occurs in isotriplet ($I=1$) and total angular momentum $J=2$ or $J=1$. At the present model we assume that all the $\bar{N}N$ states with the same angular

momentum L have the same partial cross sections.

To conclude this section we remark that the quark rearrangement and anihilation model for $\bar{N}N$ annihilation describes the feature of the branching ratios for the annihilation channels at T_{lab}= 0 $\sim$ 300 MeV except for several channels. The coupling constants g_α in model I is explained by virtue of introduction of the spatial part of the quark wave functions in hadrons. Then it is possible and necessary to introduce other processes and other interactions among quarks as a small modification in our model. Our result indicates that the quark rearrangement processes dominate in the $\bar{N}N$ S states in the energy range of T_{lab}= 0 $\sim$ 300 MeV, while they are comparable with the quark annihilation processes in the $\bar{N}N$ P and D states. Therefore, the total annihilation cross section at T_{lab}= 100 $\sim$ 300 MeV contains both contributions with similar amount. In the annihilation at rest the quark rearrangement processes dominate.

§ 5 Numerical results on $\bar{N}N$ scattering and comparison with data

This section concerns the description of the $\bar{N}N$ scattering based on the quark rearrangement and annihilation model, where the force between a nucleon and an antinucleon is described by the one-boson-exchange potential (OBEP) and a microscopic $\bar{N}N$ potential representing annihilation effect. Observables of the $\bar{P}P$ scattering are calculated and compared with data, and the characteristic features of the scattering by the optical potential given by our model are discussed[64].

The $\bar{N}N$ interaction is represented by both of the OBEP (fig. 15), where mesons are exchanged in the t-channel, and the intermediate meson configurations (fig. 16). It is well known that the OBEP for the $\bar{N}N$ system is obtained from the one for the NN system by G-parity transformation[2,3]. Let us write the OBEP for the NN system as

$$V_{OBEP}(NN) = \sum_{\alpha=\text{mesons}} V_{OBEP}(NN,\alpha), \tag{5-1}$$

where α are mesons exchanged. With the G-parity of α meson being represented by ε_α, where $\varepsilon_\alpha = 1$ for mesons with even G-parity (η, ρ, $\cdots$) and $\varepsilon_\alpha = -1$ for mesons with odd G-parity (π, ω, $\cdots$), the OBEP for the $\bar{N}N$ system becomes

$$V_{OBEP}(\bar{N}N) = \sum_{\alpha=\text{mesons}} \varepsilon_\alpha V_{OBEP}(NN,\alpha). \tag{5-2}$$

The ingredient of ω meson, which is responsible for the short range strong repulsion in the NN OBEP, turns to strong attraction in the $\bar{N}N$ OBEP (fig. 17). Here we employ the model

II of Ueda, Riewe and Green[65] as the NN OBEP. The potentials are cut off in the short range part with the form factor for the meson-nucleon vertex:

$$F(k^2) = \frac{\Lambda^2}{k^2+\Lambda^2} \,. \tag{5-3}$$

They obtain the value of the cut off parameter as

$$\begin{aligned} \Lambda &= 2532.4 \text{ MeV} \quad \text{for pion,} \\ &= 1184.3 \text{ MeV} \quad \text{for other mesons.} \end{aligned} \tag{5-4}$$

The details are found in ref. 4.

The quark rearrangement and annihilation processes lead optical potentials with intial $\bar{N}N$ S, P and D states. These partial waves are sufficient for describing the $\bar{N}N$ annihilation in the energy range of $T_{lab} \lesssim 300$ MeV, since as shown in an optical model calculation[4], contribution from the S, P and D waves to the total annihilation cross section amounts to 98 % at T_{lab}= 100 MeV and 87 % at T_{lab}= 300 MeV (Table V).

The optical potentials from the quark rearrangement and annihilation processes (fig. 18) are given in separable and energy-dependent forms such as

$$\begin{aligned} &V_{opt}(E_{CM},\vec{X},\vec{X}',II_zJJ_zLS) \\ &= \sum_{K=2,3} \sum_{F_K} \sum_{L_zL_z'} (LL_zSJ_z-L_z|JJ_z)(LL_z'SJ_z-L_z'|JJ_z) \\ &\quad \times Y^*_{LL_z}(\hat{X})\, V_L^{F_K}(X,X_o)\, \lambda^2\, I^{L\to F_K}(E_{CM},II_zJLS,F_K) \\ &\quad \times Y_{LL_z'}(\hat{X}')\, V_L^{F_K}(X',X_o), \end{aligned} \tag{5-5}$$

where F_K= α,β,γ for K=3 and F_K= α,β for K=2. (See eqs. (3-40),

(3-47), (3-51), (3-61), (3-67), (3-73) and (3-77).) The form factors of the potentials are obtained in Gaussian forms:

$$V_L^{F_K}(X,X_o) = 1/X_o^3\ (X/X_o)^L \exp(-(X/X_o)^2), \qquad (5\text{-}6)$$

corresponding to the forms of the quark wave functions. In eq. (5-6) X_o depends not only on the number of mesons K, but also on F_K owing to the difference among the sizes of the quark wave functions of pion, other s-wave mesons and p-wave mesons. Therefore there are a large number of X_o. In solving the $\bar{N}N$ scattering, for each potential of the Lth partial wave due to three or two meson annihilation, X_o is approximately set equal to the one of the channels which give main contribution to the potential (See Table XX.). We calculate $I^{L\to F_K}(E_{CM},II_zJLS,F_K)$ in the energy range of E_{CM}= 1700 $\sim$ 2000 MeV which are shown in Table XX and figs. 7 $\sim$ 13.

We summarize the important features of the optical potentials.

(i) We consider the following eight terms:

(1) S → sss, (2) S → ss, (3) S → ps,

(4) P → ssp, (5) P → ss, (6) P → ps,

(7) D → ps, (8) D → sss,

where S, P and D indicate the orbital angular momenta in the initial $\bar{N}N$ states, and s and p the s- and p-wave mesons respectively. Here we take account of the D-wave annihilation into three s-wave mesons, (8) D → sss. We have shown in section 4 that the predicted values for the branching ratios of $\bar{P}P$ → sss, especially, $\bar{P}P$ → $\omega\pi\pi$, $\rho\rho\pi$, are insufficient without

inclusion of D → sss. As in section 4 we simulate the contribution of D → sss by the one of (1) S → sss. This simulation is made by multiplying an adjustable parameter λ_D^2 in using $\sum_{F_3} I^{S\to sss}(E_{CM}, II_z JL=0\ S, F_3)$.

(ii) The parameter X_o, representing the annihilation radius, is 0.45 ∿ 0.6 fm for the three meson annihilation and 0.4 ∿ 0.45 fm for the two meson annihilation (Table XXa). The latter is smaller than the former since in the two meson annihilation processes a quark and an antiquark must occupy the same position spatially on the $\bar{q}q$ pair annihilation. The radius X_o depends also on the radius of the quark wave function. We use r_p= 0.62 fm as the nucleon root-mean-square radius according to Isgur and Karl[21]. If we use r_p= 0.7 fm, the X_o increases with ∿ 10 %.

(iii) The imaginary part of each $I^{L\to F_K}(E_{CM}, II_z JLS, F_K)$ has a peak at the energy of the sum of the masses of mesons F_K plus 300 ∿ 500 MeV (fig. 19). There the overlap of the spatial part of the wave functions is balanced well with the phase space volume of the final state mesons. As a result of the difference of the threshold energy of the final states included in each process, the potentials for $\bar{N}N \to ss$ decrease with energy (figs. 9 and 11) and others show flat or increasing energy dependences (figs. 7, 8, 10, 12 and 13). The strength of the potentials for S → sss, particularly, with I=0 and S=0 is drastically weakened below the $\bar{N}N$ threshold (E_{CM}= 1876 MeV) since the main contribution to them comes from three meson annihilations with the sum of the meson masses ∿ 1700 MeV. As

the process S → sss provides main contribution to the initial S state annihilation, this feature creates possibility of narrow-width $\bar{N}N$ bound states in the S states.

(iv) The real part of each $I^{L\to F_K}(E_{CM}, II_z JLS, F_K)$ originates from the principal part of the Green function of the intermediate meson states. It is negative at sufficiently low energies and changes its sign at a higher energy (fig. 19a). The energy of the real part having zero is almost equal to the one at which the imaginary part has a peak. Hence the real part is negative in the energy range of $T_{lab} \lesssim 300$ MeV in the channel with heavy mesons. As a result of this the real part of the potential from $\bar{N}N \to sss$, ssp is negative, the one from $\bar{N}N \to ss$ positive and the one from $\bar{N}N \to ps$ positive or negative.

(v) The annihilation potential has the separable form as shown in eq. (5-5). Hence the annihilation effect depends not only on the imaginary parts, but also sensitively on nodes of the relative wave function of $\bar{N}N$.

First we adjust the parameter λ in eq. (3-2), describing strength of potentials, to fit the $\bar{P}P$ total annihilation cross section at $T_{lab} = 100$ MeV. At the first stage, we neglect the process (8) D → sss. Only 65 % of the experimental value is reproduced at most as shown in fig. 20a.

The NN OBEP has uncertainties in the short range part where quark structure of nucleons and mesons is important. In this region the G-parity transformation is not applicable to get the $\bar{N}N$ OBEP from the NN OBEP and quark dynamics should be considered instead of the meson exchange. The $\bar{N}N$ potential

given by the G-parity transformation is strongly attractive in the short range part due to the ω meson exchange. Here as a simple case we modify phenomenologically the short range part of the $\bar{N}N$ OBEP by adding repulsive central components as follows.

$$V_{OBEP}^{mod.}(\bar{N}N) = V_{OBEP}(\bar{N}N) + V_c(I)\exp(-(X/X_c)^2), \qquad (5\text{-}7)$$

where X_c is fixed as X_c= 0.4 fm and $V_c(I)$ with isospin I=0 and I=1 are two adjustable parameters. In the optimum case 85 % of the experimental value is reproduced as shown in fig. 20b, where λ is fixed as the value given above. The central components of the $\bar{N}N$ OBEP with and without the modification are shown in fig. 17.

So far the D wave $\bar{N}N$ annihilation is assumed to occur only through the two meson annihilation process, (7) D → ps. The inclusion of (8) D → sss improves the situation and in the optimum case for λ_D^2 we reproduce 97 % of the experimental value (fig. 21c). Here as seen in Table XXa, contribution from D → sss determined by the present optical model calculation is somewhat large in comparison with the value 60 % in eq. (4-10) determined by fitting the observed branching ratios.

The total[66∿69], the elastic[63] and the charge-exchange[70] cross sections of the $\bar{P}P$ scattering below 300 MeV are displayed in fig. 21. The angular distributions of the $\bar{P}P$ elastic[63] and the charge-exchange[70] scatterings at T_{lab}= 120 MeV are shown in figs. 22 and 23 respectively, and the backward angle elastic cross section[71] is shown in fig. 24 as function of

incident momentum. We find that the present potential reproduces the observables qualitatively well. Quantitatively, however, the backward parts of the angular distributions do not fit well to data for both the elastic and the charge-exchange scatterings.

The following improvement should be taken in to remedy the fits.

(i) The treatment of the D wave annihilation should be elaborated. The annihilation potential for the transitions between the $\bar{N}N$ $^3S_1$ and the $^3D_1$ states and between the $^3D_1$ states is ignored in the present calculation. The inclusion of this would increase the partial annihilation cross section from the initial D states. We should improve the simulation of the contribution from the process D → sss by the three meson annihilation from the S states, S → sss, taking momentum transfer among quarks into consideration. In addition to this $\Delta\bar{N}$, $\bar{\Delta}N$ and $\bar{\Delta}\Delta$ annihilations make some cosiderable contribution to the $\bar{N}N$ D wave annihilation[26]. The additive D wave contributions would improve fits in the angular distribution of the $\bar{P}P$ elastic scattering at backward angles.

(ii) The modification of the short range part of the $\bar{N}N$ OBEP should be elaborated. At present we do not know how the reasonable choice of the modification should be. We can, however, remark that to add the component of the spin-dependent type $\vec{\sigma}_1\cdot\vec{\sigma}_2\ \vec{\tau}_1\cdot\vec{\tau}_2\ \exp(-(X/X_c)^2)$ to eq. (5-7) improves much the fits to the differential cross section of the charge-exchange scattering.

Both the real part of the optical potential (figs. 7 ∿ 13) and the OBEP (fig. 17) are strongly attractive at short distances, $X \lesssim 0.8$ fm. The attractive forces create a node at $X = 0.5 \sim 1$ fm in $\bar{N}N$ relative wave functions in many low angular momentum states. This feature causes some cancellation in the integral of the separable potential in Schrödinger equation. Let us define a local equivalent potential of the separable optical potential by

$$V_{local}(E_{CM},\vec{X},II_zJJ_zLS)$$
$$= \int d^3X' \; V_{opt}(E_{CM},\vec{X},\vec{X}',II_zJJ_zLS) \; \Psi_{II_zJJ_zLS}(\vec{X}')/\Psi_{II_zJJ_zLS}(\vec{X}), \tag{5-8}$$

where $V_{opt}(E_{CM},\vec{X},\vec{X}',II_zJJ_zLS)$ is defined by eq. (5-5). The equivalent local potential and the wave function are shown in fig. 25. The stronger the imaginary part is made, the stronger the real part of the optical potential bocomes and thus the wave function has a node. Then by the cancellation in the integral the annihilation effect of the optical potential is weakened. This is a reason why only 65 % of the $\bar{P}P$ annihilation cross section is reproduced without the introduction of the repulsive central component in eq. (5-7).

The repulsive central component needed is very large (fig. 17). The suitable values for $V_c(I)$ are

$$V_c(I=0) = 14.6 \text{ GeV},$$
$$V_c(I=1) = 11.0 \text{ GeV}. \tag{5-9}$$

With the repulsive central component, the node is pushed away

to a large distance, and the cancellation becomes less effective. To see this effect the magnitudes, R, of the S matrix of the partial waves at T_{lab}= 120 MeV are calculated in Table XXI, where σ is defined by

$$\sigma = (2J+1)(1-R^2) \qquad (5\text{-}10)$$

which is proportional to the partial annihilation cross section. For example, the increase of σ in the $^{11}P_1$ state by the repulsive component is just due to this effect. In other cases, for example in the $^{13}P_2$ state, the magnitude of $\Psi(X)$ around X = 0.6 fm becomes very small owing to the strong repulsion at $X \lesssim 0.5$ fm (fig. 25). This, with the node effect mentioned above, increases the imaginary part of $V_{local}(E_{CM},\vec{X},\vec{X}',II_zJJ_zLS)$ in eq. (5-8) around X = 0.6 fm. The feature at this distances is most effective to the annihilation cross section.

The repulsive components do not simply cancel the short range attraction of the OBEP, but rather produce newly the short range repulsive forces. Both I=0 and I=1 central components of the modified OBEP change from attraction to repulsion at X = 0.67 fm (See fig. 17.). Both are strongly repulsive with 1 GeV at X = 0.5 fm and most attractive with -300 MeV and -200 MeV at X = 0.85 fm respectively. This implies that a new origin for the repulsion at short distances $X \lesssim 0.4$ fm, which would be found in the realm of quark physics, must exist both in the I=0 and I=1 $\bar{N}N$ systems.

Finally, we estimate the justification of the

approximation for $b(I,{}^{2S+1}L_J,E_{CM})$ in sections 3 and 4. There we have assumed that $b(I,{}^{2S+1}L_J,E_{CM}) = b(L,E_{CM})$ and the L-dependence of the annihilation cross section is equal to the one by an optical model calculation (See eq. (3-84)). Comparison of them with the values calculated from Table XXI is given in Table XXII. We find that the approximation is valid within $\sim$ 30 % except in several partial waves.

In section 4 the relative weight between the three meson annihilation and the two meson annihilation with the same quantum numbers, I, J, L and S has been assumed to be equal to that of $I^{L\to F_K}(E_{CM},II_zJLS,F_K)$. However as the annihilation ranges, X_o, of them are different and the wave functions in several partial waves have nodes, $b(I,{}^{2S+1}L_J,E_{CM})$ is also dependent on the number of the final mesons and thus the predicted branching ratios would alter. In order to estimate this we must solve coupled channel equations with the $\bar{N}N$ channel, three meson ones and two meson ones.

§ 6 Summary and discussions

A microscopic description for the low energy $\bar{N}N$ annihilation has been proposed by a quark rearrangement and annihilation model. We have investigated the branching ratios of the final state mesons at T_{lab}= 0 ∿ 300 MeV, constructed the $\bar{N}N$ optical potentials by the model and solved the $\bar{N}N$ scattering problem.

In our model the low energy $\bar{N}N$ annihilation is characterized by the two processes: the quark rearrangement process into three mesons and the one $\bar{q}q$-pair annihilation process into two mesons. The amplitudes of the processes are given by the overlap of the spin-isospin and the spatial parts of the wave functions and the assumption that a $\bar{q}q$ pair annihilates from the $^3s_1$ state. We take in the p-wave mesons as well as the s-wave mesons in the final states. Our model contains four parameters: the ratio of the strengths for the three meson and the two meson annihilations, the proton charge radius, the pion radius and the p-wave meson radius. The model describes well the branching ratios for the annihilation channels both at rest (T_{lab}= 0 MeV) and in flight (T_{lab}= 50 ∿ 300 MeV) except for several channels.

The fractions of the three meson states and the two meson states in $\sigma(2\pi^+2\pi^-)$ and $\sigma(2\pi^+2\pi^-\pi^\circ)$ have favorable abundances and energy dependences. The energy dependences give us a clue to clarify from what initial $\bar{P}P$ state each three meson or two meson annihilation occurs. For example, the rapidly increasing energy dependence of the $f^\circ\rho^\circ$ channel indicates that

the main contribution to it comes from the initial D states.

Our model predicts that the quark rearrangement process dominates at rest, while it is comparable with the quark annihilation process at T_{lab}= 100 ∿ 300 MeV. This is the case for the total annihilation cross section. For the annihilation from the initial S states the quark rearrangement process dominates all in the energy range of T_{lab}= 0 ∿ 300 MeV.

We have also investigated the case of the $^3p_0$ $\bar{q}q$-pair annihilation. Although the interaction is found unfavorable for reproducing data if only this works, we cannot remove the possibility of coexistence of $\bar{q}q$-pair annihilations from several $\bar{q}q$ states.

The experimental abundances of the three s-wave meson channels, $\omega\pi\pi$ and $\rho\rho\pi$, and their increasing energy dependences require considerable contribution from the process D → sss which is predicted to have very small contribution by our original amplitudes. From experimental data we have estimated that this contribution should amount to about 60 % of the D state annihilation. The possible origins of this process have been discussed.

Our predictions for $\sigma(\pi\pi)$, $\sigma(\rho\pi)$ and $\sigma(\rho\rho)$ are too small. However the absolute values of these cross sections are small. We have interpreted this disagreement being due to the neglect of two $\bar{q}q$-pair annihilation processes etc.

The optical potentials due to the quark rearrangement and annihilation amplitudes become separable, and energy- and state-dependent. The form factors have Gaussian forms with

the range of $X_0 = 0.4 \sim 0.7$ fm, which originate from the ones of hadron internal wave functions. The energy dependence of the optical potential depends on the intermediate meson states.

The imaginary part of the optical potential for $\bar{N}N \to ss$ shows decreasing energy dependence near the $\bar{N}N$ threshold, since the meson states included have their threshold at far lower energy than the $\bar{N}N$ threshold. On the other hand, the one for $\bar{N}N \to sss$ shows rapidly increasing energy dependence, since many meson states open their threshold near the $\bar{N}N$ threshold. This feature creates the possibility of narrow-width bound states in some channels.

The feature of the real part of the optical potential is also determined by the positions of the thresholds of the intermediate meson states included. The real part has been obtained to be strongly attractive as a whole.

By using the $\bar{N}N$ optical potential and the $\bar{N}N$ OBEP we have calculated several cross sections. We have reproduced the qualitative feature of the observables below $T_{lab} = 300$ MeV. We find that to reproduce the annihilation cross section strong repulsion is needed at short distances. Without it the $\bar{P}P$ annihilation cross section is short by $20 \sim 30$ %. This is owing to the cancellation in the integral of separable potential in Schrödinger equation due to nodes of the $\bar{P}P$ relative wave functions. The existence of the additional process $D \to sss$ has been supported in the estimation of the annihilation cross section.

The angular distributions of the $\bar{P}P$ elastic and the

charge-exchange scatterings at backward angles are dependent on ambiguities in our model, for example, the treatment of the short range part of the $\bar{N}N$ OBEP and additional D wave annihilation potentials due to the $\Delta\bar{N}$, $\bar{\Delta}N$ and $\bar{\Delta}\Delta$ annihilation.

The quark rearrangement and annihilation model is suitable for describing the gross feature of the low energy $\bar{N}N$ scattering, although to refine the model it is necessary that further investigation is performed in several channels and more detailed experimental data are required.

The following questions come up as the next step. How can we develop the quark rearrangement and the quark annihilation model to describe the $\bar{N}N$ annihilation more quantitatively ? Is it right that we assume that spins and isospins of quarks do not flip in the rearrangement processes and a $\bar{q}q$ pair annihilates in the $\bar{q}q$ $^3s_1$ state ? The following approaches are expected to answer the questions.

(i) To study specific meson channels elaborately. Some observables would be sensitively dependent on quark dynamics. For example, comparison of the process $\bar{P}P \to K^+K^-$ with the one $\bar{P}P \to \pi^+\pi^-$ is expected to reveal mechanism of the two meson annihilation. Since a pair creation with a strange quark and a strange antiquark is needed for the K^+K^- production, energy dependence of the cross section and angular distribution for $\bar{P}P \to K^+K^-$ should be different from the ones for $\bar{P}P \to \pi^+\pi^-$. In fact, it has been reported in an experiment by bubble chamber that the difference was observed[72].

(ii) To make the model consistent with the description of other

hadron reactions. Decays of hadrons due to strong interaction, for example, $\rho^{\circ} \rightarrow \pi^{+}\pi^{-}$, and interactions among baryons and mesons should be accompanied by quark rearrangement and $\bar{q}q$ pair creations or annihilations.

(iii) To relate the present model to the fundamantal theory of strong interaction, QCD. Hadron interactions cause deformation of the boundary between physical vacuum and perturbative one, which makes the situation difficult. It is necessary to introduce the theory able to treat the situation such as the soliton bag model[73].

Acknowledgements

The author wishes to acknowledge to Professor S. Takagi and Dr. T. Ueda for many valuable discussions, helpful advices and careful reading through the manuscript. Especially, he is deeply indebted to Dr. T. Ueda for the collaboration to a series of works. He also wishes to express his gratitude to Professor T. Sawada, Dr. O. Miyamura and the members of Department of Applied Mathematics, Faculty of Engineering Science, Osaka University, for their kind supports and continuous encouragements.

The numerical calculations for this work have been carried out on the Computer System at the Computation Center of Osaka University. They have been financially supported in part by Institute for Nuclear Study, Tokyo University.

Appendix A Phase space volume of the final state with three mesons

The phase space integral

$$\int \frac{d^3p_1}{E_1}\frac{d^3p_2}{E_2}\frac{d^3p_3}{E_3}\,\delta^3(\vec{p}_1+\vec{p}_2+\vec{p}_3)\,\delta(E_1+E_2+E_3-E_{CM}) \qquad (A\text{-}1)$$

are carried and written as the form:

$$8\pi^2E_{CM}^2\int_{M_2}^{1-M_1-M_3} dY \int_{Z_{min}}^{Z_{max}} dZ\ . \qquad (A\text{-}2)$$

Here $M_i = m_i/E_{CM}$ $(i=1,2,3)$, and Z_{max} and Z_{min} are given by the solutions of the equation,

$$4(1+M_2^2-2Y)Z^2 -4(Z-1)(2Y-1-M_1^2-M_2^2+M_3^2)Z +4(1+M_1^2)Y^2$$

$$-4(1+M_1^2+M_2^2-M_3^2)Y +(1+(M_1+M_2)^2-M_3^2)(1+(M_1-M_2)^2-M_3^2) = 0. \qquad (A\text{-}3)$$

Appendix B Approximation of the form factor of the optical potentials

From eq. (3-39) we obtain the form factor of the potential for S → ps as

$$[12B_2 +6E_2gf +dhp_1^2 +\{\frac{c}{2b}(eh+dj)p_1^2 +\frac{3ej}{2b}\}(1-\frac{X^2}{6b})]\ V_0(X,X_o) \qquad (B\text{-}1)$$

instead of

$$[12B_2 +6E_2gf +dhp_1^2]\ V_0(X,X_o) \qquad (B\text{-}2)$$

in eq.(3-61), where

$$c = B_2(1/D_\alpha^2+1/D_N^2)/(8D_N^2)$$

$$-\frac{1}{4}E_2\{1/D_\beta^2+1/D_N^2+B_2(1/D_\alpha^2+1/D_N^2)/(2D_N^2)\}\{1/D_N^2-(A_2+B_2)/(2D_N^2)^2\}, \quad \text{(B-3)}$$

$$e = (B_2-A_2)[1/(2D_N^2)-E_2\{1/D_N^2-(A_2+B_2)/(2D_N^2)^2\}/(2D_N^2)] \quad \text{(B-4)}$$

and

$$j = B_2/D_N^2-B_2E_2\{1/D_N^2-(A_2+B_2)/(2D_N^2)^2\}/D_N^2 \ . \quad \text{(B-5)}$$

Using the values in eqs. (3-20) and (3-25):

$$D_N = 0.81 \text{ fm}^{-1} \quad \text{(B-6)}$$

and

$$D_\alpha = 0.87 \text{ fm}^{-1}, \quad \text{(B-7)}$$

we estimate the ratio of the last term to the first and the second terms in eq. (B-1):

$$\frac{1}{12B_2+6E_2gf}\{\frac{c}{2b}(eh+dj)p_1^2+\frac{3ej}{2b}\}(1-\frac{X^2}{6b})$$

$$= (-0.01p_1^2+0.53)\{1-(\frac{X}{0.54 \text{ fm}})^2\}. \quad \text{(B-8)}$$

The last term changes its sign at X = 0.54 fm. Hence this term should be considered, particularly, when the wave function has some nodes near this distance.

References

[1] U. Gastaldi and R. Klapisch, Proc. Int. School of Physics, "Enrico Fermi" LXXIX (North Holland 1981) p.462.

[2] J.S. Ball and G.F. Chew, Phys. Rev. 109 (1958) 1385.

[3] R.A. Bryan and R.J.N. Phillips, Nucl. Phys. B5 (1968) 201; R.J.N. Phillips, Rev. Mod. Phys. 39 (1967) 681.

[4] T. Ueda, Prog. Theor. Phys. 62 (1979) 1670; 63 (1980) 195.

[5] I.S. Shapiro, Phys. Reports 35C (1978) 129; L.N. Bogdanova, O.D. Dalkarov and I.S. Shapiro, Ann. Phys. 84 (1974) 261.

[6] J. Côté, M. Lacombe, B. Loiseau, B. Moussallam and R. Vinh Mau, Phys. Rev. Lett. 48 (1982) 1319.

[7] C.B. Dover and J.M. Richard, Phys. Rev. C21 (1980) 1466.

[8] A.M. Badalyan, L.P. Kok, M.I. Polikarpov and Y. Simonov, Phys. Reports 82C (1982) 31.

[9] F. Myhrer and A.W. Thomas, Phys. Lett. 64B (1976) 59.

[10] A.M. Green and S. Wycech, Nucl. Phys. A377 (1982) 441.

[11] A.M. Green, W. Stepien-Rudzka and S. Wycech, Nucl. Phys. A399 (1983) 307.

[12] O.D. Dalkarov and F. Myhrer, Nuovo Cim. 40A (1977) 152.

[13] W.B. Kaufmann, Phys. Rev. 19C (1979) 440.

[14] B.O. Kerbikov, A.E. Kudryavtsev, V.E. Markushin and I.S. Shapiro, JETP Lett. 26 (1977) 368.

[15] A.E. Kudryavtsev and R.T. Tyapaev, Sov. J. Nucl. Phys. 30 (1979) 835.

[16] D.H. Timmers, W.A. Van Der Sanden and J.J. De Swart,

Phys. Rev. D29 (1984) 1928.

[17] M. Van Der Velde, Ph. D. thesis, Vrije Universiteit te Amsterdam, 1980.

[18] H.R. Rubinstein and H. Stern, Phys. Lett. 21 (1966) 447.

[19] J. Harte, R.H. Socolow and J. Vandermeulen, Nuovo Cim. 49A (1967) 555.

[20] M. Maruyama and T. Ueda, Nucl. Phys. A364 (1981) 297.

[21] N. Isgur and G. Karl, Phys. Rev. D20 (1979) 1191.

[22] N. Isgur and G. Karl, Phys. Rev. D18 (1978) 4187.

[23] A. Chodos, R.L. Jaffe, K. Johnson, C.B. Thorn and V.F. Weisskopf, Phys. Rev. D9 (1974) 3471; A. Chodos, R.L. Jaffe, K. Johnson and C.B. Thorn, Phys. Rev. D10 (1974) 2599.

[24] M. Maruyama, Prog. Theor. Phys. 69 (1983) 937.

[25] M. Maruyama and T. Ueda, Phys. Lett. 124B (1983) 121.

[26] A.M. Green and J.A. Niskanen, Nucl. Phys. A412 (1984) 448.

[27] A.M. Green and J.A. Niskanen, International Review of Nuclear Physics Vol. II, ed. T.T.S. Kuo (World Scientific Co. Singapore 1984).

[28] S. Furui, A. Faessler and S.B. Khadkikar, Nucl. Phys. A424 (1984) 495.

[29] C. Baltay et al., Phys. Rev. Lett. 15 (1965) 532; B. Conforto et al., Nucl. Phys. B3 (1967) 469; A. Astier et al., Nucl. Phys. B10 (1969) 65.

[30] R. Bizzarri et al., Nucl. Phys. B14 (1969) 169.

[31] T. Fields, Phys. Rev. Lett. 36 (1976) 489.

[32] R.K. Logan, S. Kogitz and S. Tanaka, Can. J. Phys. 55 (1977) 2059; S. Kogitz, R.K. Logan and S. Tanaka, Proc. III European Symp. on $\bar{N}N$ Interactions, Stockholm (Sweden) 1982, p 541.

[33] P. Pavlopoulos et al., Proc. 2nd Int. Conf. on nucleon-nucleon interaction, Vancouver, 1977 (AIP Conf. Proc. No. 41), p. 340.

[34] L.D. Jacobs, Phys. Rev. D6 (1972) 1291; J. Pisút and M. Roos. Nucl. Phys. B6 (1968) 325.

[35] R. Gessaroli et al., Nucl. Phys. B126 (1977) 382.

[36] C. Baltay et al., Phys. Rev. 145 (1966) 1103.

[37] C. Baltay et al., Phys. Rev. 140 (1965) B1042.

[38] F.N. Ndili, Phys. Rev. 138 (1965) B460.

[39] M. Foster et al., Nucl. Phys. B6 (1968) 107.

[40] M. Foster et al., Nucl. Phys. B8 (1968) 174.

[41] P. Espigat, C. Ghesquière, E. Lillestol and L. Montanet, Nucl. Phys. B36 (1972) 93.

[42] T.E. Kalogeropoulos et al., Phys. Rev. Lett. 33 (1974) 1631.

[43] S. Devons et al., Phys. Lett. 47B (1973) 271.

[44] M. Bloch, G. Fontaine and E. Lillestol, Nucl. Phys. B23 (1970) 221.

[45] S. Devons et al., Phys. Rev. Lett. 27 (1971) 1614.

[46] S.J. Orfanidis and V. Rittenberg, Nucl. Phys. B59 (1973) 570; A. Bettini et al., Nuovo Cim. 47A (1967) 642; P. Anninos et al., Phys. Rev. Lett. 20 (1968) 402; T.E. Kalogeropoulos et al., Phys. Rev. Lett. 33 (1974) 1631.

[47] P. Pavlopoulos et al., Phys. Lett. 72B (1978) 415.

[48] C.B. Dover, J.M. Richard and M.C. Zabek, Ann. Phys. 130 (1980) 70; O.D. Dal'karov, V.M. Samoilov and I.S. Shapiro, Sov. J. Nucl. Phys. 17 (1973) 566.

[49] B.R. Desai, Phys. Rev. 119 (1960) 1390.

[50] C. Defoix et al., Nucl. Phys. B162 (1980) 12.

[51] F. Sai, S. Sakamoto and S.S. Yamamoto, Nucl. Phys. B213 (1983) 371; S. Sakamoto, Y. Kubota, F. Sai and S. Yamamoto, Tokyo Univ. preprint UT-HE-83/05.

[52] M. Maruyama and T. Ueda, Contribution paper to the 10th International Conference on Few Body Problems in Physics, Karlsruhe (Germany), August, 1983 - vol. II.

[53] M. Maruyama and T. Ueda, Osaka Univ. preprint OUAM 84-3-1; Contribution paper to International Symposium on "Nuclear Spectroscopy and Nuclear Interactions", Osaka, March 21-24, 1984.

[54] A. Le Yaouanc, L. Oliver, O. Pène and J.C. Raynal, Phys. Rev. D8 (1973) 2223; D11 (1975) 1272.

[55] "Compilation of coupling constants and low-energy parameters", Nucl. Phys. B147 (1979) 189.

[56] R. Hamatsu et al., Nucl. Phys. B123 (1977) 189.

[57] R.R. Burns, P.E. Condon, J. Donahue, M.A. Mandelkern and J. Schultz, Nucl. Phys. B27 (1971) 109; B73 (1974) 219; R.R. Burns, P.E. Condon, J. Donahue, M.A. Mandelkern, L.R. Price and J. Schultz, Nucl. Phys. B85 (1975) 337.

[58] T.C. Bacon et al., Phys. Rev. D7 (1973) 577.

[59] P. Espigat et al., Nucl. Phys. B162 (1980) 41.

[60] "Review of Particle Properties", Rev. Mod. Phys. 52 (1980) No. 2 Part II.

[61] H. Genz, Phys. Rev. D28 (1983) 1094.

[62] C.B. Dover and P.M. Fishbane, Orsay preprint IPNO/TH 84-8 (1984).

[63] T. Kageyama et al., private communication.

[64] M. Maruyama and T. Ueda, Osaka Univ. preprint OUAM 84-6-2 (1984), to be published in Physics Letters B.

[65] T. Ueda, F.E. Riewe and A.E.S. Green, Phys. Rev. C17 (1978) 1763.

[66] A.S. Carroll et al., Phys. Rev. Lett. 32 (1974) 247; V. Chaloupka et al., Phys. Lett. 61B (1976) 487; W. Bruckner et al., Phys. Lett. 67B (1977) 222.

[67] B. Conforto et al., Nuovo Cim. 54A (1968) 441.

[68] D. Spencer and D.N. Edwards, Nucl. Phys. B19 (1970) 501.

[69] B. Cork, O.I. Dahl, D.H. Miller, A.G. Tenner and C.L. Wang, Nuovo Cim. 25 (1962) 497; C.A. Coombes, B. Cork, W. Galbraith, G.R. Lambertson and W.A. Wenzel, Phys. Rev. 112 (1958) 1303; U. Amaldi jr. et al., Nuovo Cim. 46A (1966) 171; M. Coupland, E. Eisenhandler, W.R. Gibson, P.I.P. Kalmus and A. Astbury, Phys. Lett. 71B (1977) 460.

[70] K. Nakamura et al., Tokyo Univ. preprint UT-HE-84/04.

[71] M. Alston-Garnjost et al., Phys. Rev. Lett. 43 (1979) 1901.

[72] K. Nakamura and T. Tanimoto, Tokyo Univ. preprint UT-HE-84/11.

[73] R. Friedberg and T.D. Lee, Phys. Rev. D15 (1977) 1694; D16 (1977) 1096.

Table Ia Meson branching ratios in the $\bar{P}P$ annihilation at rest (T_{lab}= 0 MeV) in units of %. Contribution from two meson annihilation is removed. Asterisks (*) indicate the fitted data, where brackets mean that the sum of the data is fitted.

Channels	Experiment[33]	Our model	Harte et al.
* $m\pi^\circ (m \geq 1)$	3.2	3.4	12.9
$\pi^+\pi^-\pi^\circ$	3.6,2.0,1.0	0.9	7.4
$\pi^+\pi^-2\pi^\circ$	7.3 ± 3.0	3.3	
$\pi^+\pi^-3\pi^\circ$	23.2 ± 3.0	20.2	22.3
$\pi^+\pi^-m\pi^\circ (m \geq 4)$	2.8 ± 0.7	6.0	
* $2\pi^+2\pi^-(\rho^\circ\pi^+\pi^-)$	5.4 ± 0.3	5.4	25.6
$2\pi^+2\pi^-\pi^\circ$	18.0 ± 0.9	19.2	28.5
* $\eta^\circ\pi^+\pi^-$	0.28± 0.07	0.28	1.4
* $\omega^\circ\pi^+\pi^-$	3.4 ± 0.4	3.4	24.0
* $\rho^\circ\pi^\pm\pi^-\pi^\circ$	7.3 ± 1.7	7.7	1.4
* $\rho^\pm\pi^\mp\pi^+\pi^-$	6.4 ± 1.8	6.4	4.3
* $2\pi^+2\pi^-2\pi^\circ$	15.5 ± 1.0	13.9	3.1
* $2\pi^+2\pi^-m\pi^\circ (m \geq 3)$	4.2 ± 1.0	6.5	
$3\pi^+3\pi^-$	1.9 ± 0.2	1.1	
$3\pi^+3\pi^-\pi^\circ$	1.6 ± 0.3	1.2	
$\omega^\circ 2\pi^+2\pi^-$	1.2 ± 0.3	0.5	0.1
$\eta^\circ 2\pi^+2\pi^-$	0.14± 0.05	0.7	
$3\pi^+3\pi^-m\pi^\circ (m \geq 2)$	0.3 ± 0.1	0.3	

Table Ib Experimental data at rest (T_{lab}= 0 MeV).

Channel	ref. 33 (36)	ref. 29	refs. 37∿45
$2\pi^\circ$	∿ 0.04		0.048± 0.010 [45]
$\eta^\circ\pi^\circ$			0.008± 0.002 [42]
$3\pi^\circ$			0.76± 0.23 [43]
$\eta^\circ 2\pi^\circ$			0.34± 0.1 [42]
			0.35± 0.1 [43]
$m\pi^\circ (m \geq 3)$	3.2 ± 0.5	3.2	
$\pi^+\pi^-$	0.33± 0.04	0.375±0.03	0.389±0.074 [38]
$\pi^+\pi^-\pi^\circ$	(7.8 ± 0.9)	6.9 ± 0.35	4.0 ± 0.23 [38]
			6.9 ± 0.4 [39]
$\pi^+\pi^-\pi^\circ$	3.7		2.1 ± 0.1 [38]
			1.1 ± 0.4 [39]
$\rho^\circ\pi^\circ$	1.4 ± 0.2		2.1 ± 0.1 [38]
$\rho^\pm\pi^\mp$	2.7 ± 0.4		5.8 ± 0.3 [39]
$\pi^+\pi^-2\pi^\circ$	9.3 ± 3.0	15.6	
$\omega^\circ\pi^\circ$			0.15 ± 0.05 [38]
			0.8 ± 0.3 [42]
$\pi^+\pi^-3\pi^\circ$	23.3 ± 3.0	16.4	
$\pi^+\pi^-m\pi^\circ (m \geq 4)$	2.8 ± 0.7	3.1	
$2\pi^+2\pi^-$	5.8 ± 0.3	6.9 ± 0.6	
$\rho^\circ\rho^\circ$	(0.4 ± 0.3)		
$2\pi^+2\pi^-\pi^\circ$	(18.7 ± 0.9)	19.6 ± 0.7	
$\omega^\circ\pi^+\pi^-$	3.4 ± 0.4		3.9 ± 0.5 [37]
$\omega^\circ\rho^\circ$	0.6 ± 0.3		0.7 ± 0.3 [37]
$\rho^\circ\pi^+\pi^-\pi^\circ$	7.3 ± 1.7		
$\rho^\pm\pi^\mp\pi^+\pi^-$	6.4 ± 1.8		
$\eta^\circ\pi^+\pi^-$	0.28± 0.07		0.30± 0.03 [40]
			0.32± 0.04 [41]
$\eta^\circ\rho^\circ$	0.052±0.04		0.15± 0.02 [40]
$2\pi^+2\pi^-2\pi^\circ$	16.6 ± 1.0	15.5	
$\omega^\circ\omega^\circ$			1.1 ± 0.5 [44]
$2\pi^+2\pi^-m\pi^\circ (m \geq 3)$	4.2 ± 1.0	4.8	
$3\pi^+3\pi^-$	1.9 ± 0.2	2.1 ± 0.25	
$3\pi^+3\pi^-\pi^\circ$	(1.6 ± 0.3)	1.85± 0.15	
$\omega^\circ 2\pi^+2\pi^-$	1.2 ± 0.3		1.1 ± 0.3 [42]
$\eta^\circ 2\pi^+2\pi^-$	0.14± 0.05		0.12± 0.05 [42]
$3\pi^+3\pi^-m\pi^\circ (m \geq 2)$	(0.3 ± 0.1)	0.3 ± 0.1	

Table Ic Two meson annihilation at rest[33,37~40,42,44,45].

Channel	Experiment
$\pi^\circ\pi^\circ$	0.048±0.010
$\pi^+\pi^-$	0.33± 0.04
$\eta^\circ\pi^\circ$	0.02± 0.005
$\rho^\circ\pi^\circ$	1.4 ± 0.2
$\rho^\pm\pi^\mp$	2.7 ± 0.4 } 2.1, 5.8
$\omega^\circ\pi^\circ$	0.17± 0.06, 0.9 ± 0.45
$\eta^\circ\eta^\circ$	
$\eta^\circ\rho^\circ$	0.22± 0.17
$\eta^\circ\omega^\circ$	
$\rho^\circ\rho^\circ$	0.4 ± 0.3
$\rho^+\rho^-$	
$\rho^\circ\omega^\circ$	0.7 ± 0.3
$\omega^\circ\omega^\circ$	1.4 ± 0.6

Table II C(IS,αβγ) and phase space volume.

α β γ	I^G,S	C(IS,αβγ) (×1296)	×(phase space)	× b(I,S) × $g_\alpha g_\beta g_\gamma$
$\pi^\circ\pi^\circ\pi^\circ$	1^-,0	81	1.00	1.00
$\pi^\circ\pi^+\pi^-$	1^-,0	54	0.66	0.66
$\eta^\circ\pi^\circ\pi^\circ$	0^+,0	27	0.19	1.41
$\eta^\circ\pi^+\pi^-$	0^+,0	54	0.38	2.83
$\rho^\circ\pi^\circ\pi^\circ$	1^+,1	27	0.11	1.90
$\rho^\circ\pi^+\pi^-$	1^+,1	150	0.63	10.38
$\rho^\pm\pi^\mp\pi^\circ$	1^-,1	12	0.05	0.84
$\eta^\circ\eta^\circ\pi^\circ$	1^-,0	27	0.08	4.51
$\rho^\circ\eta^\circ\pi^\circ$	0^-,1	6	0.01	0.93
$\rho^\pm\eta^\circ\pi^\mp$	0^-,1	12	0.02	1.84
$\rho^\circ\rho^\circ\pi^\circ$	1^-,0	81	0.03	8.93
$\rho^\circ\rho^\pm\pi^\mp$	0^-,1	216	0.08	23.31
	1^-,0	36	0.01	3.91
$\rho^+\rho^-\pi^\circ$	0^-,1	108	0.04	11.90
	1^-,0	450	0.18	49.63
$\omega^\circ\pi^\circ\pi^\circ$	0^-,1	75	0.29	3.67
$\omega^\circ\pi^+\pi^-$	0^-,1	150	0.57	7.23
$\omega^\circ\eta^\circ\pi^\circ$	1^+,1	6	0.01	0.61
$\omega^\circ\rho^\circ\pi^\circ$	0^+,0	18	0.01	1.19
$\omega^\circ\rho^\pm\pi^\mp$	1^+,1	216	0.07	13.85
	0^+,0	36	0.01	2.30
$\omega^\circ\omega^\circ\pi^\circ$	1^-,0	225	0.05	8.46
$\eta^\circ\eta^\circ\eta^\circ$	0^+,0	81	0.04	16.49
$\rho^\circ\eta^\circ\eta^\circ$	1^+,1	75	0.01	5.27
$\rho^\circ\rho^\circ\eta^\circ$	0^+,0	225	0.003	6.73
$\rho^+\rho^-\eta^\circ$	1^+,1	108	0.002	3.26
	0^+,0	450	0.01	13.66
$\rho^\circ\rho^\circ\rho^\circ$	1^+,1	135	0.0004	1.80
$\rho^\circ\rho^+\rho^-$	1^+,1	378	0.001	5.03
	0^+,0	324	0.001	4.57
$\omega^\circ\eta^\circ\eta^\circ$	0^-,1	27	0.001	0.69
$\omega^\circ\rho^\circ\eta^\circ$	1^-,0	18	0.0001	0.15
$\omega^\circ\rho^\circ\rho^\circ$	0^-,1	189	0.0003	1.04
$\omega^\circ\rho^+\rho^-$	0^-,1	378	0.001	2.08
	1^-,0	324	0.001	1.74
$\omega^\circ\omega^\circ\eta^\circ$	0^+,0	81	0.0003	0.35
$\omega^\circ\omega^\circ\rho^\circ$	1^+,1	189	0.0001	0.26
$\omega^\circ\omega^\circ\omega^\circ$	0^-,1	135	0.00004	0.08

Table III Decay branching ratios of η, ρ and ω.

Decay modes		branching ratio(%)
$\eta^{\circ} \rightarrow$	$\gamma\gamma$	38.0
	$3\pi^{\circ}$	29.9
	$\pi^{\circ}\pi^{+}\pi^{-}$	23.6
	$\pi^{+}\pi^{-}\gamma$	4.9
	$\pi^{\circ}\gamma\gamma$	3.1
$\rho \rightarrow$	2π	100
$\omega^{\circ} \rightarrow$	$\pi^{\circ}\pi^{+}\pi^{-}$	89.9
	$\pi^{+}\pi^{-}$	1.4
	$\pi^{\circ}\gamma$	8.8

Table IV Meson branching ratios in PN annihilation at rest in units of %.

Channel	Experiment[46]	Prediction
1 prong	17.65± 0.8	14.3
$\pi^-2\pi^\circ$		0.4
$\pi^-3\pi^\circ$		9.7
$\pi^-m\pi^\circ(m\geq 4)$		2.7
3 prong	59.2 ± 2	53.0
$\pi^+2\pi^-$	2.3 ± 0.3	1.1
$\pi^+2\pi^-\pi^\circ$	17 ± 2	12.8
$\pi^+2\pi^-m\pi^\circ(m\geq 2)$	39.7 ± 2	39.1
5 prong	22.8 ± 1	28.8
$2\pi^+3\pi^-$	4.2 ± 0.2	10.0
$2\pi^+3\pi^-\pi^\circ$	12 ± 1	13.0
$2\pi^+3\pi^-m\pi^\circ(m\geq 2)$	6.6 ± 1	5.8
7 prong	0.35± 0.03	0
$\eta^\circ\pi^+2\pi^-$	< 0.3	0
$\omega^\circ\pi^+2\pi^-$	6 ~ 10	9.1
$\rho\ \pi\ \pi$	~ 8.7	11.5
$\rho^\circ\rho^\circ\pi^-$	~ 5.15	9.9

Table V The orbital angular momentum dependence of the annihilation cross sections by the optical model calculation[4]. The cross sections below are normalized as

$$\frac{8k_{CM}}{\pi}\,\sigma_{annih.}(L) = \sum_{SIJ} (2J+1)\,(1-|\eta(I,{}^{2S+1}L_J)|^2).$$

L	optical limit (η = 0)	T_{lab}= 100 MeV	T_{lab}= 300 MeV
0	8	7.4 (22.9%)	7.7 (12.7%)
1	24	17.3 (53.6%)	21.4 (35.3%)
2	40	7.1 (22.0%)	23.8 (39.3%)
3	56	0.5 (1.5%)	7.7 (12.7%)

Table VI Masses, widths and branching ratios of p-wave mesons which we use[60].

meson	mass(MeV)	width(MeV)	$spin^{parity}$	isospin
H	1190	320	1^+	0
ε	1300	400	0^+	0
D	1283	26	1^+	0
f	1273	179	2^+	0
B	1233	137	1^+	1
δ	983	54	0^+	1
A_1	1275	315	1^+	1
A_2	1318	110	2^+	1

H →	$\pi^+\pi^-\pi^\circ$	100 %	A_1° →	$\pi^+\pi^-\pi^\circ$	100 %
ε →	$\pi^+\pi^-$	60	$A_1^\pm$ →	$\pi^\pm 2\pi^\circ$	50
	$2\pi^\circ$	30		$2\pi^\pm\pi^\mp$	50
D →	$\pi^+\pi^-2\pi^\circ$	26.7	A_0° →	$\pi^+\pi^-\pi^\circ$	70.1
	$\pi^+\pi^-2\pi^\circ$	14.6		$2\pi^+2\pi^-\pi^\circ$	9.5
	$2\pi^+2\pi^-$	13.3		$2\pi^\circ$	5.7
	$\pi^+\pi^-\pi^\circ$	13.0		$4\pi^\circ$	4.6
	$2\pi^+2\pi^-\pi^\circ$	7.9		$\pi^+\pi^-2\pi^\circ$	4.3
	$3\pi^\circ$	6.5			
	$5\pi^\circ$	5.3	$A_2^\pm$ →	$2\pi^\pm\pi^\mp$	35.1
f →	$\pi^+\pi^-$	55.4		$\pi^\pm 2\pi^\circ$	35.1
	$2\pi^\circ$	27.7		$2\pi^\pm\pi^\mp 2\pi^\circ$	9.5
	$2\pi^+2\pi^-$	2.8		$\pi^\pm\pi^\circ$	5.7
B° →	$\pi^+\pi^-2\pi^\circ$	89.9		$\pi^\pm 3\pi^\circ$	4.6
	$3\pi^\circ$	8.7		$2\pi^\pm\pi^\mp\pi^\circ$	4.3
	$\pi^+\pi^-\pi^\circ$	1.4			
B± →	$2\pi^\pm\pi^\mp\pi^\circ$	89.9			
	$\pi^\pm 2\pi^\circ$	8.7			
	$2\pi^\pm\pi^\mp$	1.4			
δ° →	$2\pi^\circ$	39.1			
	$4\pi^\circ$	31.8			
	$\pi^+\pi^-2\pi^\circ$	23.7			
δ± →	$\pi^\pm\pi^\circ$	39.1			
	$\pi^\pm 3\pi^\circ$	31.8			
	$2\pi^\pm\pi^\mp\pi^\circ$	23.7			

Table VII $\sigma_3(F_3,I,{}^{2S+1}L_J,E_{CM}=2M_N)/b(I,{}^{2S+1}L_J,E_{CM})$ with L=0 at rest. Model I is given in section 2[20] and Model II in section III[25].

Channel	Model I	Model II		
		r_p=0.62 fm D_π/D_s=2.3	r_p=0.62 fm D_π/D_s=2.0	r_p=0.70 fm D_π/D_s=1.4
$\pi^\circ\pi^\circ\pi^\circ$	0.53	0.45	0.51	0.32
$\pi^\circ\pi^+\pi^-$	0.35	0.30	0.34	0.22
$\eta^\circ\pi^\circ\pi^\circ$	0.75	0.62	0.62	0.44
$\eta^\circ\pi^+\pi^-$	1.48	1.25	1.25	0.90
$\rho^\circ\pi^\circ\pi^\circ$	1.00	1.00	1.00	1.00
$\rho^\circ\pi^+\pi^-$	5.48	5.58	5.58	5.60
$\rho^\pm\pi^\mp\pi^\circ$	0.44	0.45	0.45	0.45
$\eta^\circ\eta^\circ\pi^\circ$	2.38	2.21	1.94	1.57
$\rho^\circ\eta^\circ\pi^\circ$	0.49	0.53	0.46	0.50
$\rho^\pm\eta^\circ\pi^\mp$	0.97	1.05	0.92	0.99
$\rho^\circ\rho^\circ\pi^\circ$	4.72	4.91	4.32	5.29
$\rho^\circ\rho^\pm\pi^\mp$	12.32	13.15	11.57	14.17
	2.07	2.19	1.93	2.36
$\rho^+\rho^-\pi^\circ$	6.29	6.55	5.76	7.05
	26.23	27.29	24.00	29.38
$\omega^\circ\pi^\circ\pi^\circ$	1.94	2.11	2.11	2.18
$\omega^\circ\pi^+\pi^-$	3.82	4.24	4.24	4.39
$\omega^\circ\eta^\circ\pi^\circ$	0.32	0.39	0.35	0.39
$\omega^\circ\rho^\circ\pi^\circ$	0.63	0.69	0.61	0.79
$\omega^\circ\rho^\pm\pi^\mp$	7.32	8.18	7.19	9.37
	1.22	1.36	1.20	1.56
$\omega^\circ\omega^\circ\pi^\circ$	4.47	5.14	4.52	6.42
$\eta^\circ\eta^\circ\eta^\circ$	8.72	12.68	9.72	9.42
$\rho^\circ\eta^\circ\eta^\circ$	2.79	3.58	2.74	2.77
$\rho^\circ\rho^\circ\eta^\circ$	3.56	3.84	2.94	3.01
$\rho^+\rho^-\eta^\circ$	1.72	1.84	1.41	1.44
	7.22	7.67	5.88	6.02
$\rho^\circ\rho^\circ\rho^\circ$	0.97	0.89	0.69	0.70
$\rho^\circ\rho^+\rho^-$	2.66	2.50	1.92	1.97
	2.42	2.15	1.65	1.69
$\omega^\circ\eta^\circ\eta^\circ$	0.37	0.25	0.19	0.21
$\omega^\circ\rho^\circ\eta^\circ$	0.08	0.09	0.07	0.07
$\omega^\circ\rho^\circ\rho^\circ$	0.55	0.34	0.26	0.28
$\omega^\circ\rho^+\rho^-$	1.10	0.67	0.52	0.56
	0.92	0.58	0.44	0.48
$\omega^\circ\omega^\circ\eta^\circ$	0.19	0.03	0.03	0.03
$\omega^\circ\omega^\circ\rho^\circ$	0.14	0.05	0.04	0.04
$\omega^\circ\omega^\circ\omega^\circ$	0.04	0.002	0.002	0.002

Table VIII The effective couplings $g_\alpha^{eff.}$ defined by eq. (4-2) and the deviations ν defined by eq. (4-3) in the case of $r_p = 0.62$ fm and $D_\pi/D_s = 2.3$[25].

α	$g_\alpha^{eff.}/g_\pi^{eff.}$	Channel	ν
η	6.49	$\eta\pi\pi$	0.97
ρ	17.48	$\eta\eta\pi$	1.08
ω	14.46	$\rho\eta\pi$	1.07
		$\omega\eta\pi$	1.09
		$\omega\rho\pi$	0.99
		$\omega\omega\pi$	0.97
		$\eta\eta\eta$	1.31
		$\rho\eta\eta$	1.19
		$\rho\rho\eta$	1.05
		$\rho\rho\rho$	0.94
		$\omega\eta\eta$	0.95
		$\omega\rho\eta$	0.93
		$\omega\rho\rho$	0.82
		$\omega\omega\eta$	0.59
		$\omega\omega\rho$	0.59
		$\omega\omega\omega$	0.34

Table IXa $C(II_zJJ_zLS,\alpha\beta\gamma)$ and $I^{S\to sss}(E_{CM},II_zJLS,\alpha\beta\gamma)$ in $(I=0,\ ^3S_1)$ channel.

Channel	$C(IJLS,\alpha\beta\gamma)$	T_{lab}= 100 MeV Re I	Im I	T_{lab}= 300 MeV Re I	Im I
$\rho^\circ\eta^\circ\pi^\circ$	6	+0.005	-0.009	+0.007	-0.006
$\rho^\pm\eta^\circ\pi^\mp$	12	+0.011	-0.018	+0.013	-0.013
$\rho^\circ\rho^\pm\pi^\mp$	216	-0.109	-0.285	+0.049	-0.276
$\rho^+\rho^-\pi^\circ$	108	-0.055	-0.144	+0.025	-0.138
$\omega^\circ\pi^\circ\pi^\circ$	75	+0.052	-0.024	+0.046	-0.015
$\omega^\circ\pi^+\pi^-$	150	+0.104	-0.049	+0.091	-0.029
$\omega^\circ\eta^\circ\eta^\circ$	27	-0.078	-0.028	-0.062	-0.072
$\omega^\circ\rho^\circ\rho^\circ$	189	-0.079	-0.018	-0.094	-0.040
$\omega^\circ\rho^+\rho^-$	378	-0.158	-0.036	-0.188	-0.079
$\omega^\circ\omega^\circ\omega^\circ$	135	-0.053	-0.001	-0.062	-0.002
total		-0.360	-0.598	-0.176	-0.642

Table IXb $C(II_zJJ_zLS,\alpha\beta\gamma)$ and $I^{S\to sss}(E_{CM},II_zJLS,\alpha\beta\gamma)$ in $(I=1,\ ^3S_1)$ channel.

Channel	$C(IJLS,\alpha\beta\gamma)$	T_{lab}= 100 MeV Re I	Im I	T_{lab}= 300 MeV Re I	Im I
$\rho^\circ\pi^\circ\pi^\circ$	27	+0.019	-0.008	+0.016	-0.005
$\rho^\circ\pi^+\pi^-$	150	+0.104	-0.045	+0.091	-0.027
$\rho^\pm\pi^\mp\pi^\circ$	12	+0.008	-0.004	+0.007	-0.
$\omega^\circ\eta^\circ\pi^\circ$	6	+0.005	-0.010	+0.006	-0.007
$\omega^\circ\rho^\pm\pi^\mp$	216	-0.130	-0.288	+0.031	-0.292
$\rho^\circ\eta^\circ\eta^\circ$	75	-0.229	-0.132	-0.155	-0.202
$\rho^+\rho^-\eta^\circ$	108	-0.094	-0.064	-0.130	-0.107
$\rho^\circ\rho^\circ\rho^\circ$	135	-0.058	-0.027	-0.070	-0.050
$\rho^\circ\rho^+\rho^-$	378	-0.163	-0.076	-0.196	-0.140
$\omega^\circ\omega^\circ\rho^\circ$	189	-0.076	-0.005	-0.091	-0.016
total		-0.616	-0.646	-0.490	-0.828

Table IXc $C(II_zJJ_zLS,\alpha\beta\gamma)$ and $I^{S\to sss}(E_{CM},II_zJLS,\alpha\beta\gamma)$ in $(I=0,\ ^1S_0)$ channel.

Channel	C(IJLS,αβγ)	T_{lab}= 100 MeV		T_{lab}= 300 MeV	
		Re I	Im I	Re I	Im I
$\eta^\circ\pi^\circ\pi^\circ$	27	+0.018	-0.003	+0.015	-0.002
$\eta^\circ\pi^+\pi^-$	54	+0.036	-0.006	+0.031	-0.003
$\omega^\circ\rho^\circ\pi^\circ$	18	-0.011	-0.024	+0.003	-0.024
$\omega^\circ\rho^\pm\pi^\mp$	36	-0.022	-0.048	+0.005	-0.049
$\eta^\circ\eta^\circ\eta^\circ$	81	+0.019	-0.361	+0.137	-0.281
$\rho^\circ\rho^\circ\eta^\circ$	225	-0.196	-0.133	-0.272	-0.224
$\rho^+\rho^-\eta^\circ$	450	-0.392	-0.267	-0.544	-0.448
$\rho^\circ\rho^+\rho^-$	324	-0.140	-0.065	-0.168	-0.120
$\omega^\circ\omega^\circ\eta^\circ$	81	-0.064	-0.006	-0.086	-0.021
total		-0.752	-0.882	-0.879	-1.139

Table IXd $C(II_zJJ_zLS,\alpha\beta\gamma)$ and $I^{S\to sss}(E_{CM},II_zJLS,\alpha\beta\gamma)$ in $(I=1,\ ^1S_0)$ channel.

Channel	C(IJLS,αβγ)	T_{lab}= 100 MeV		T_{lab}= 300 MeV	
		Re I	Im I	Re I	Im I
$\pi^\circ\pi^\circ\pi^\circ$	27	+0.028	-0.001	+0.025	-0.001
$\pi^\circ\pi^+\pi^-$	54	+0.019	-0.001	+0.017	-0.001
$\eta^\circ\eta^\circ\pi^\circ$	27	+0.037	-0.023	+0.034	-0.013
$\rho^\circ\rho^\circ\pi^\circ$	81	-0.041	-0.108	+0.018	-0.104
$\rho^\circ\rho^\pm\pi^\mp$	36	-0.018	-0.048	+0.008	-0.046
$\rho^+\rho^-\pi^\circ$	450	-0.229	-0.599	+0.102	-0.576
$\omega^\circ\omega^\circ\pi^\circ$	225	-0.157	-0.300	+0.013	-0.317
$\omega^\circ\rho^\circ\eta^\circ$	18	-0.015	-0.006	-0.020	-0.012
$\omega^\circ\rho^+\rho^-$	324	-0.136	-0.031	-0.161	-0.068
total		-0.511	-1.107	+0.036	-1.129

Table Xa $C(II_zJJ_zLS,\alpha\beta\gamma)$ and $I^{P\to ssp}(E_{CM},II_zJLS,\alpha\beta\gamma)$ in $(I=0,\ ^3P_2)$ channel.

Channel	$C(IJLS,\alpha\beta\gamma)$	T_{lab}= 100 MeV		T_{lab}= 300 MeV	
		Re I	Im I	Re I	Im I
$A_2{}^\circ\eta^\circ\pi^\circ$	6	-0.0008	-0.0001	-0.0012	-0.0004
$A_2{}^\pm\eta^\circ\pi^\mp$	12	-0.0016	-0.0002	-0.0023	-0.0008
$H^\circ\rho^\circ\pi^\circ$	6	-0.0005	-0.0003	-0.0007	-0.0005
$H^\circ\rho^\pm\pi^\mp$	12	-0.0011	-0.0006	-0.0021	-0.0011
$B^\circ\rho^\circ\eta^\circ$	6	-0.0003	-0.	-0.0004	-0.
$B^\pm\rho^\mp\eta^\circ$	12	-0.0007	-0.	-0.0007	-0.
$A_1{}^\circ\rho^\pm\pi^\mp$	54	-0.0038	-0.0015	-0.0047	-0.0028
$A_1{}^\pm\rho^\circ\pi^\mp$	54	-0.0038	-0.0015	-0.0047	-0.0028
$A_1{}^\pm\rho^\mp\pi^\circ$	54	-0.0038	-0.0015	-0.0047	-0.0028
$A_2{}^\circ\rho^\pm\pi^\mp$	162	-0.0034	-0.0012	-0.0041	-0.0036
$A_2{}^\pm\rho^\circ\pi^\mp$	162	-0.0034	-0.0012	-0.0041	-0.0036
$A_2{}^\pm\rho^\mp\pi^\circ$	162	-0.0034	-0.0012	-0.0041	-0.0036
$B^\circ\rho^+\rho^-$	108	-0.0055	-0.	-0.0061	-0.0001
$B^\pm\rho^\mp\rho^\circ$	216	-0.0110	-0.	-0.0121	-0.0001
$f^\circ\pi^\circ\pi^\circ$	75	-0.0023	-0.0186	+0.0046	-0.0170
$f^\circ\pi^+\pi^-$	150	-0.0045	-0.0375	+0.0091	-0.0339
$B^\circ\omega^\circ\pi^\circ$	150	-0.0113	-0.0005	-0.0143	-0.0020
$B^\pm\omega^\circ\pi^\mp$	300	-0.0227	-0.0009	-0.0286	-0.0041
$f^\circ\rho^\circ\rho^\circ$	176	-0.0056	-0.0002	-0.0061	-0.0004
$f^\circ\rho^+\rho^-$	352	-0.0112	-0.0004	-0.0123	-0.0008
$\delta^\circ\omega^\circ\rho^\circ$	32	-0.0017	-0.	-0.0019	-0.
$\delta^\pm\omega^\circ\rho^\mp$	64	-0.0034	-0.	-0.0038	-0.0001
$A_1{}^\circ\omega^\circ\rho^\circ$	126	-0.0039	-0.	-0.0043	-0.
$A_1{}^\pm\omega^\circ\rho^\mp$	252	-0.0078	-0.	-0.0085	-0.
$A_2{}^\pm\omega^\circ\rho^\circ$	220	-0.0064	-0.	-0.0069	-0.
$A_2{}^\pm\omega^\circ\rho^\mp$	440	-0.0127	-0.	-0.0139	-0.
total		-0.1551	-0.0657	-0.1589	-0.0739

$f^\circ\omega^\circ\omega^\circ$ 288 $f^\circ\eta^\circ\eta^\circ$ 27 $D^\circ\omega^\circ\omega^\circ$ 81 $D^\circ\rho^\circ\rho^\circ$ 9 $D^\circ\rho^+\rho^-$ 18
$\varepsilon^\circ\omega^\circ\omega^\circ$ 36 $\varepsilon^\circ\rho^\circ\rho^\circ$ 4 $\varepsilon^\circ\rho^+\rho^-$ 8 $H^\circ\omega^\circ\eta^\circ$ 54

Table Xb $C(II_zJJ_zLS,\alpha\beta\gamma)$ and $I^{P\to ssp}(E_{CM},II_zJLS,\alpha\beta\gamma)$ in $(I=0,\ ^3P_1)$ channel.

Channel	$C(IJLS,\alpha\beta\gamma)$	T_{lab}= 100 MeV Re I	Im I	T_{lab}= 300 MeV Re I	Im I
$A_1\,^\circ\eta^\circ\pi^\circ$	6	-0.0010	-0.0005	-0.0017	-0.0009
$A_1\,^\pm\eta^\circ\pi^{\mp}$	12	-0.0020	-0.0010	-0.0034	-0.0018
$H^\circ\rho^\circ\pi^\circ$	6	-0.0005	-0.0003	-0.0007	-0.0005
$H^\circ\rho^\pm\pi^{\mp}$	12	-0.0011	-0.0016	-0.0014	-0.0011
$B^\circ\rho^\circ\eta^\circ$	6	-0.0003	-0.	-0.0004	-0.
$B\,^\pm\rho^{\mp}\eta^\circ$	12	-0.0007	-0.	-0.0007	-0.
$\delta^\circ\rho^\pm\pi^{\mp}$	72	-0.0180	-0.0100	-0.0189	-0.0164
$\delta\,^\pm\rho^\circ\pi^{\mp}$	72	-0.0180	-0.0100	-0.0189	-0.0164
$\delta\,^\pm\rho^{\mp}\pi^\circ$	72	-0.0180	-0.0100	-0.0189	-0.0164
$A_1\,^\circ\rho^\pm\pi^{\mp}$	54	-0.0038	-0.0015	-0.0047	-0.0028
$A_1\,^\pm\rho^\circ\pi^{\mp}$	54	-0.0038	-0.0015	-0.0047	-0.0028
$A_1\,^\pm\rho^{\mp}\pi^\circ$	54	-0.0038	-0.0015	-0.0047	-0.0028
$A_2\,^\circ\rho^\pm\pi^{\mp}$	90	-0.0056	-0.0013	-0.0068	-0.0034
$A_2\,^\pm\rho^\circ\pi^{\mp}$	90	-0.0056	-0.0013	-0.0068	-0.0034
$A_2\,^\pm\rho^{\mp}\pi^\circ$	90	-0.0056	-0.0013	-0.0068	-0.0034
$B^\circ\rho^+\rho^-$	108	-0.0037	-0.	-0.0040	-0.
$B\,^\pm\rho^{\mp}\rho^\circ$	216	-0.0073	-0.	-0.0081	-0.0001
$D^\circ\pi^\circ\pi^\circ$	75	-0.0031	-0.0221	+0.0039	-0.0199
$D^\circ\pi^+\pi^-$	150	-0.0062	-0.0442	+0.0078	-0.0399
$B^\circ\omega^\circ\pi^\circ$	150	-0.0113	-0.0005	-0.0143	-0.0020
$B\,^\pm\omega^\circ\pi^{\mp}$	300	-0.0227	-0.0009	-0.0286	-0.0041
$f^\circ\rho^\circ\rho^\circ$	15	-0.0005	-0.	-0.0005	-0.
$f^\circ\rho^+\rho^-$	30	-0.0010	-0.	-0.0010	-0.
$\delta^\circ\omega^\circ\rho^\circ$	72	-0.0038	-0.	-0.0043	-0.0001
$\delta\,^\pm\omega^\circ\rho^{\mp}$	144	-0.0075	-0.	-0.0085	-0.0001
$A_1\,^\circ\rho^\circ\omega^\circ$	96	-0.0030	-0.	-0.0033	-0.
$A_1\,^\pm\rho^{\mp}\omega^\circ$	192	-0.0059	-0.	-0.0065	-0.
$A_2\,^\circ\rho^\circ\omega^\circ$	210	-0.0061	-0.	-0.0066	-0.
$A_2\,^\pm\rho^{\mp}\omega^\circ$	420	-0.0121	-0.	-0.0132	-0.
total		-0.2159	-0.1070	-0.2242	-0.1342

$f^\circ\omega^\circ\omega^\circ$ 135 $D^\circ\omega^\circ\omega^\circ$ 270 $D^\circ\rho^\circ\rho^\circ$ 174 $D^\circ\rho^+\rho^-$ 348
$D^\circ\eta^\circ\eta^\circ$ 27 $H^\circ\omega^\circ\eta^\circ$ 54

Table Xc $C(II_zJJ_zLS,\alpha\beta\gamma)$ and $I^{P\to ssp}(E_{CM},II_zJLS,\alpha\beta\gamma)$ in $(I=0,\ ^3P_0)$ channel.

Channel	C(IJLS,αβγ)	T_{lab}= 100 MeV Re I	Im I	T_{lab}= 300 MeV Re I	Im I
δ°η°π°	6	-0.0008	-0.0026	+0.0003	-0.0025
δ±η°π∓	12	-0.0015	-0.0051	+0.0006	-0.0049
H°ρ°π°	6	-0.0005	-0.0003	-0.0007	-0.0005
H°ρ±π∓	12	-0.0011	-0.0006	-0.0014	-0.0011
B°ρ°η°	6	-0.0003	-0.	-0.0004	-0.
B±ρ∓η°	12	-0.0007	-0.	-0.0007	-0.
A_1°ρ±π∓	216	-0.0151	-0.0059	-0.0187	-0.0113
A_1±ρ°π∓	216	-0.0151	-0.0059	-0.0187	-0.0113
A_1±ρ∓π°	216	-0.0151	-0.0059	-0.0187	-0.0113
B°ρ+ρ-	108	-0.0037	-0.	-0.0040	-0.
B±ρ∓ρ°	216	-0.0073	-0.	-0.0081	-0.0001
ε°π°π°	75	-0.0046	-0.0141	+0.0028	-0.0143
ε°π+π-	150	-0.0092	-0.0292	+0.0055	-0.0285
B°ω°π°	150	-0.0113	-0.0005	-0.0143	-0.0020
B±ω°π∓	300	-0.0227	-0.0020	-0.0286	-0.0041
f°ρ°ρ°	20	-0.0006	-0.	-0.0007	-0.0001
f°ρ+ρ-	40	-0.0013	-0.	-0.0014	-0.0002
δ°ρ°ω°	2	-0.0001	-0.	-0.0001	-0.
δ±ρ∓ω°	4	-0.0002	-0.	-0.0002	-0.
A_1°ρ°ω°	216	-0.0067	-0.	-0.0073	-0.
A_1±ρ∓ω°	432	-0.0133	-0.	-0.0146	-0.0001
A_2°ρ°ω°	160	-0.0046	-0.	-0.0050	-0.
A_2±ρ∓ω°	320	-0.0092	-0.	-0.0101	-0.
ε°ρ°ρ°	169	-0.0051	-0.0005	-0.0056	-0.0010
ε°ρ+ρ-	338	-0.0103	-0.0010	-0.0113	-0.0019
total		-0.1778	-0.0739	-0.1807	-0.0956

f°ω°ω° 180 ε°ω°ω° 225 ε°ρ°ρ° 169 ε°ρ+ρ- 338
ε°η°η° 27 H°ω°η° 54

Table Xd $C(II_zJJ_zLS,\alpha\beta\gamma)$ and $I^{P\to ssp}(E_{CM},II_zJLS,\alpha\beta\gamma)$ in $(I=1,\ ^3P_2)$ channel.

Channel	C(IJLS,αβγ)	T_{lab}= 100 MeV Re I	Im I	T_{lab}= 300 MeV Re I	Im I
$A_2°\pi°\pi°$	27	-0.0022	-0.0072	+0.0005	-0.0069
$A_2°\pi+\pi-$	150	-0.0123	-0.0397	+0.0029	-0.0383
$A_2\pm\pi\mp\pi°$	12	-0.0010	-0.0032	+0.0002	-0.0031
$B°\rho°\pi°$	54	-0.0042	-0.0010	-0.0054	-0.0025
$B\pm\rho°\pi\mp$	300	-0.0236	-0.0058	-0.0300	-0.0138
$B\pm\rho\mp\pi°$	12	-0.0009	-0.0002	-0.0012	-0.0006
$B°\rho\pm\pi\mp$	12	-0.0009	-0.0002	-0.0012	-0.0006
$D°\rho\pm\pi\mp$	54	-0.0037	-0.0004	-0.0046	-0.0013
$f°\rho\pm\pi\mp$	162	-0.0114	-0.0041	-0.0141	-0.0075
$A_1\pm\omega°\pi\mp$	54	-0.0036	-0.0006	-0.0045	-0.0015
$A_2\pm\omega°\pi\mp$	162	-0.0098	-0.0003	-0.0118	-0.0010
$H°\rho°\eta°$	150	-0.0089	-0.0002	-0.0101	-0.0008
$A_1\pm\rho\mp\eta°$	54	-0.0027	-0.	-0.0031	-0.0001
$H°\rho+\rho-$	108	-0.0039	-0.0001	-0.0044	-0.0002
$\delta°\rho°\rho°$	36	-0.0019	-0.0001	-0.0022	-0.0002
$\delta°\rho+\rho-$	8	-0.0004	-0.	-0.0005	-0.
$\delta\pm\rho\mp\rho°$	64	-0.0034	-0.0001	-0.0039	-0.0003
$A_1°\rho°\rho°$	81	-0.0026	-0.	-0.0028	-0.0001
$A_1°\rho+\rho-$	18	-0.0006	-0.	-0.0006	-0.
$A_1\pm\rho\mp\rho°$	252	-0.0080	-0.0001	-0.0088	-0.0002
$A_2°\rho°\rho°$	288	-0.0085	-0.	-0.0093	-0.
$A_2°\rho+\rho-$	352	-0.0104	-0.	-0.0114	-0.
$A_2\pm\rho\mp\rho°$	440	-0.0130	-0.	-0.0142	-0.0001
$A_2\pm\rho\mp\eta°$	162	-0.0076	-0.	-0.0084	-0.0001
$A_2°\eta°\eta°$	75	-0.0058	-0.	-0.0067	-0.0001
$f°\omega°\rho°$	220	-0.0068	-0.0001	-0.0075	-0.0003
$B\pm\omega°\rho\mp$	216	-0.0071	-0.	-0.0079	-0.
total		-0.1776	-0.0639	-0.1794	-0.0805

$f°\eta°\pi°$ 6 $D°\omega°\rho°$ 126 $\varepsilon°\omega°\rho°$ 32 $A_2°\omega°\omega°$ 176
$A_1°\omega°\omega°$ 9 $\delta°\omega°\omega°$ 4 $H°\omega°\pi°$ 6 $B°\omega°\eta°$ 6

Table Xe $C(II_zJJ_zLS,\alpha\beta\gamma)$ and $I^{P\to ssp}(E_{CM},II_zJLS,\alpha\beta\gamma)$ in $(I=1,\ ^3P_1)$ channel

Channel	C(IJLS,αβγ)	T_{lab}= 100 MeV Re I	Im I	T_{lab}= 300 MeV Re I	Im I
$A_1°\pi°\pi°$	27	-0.0009	-0.0063	+0.0016	-0.0060
$A_1°\pi+\pi-$	150	-0.0049	-0.0353	+0.0089	-0.0331
$A_1\pm\pi\mp\pi°$	12	-0.0004	-0.0028	+0.0007	-0.0026
$B°\rho°\pi°$	54	-0.0042	-0.0010	-0.0054	-0.0025
$B\pm\rho°\pi\mp$	300	-0.0236	-0.0058	-0.0300	-0.0138
$B\pm\rho\mp\pi°$	12	-0.0009	-0.0002	-0.0012	-0.0006
$B°\rho\pm\pi\mp$	12	-0.0009	-0.0002	-0.0012	-0.0006
$\varepsilon°\rho\pm\pi\mp$	72	-0.0047	-0.0030	-0.0058	-0.0044
$D°\rho\pm\pi\mp$	54	-0.0037	-0.0004	-0.0046	-0.0013
$f°\rho\pm\pi\mp$	90	-0.0063	-0.0023	-0.0079	-0.0042
$\delta\pm\omega°\pi\mp$	72	-0.0137	-0.0052	-0.0196	-0.0138
$A_1\pm\omega°\pi\mp$	54	-0.0036	-0.0006	-0.0045	-0.0015
$A_2\pm\omega°\pi\mp$	90	-0.0055	-0.0002	-0.0066	-0.0005
$A_1°\eta°\eta°$	75	-0.0064	-0.	-0.0074	-0.0004
$H°\rho°\eta°$	150	-0.0089	-0.0002	-0.0101	-0.0008
$\delta\pm\rho\mp\eta°$	72	-0.0068	-0.0002	-0.0081	-0.0010
$A_1\pm\rho\mp\eta°$	54	-0.0027	-0.	-0.0031	-0.0001
$H°\rho+\rho-$	108	-0.0039	-0.0001	-0.0044	-0.0002
$\delta\pm\rho\mp\rho°$	144	-0.0078	-0.0002	-0.0088	-0.0007
$A_1°\rho°\rho°$	270	-0.0086	-0.0001	-0.0094	-0.0002
$A_1°\rho+\rho-$	348	-0.0110	-0.0001	-0.0121	-0.0003
$A_1\pm\rho\mp\rho°$	192	-0.0061	-0.	-0.0067	-0.0001
$A_2°\rho°\rho°$	135	-0.0040	-0.	-0.0044	-0.
$A_2°\rho+\rho-$	30	-0.0009	-0.	-0.0010	-0.
$A_2\pm\rho\mp\rho°$	420	-0.0124	-0.	-0.0136	-0.0001
total		-0.1831	-0.0646	-0.1984	-0.0899

$f°\omega°\eta°$	210	$D\cdot\cdot\omega°\rho°$	96	$D°\eta°\pi°$	6	$\varepsilon°\omega°\rho°$	72	$A_2\pm\rho\mp\eta°$	90
$A_2°\omega°\omega°$	15	$H°\omega°\pi°$	6	$B\pm\omega°\rho\mp$	216	$B°\omega°\eta°$	6	$A_1°\omega°\omega°$	174

Table Xf: $C(II_zJJ_zLS,\alpha\beta\gamma)$ and $I^{P\to ssp}(E_{CM},II_zJLS,\alpha\beta\gamma)$ in $(I=1,\ ^3P_0)$ channel.

Channel	C(IJLS,αβγ)	T_{lab}= 100 MeV Re I	Im I	T_{lab}= 300 MeV Re I	Im I
δ°π°π°	27	+0.0048	-0.0048	+0.0048	-0.0031
δ°π+π-	150	+0.0268	-0.0266	+0.0268	-0.0171
δ±π∓π°	12	+0.0021	-0.0021	+0.0021	-0.0014
B°ρ°π°	54	-0.0042	-0.0010	+0.0054	-0.0025
B±ρ°π∓	300	-0.0236	-0.0058	-0.0300	-0.0138
B±ρ∓π°	12	-0.0009	-0.0002	-0.0012	-0.0006
B°ρ±π∓	12	-0.0009	-0.0002	-0.0012	-0.0006
D°ρ±π∓	216	-0.0148	-0.0014	-0.0183	-0.0051
A_1 ±ω°π∓	216	-0.0146	-0.0025	-0.0179	-0.0061
δ°η°η°	75	-0.0142	-0.0001	-0.0198	-0.0010
H°ρ°η°	150	-0.0089	-0.0002	-0.0101	-0.0008
A_1 ±ρ∓η°	216	-0.0109	-0.0001	-0.0122	-0.0005
H°ρ+ρ-	108	-0.0039	-0.0001	-0.0044	-0.0002
δ°ρ°ρ°	225	-0.0118	-0.0003	-0.0138	-0.0011
δ°ρ+ρ-	338	-0.0177	-0.0005	-0.0207	-0.0017
δ±ρ∓ρ°	14	-0.0007	-0.	-0.0009	-0.0001
A_1 ±ρ∓ρ°	432	-0.0137	-0.0001	-0.0150	-0.0003
A_2°ρ°ρ°	180	-0.0053	-0.	-0.0058	-0.
A_2°ρ+ρ-	40	-0.0012	-0.	-0.0013	-0.
A_2±ρ∓ρ°	320	-0.0095	-0.	-0.0103	-0.0001
total		-0.1530	-0.0469	-0.1873	-0.0572

f°ω°ρ°	160	D°ω°ρ°	216	ε°ω°ρ°	2	ε°η°π°	6	A_2°ω°ω°	20
δ°ω°ω°	169	H°ω°π°	6	B±ω°ρ∓	216	B°ω°η°	6		

Table Xg $C(II_zJJ_zLS,\alpha\beta\gamma)$ and $I^{P\to ssp}(E_{CM},II_zJLS,\alpha\beta\gamma)$ in $(I=0,\ ^1P_1)$ channel.

Channel	C(IJLS,αβγ)	T_{lab}= 100 MeV Re I	Im I	T_{lab}= 300 MeV Re I	Im I
H°π°π°	27	+0.0015	-0.0070	+0.0032	-0.0060
H°π+π-	54	+0.0031	-0.0140	+0.0065	-0.0121
B°η°π°	54	-0.0112	-0.0031	-0.0164	-0.0098
B±η°π∓	108	-0.0223	-0.0065	-0.0328	-0.0195
D°ρ°π°	6	-0.0004	-0.	-0.0005	-0.0001
D°ρ±π∓	12	-0.0008	-0.0001	-0.0010	-0.0003
f°ρ°π°	10	-0.0007	-0.0003	-0.0009	-0.0005
f°ρ±π∓	20	-0.0014	-0.0005	-0.0017	-0.0009
δ°ω°π°	2	-0.0004	-0.0001	-0.0005	-0.0004
δ±ω°π∓	4	-0.0008	-0.0003	-0.0011	-0.0008
A_1°ω°π°	6	-0.0004	-0.0001	-0.0005	-0.0002
A_1±ω°π∓	12	-0.0008	-0.0001	-0.0010	-0.0003
A_2°ω°π°	10	-0.0006	-0.	-0.0007	-0.0001
A_2±ω°π∓	20	-0.0012	-0.	-0.0015	-0.0001
H°η°η°	243	-0.0251	-0.0002	-0.0301	-0.0032
δ°ρ°η°	50	-0.0047	-0.0001	-0.0056	-0.0007
δ±ρ∓η°	100	-0.0094	-0.0002	-0.0112	-0.0015
A_1°ρ°η°	150	-0.0076	-0.0001	-0.0085	-0.0003
A_1±ρ∓η°	300	-0.0151	-0.0001	-0.0170	-0.0006
A_2°ρ°η°	250	-0.0117	-0.	-0.0130	-0.0001
A_2±ρ∓η°	500	-0.0233	-0.	-0.0260	-0.0001
H°ρ°ρ°	225	-0.0082	-0.0001	-0.0091	-0.0004
H°ρ+ρ-	450	-0.0164	-0.0002	-0.0181	-0.0008
δ°ρ+ρ-	36	-0.0019	-0.0001	-0.0022	-0.0002
δ±ρ∓ρ°	72	-0.0039	-0.0001	-0.0066	-0.0004
A_1°ρ+ρ-	108	-0.0034	-0.	-0.0038	-0.0001
A_1±ρ∓ρ°	216	-0.0068	-0.	-0.0075	-0.0002
A_2°ρ+ρ-	180	-0.0053	-0.	-0.0058	-0.
A_2±ρ∓ρ°	360	-0.0107	-0.	-0.0116	-0.
total		-0.2028	-0.0342	-0.2372	-0.0605

f°ω°η°	90	D°ω°η°	54	ε°ω°η°	18	ε°ρ°π°	2	ε°ρ±π∓	4
H°ω°ω°	81	B°ω°ρ°	18	B±ω°ρ∓	36				

Table Xh $C(II_zJJ_zLS,\alpha\beta\gamma)$ and $I^{P\to ssp}(E_{CM},II_zJLS,\alpha\beta\gamma)$ in $(I=1,\ ^1P_1)$ channel.

Channel	C(IJLS,αβγ)	T_{lab}= 100 MeV Re I	Im I	T_{lab}= 300 MeV Re I	Im I
B°π°π°	243	+0.0033	-0.0700	+0.0225	-0.0598
B°π+π-	54	+0.0007	-0.0156	+0.0050	-0.0133
B±π∓π°	108	+0.0015	-0.0311	+0.0100	-0.0266
H°η°π°	54	-0.0155	-0.0085	-0.0153	-0.0131
B°η°η°	27	-0.0025	-0.	-0.0030	-0.
δ°ρ°π°	18	-0.0045	-0.0029	-0.0047	-0.0048
δ°ρ±π∓	4	-0.0010	-0.0007	-0.0011	-0.0011
δ±ρ°π∓	4	-0.0010	-0.0007	-0.0011	-0.0011
δ±ρ∓π°	100	-0.0250	-0.0163	-0.0263	-0.0265
A_1°ρ°π°	54	-0.0038	-0.0015	-0.0047	-0.0028
A_1°ρ±π∓	12	-0.0008	-0.0003	-0.0010	-0.0006
A_1±ρ°π∓	12	-0.0008	-0.0003	-0.0010	-0.0006
A_1±ρ∓π°	300	-0.0210	-0.0082	-0.0260	-0.0157
A_2°ρ°π°	90	-0.0056	-0.0007	-0.0068	-0.0020
A_2°ρ±π∓	20	-0.0013	-0.0002	-0.0015	-0.0004
A_2±ρ°π∓	20	-0.0013	-0.0002	-0.0015	-0.0004
A_2±ρ∓π°	500	-0.0314	-0.0041	-0.0380	-0.0111
B°ρ°ρ°	81	-0.0027	-0.	-0.0030	-0.
B°ρ+ρ-	450	-0.0153	-0.	-0.0168	-0.0002
B±ρ∓ρ°	36	-0.0012	-0.	-0.0013	-0.
ε°ω°π°	50	-0.0032	-0.0014	-0.0038	-0.0021
D°ω°π°	150	-0.0099	-0.0001	-0.0121	-0.0005
f°ω°π°	250	-0.0170	-0.0032	-0.0209	-0.0058
f°ρ+ρ-	180	-0.0057	-0.0002	-0.0063	-0.0004
δ±ω°ρ∓	72	-0.0038	-0.	-0.0043	-0.0001
total		-0.2000	-0.1633	-0.1975	-0.1843

f°ρ°η° 10 D°ρ°η° 6 A_2±ω°ρ∓ 360 A_1°ω°η° 4 B°ω°ω° 225
D°ρ+ρ- 108 ε°ρ+ρ- 36 A_1±ω°ρ∓ 216 δ°ω°η° 2 ε°ρ°η° 2
A_2°ω°η° 10 H°ω°ρ° 18

Table XIa $N_i(S\to ss)$, $Q_i^{(1)}(S\to ss)$, $Q_i^{(2)}(S\to ss)$ and $I^{S\to ss}(E_{CM}, II_z JLS, \alpha\beta)$ in $(I=0, {}^3S_1)$ channel.

Channel	N_i	$Q_i^{(1)}$	$Q_i^{(2)}$	T_{lab}= 100 MeV Re I	Im I	T_{lab}= 300 MeV Re I	Im I
$\rho^\circ\pi^\circ$	4	5	-6	+0.1062	-0.0167	+0.0903	-0.0081
$\rho^\pm\pi^\mp$	8	5	-6	+0.2123	-0.0394	+0.1807	-0.0162
$\omega^\circ\eta^\circ$	4	3	0	+0.0124	-0.0059	+0.0106	-0.0030
total				+0.3331	-0.0559	+0.2835	-0.0273

Table XIb $N_i(S\to ss)$, $Q_i^{(1)}(S\to ss)$, $Q_i^{(2)}(S\to ss)$ and $I^{S\to ss}(E_{CM}, II_z JLS, \alpha\beta)$ in $(I=1, {}^3S_1)$ channel.

Channel	N_i	$Q_i^{(1)}$	$Q_i^{(2)}$	T_{lab}= 100 MeV Re I	Im I	T_{lab}= 300 MeV Re I	Im I
$\rho^+\rho^-$	4 8	3 0	-3 3	+0.0543	-0.0689	+0.0602	-0.0451
$\rho^\circ\eta^\circ$	4	1	0	+0.0013	-0.0006	+0.0012	-0.0003
$\omega^\circ\pi^\circ$	4	1	-6	+0.0538	-0.0094	+0.0455	-0.0046
$\pi^+\pi^-$	2	6	-6	+0.0398	-0.0007	+0.0360	-0.0003
total				+0.1502	-0.0796	+0.1438	-0.0503

Table XIc $N_i(S\to ss)$, $Q_i^{(1)}(S\to ss)$, $Q_i^{(2)}(S\to ss)$ and $I^{S\to ss}(E_{CM}, II_z JLS, \alpha\beta)$ in $(I=0, {}^1S_0)$ channel.

Channel	N_i	$Q_i^{(1)}$	$Q_i^{(2)}$	T_{lab}= 100 MeV Re I	Im I	T_{lab}= 300 MeV Re I	Im I
$\omega^\circ\omega^\circ$	6	3	-3	+0.0514	-0.0851	+0.0623	-0.0556
$\rho^\circ\rho^\circ$	6	1	-1	+0.0060	-0.0077	+0.0067	-0.0050
$\rho^+\rho^-$	12	1	-1	+0.0121	-0.0153	+0.0134	-0.0100
total				+0.0699	-0.1080	+0.0829	-0.0706

Table XId $N_i(S\to ss)$, $Q_i^{(1)}(S\to ss)$, $Q_i^{(2)}(S\to ss)$ and $I^{S\to ss}(E_{CM}, II_z JLS, \alpha\beta)$ in $(I=1, {}^1S_0)$ channel.

Channel	N_i	$Q_i^{(1)}$	$Q_i^{(2)}$	T_{lab}= 100 MeV Re I	Im I	T_{lab}= 300 MeV Re I	Im I
$\rho^\circ\omega^\circ$	12	5	1	+0.0470	-0.0681	+0.0544	-0.0445
$\rho^\pm\pi^\mp$	12	0	6	+0.1280	-0.0210	+0.1090	-0.0103
total				+0.1762	-0.0890	+0.1654	-0.0548

Table XIIa $N_i(S\to ps)$, $Q_i^{(1)}(S\to ps)$, $Q_i^{(2)}(S\to ps)$ and $I^{S\to ps}(E_{CM}, II_z JLS, \alpha\beta)$ in $(I=0, {}^3S_1)$ channel.

Channel	N_i	$Q_i^{(1)}$	$Q_i^{(2)}$	T_{lab}= 100 MeV Re I	Im I	T_{lab}= 300 MeV Re I	Im I
$\varepsilon°\omega°$	2/3	30	0	-0.1990	-0.1906	-0.1678	-0.2663
$D°\omega°$	2	0	15	-0.0064	-0.0003	-0.0087	-0.0011
$f°\omega°$	10/3	6	-9	-0.0788	-0.0333	-0.0886	-0.0677
$\delta°\rho°$	8/3	1	-6	-0.0044	-0.0102	+0.	-0.0113
$\delta\pm\rho\mp$	16/3	1	-6	-0.0087	-0.0204	+0.0001	-0.0226
$A_1°\rho°$	2	6	-1	-0.0296	-0.0337	-0.0218	-0.0454
$A_1\pm\rho\mp$	4	6	-1	-0.0591	-0.0674	-0.0436	-0.0908
$A_2°\rho°$	10/3	4	-3	-0.0300	-0.0166	-0.0308	-0.0291
$A_2\pm\rho\mp$	20/3	4	-3	-0.0600	-0.0331	-0.0617	-0.0582
total				-0.4759	-0.4056	-0.4229	-0.5925

Table XIIb $N_i(S\to ps)$, $Q_i^{(1)}(S\to ps)$, $Q_i^{(2)}(S\to ps)$ and $I^{S\to ps}(E_{CM}, II_z JLS, \alpha\beta)$ in $(I=1, {}^3S_1)$ channel.

Channel	N_i	$Q_i^{(1)}$	$Q_i^{(2)}$	T_{lab}= 100 MeV Re I	Im I	T_{lab}= 300 MeV Re I	Im I
$\delta°\omega°$	8/3	1	6	+0.0016	-0.0015	+0.0004	-0.0011
$A_1°\omega°$	2	6	7	-0.0256	-0.0239	-0.0208	-0.0364
$A_2°\omega°$	10/3	4	-9	-0.0372	-0.0067	-0.0480	-0.0177
$\varepsilon°\rho°$	2/3	26	0	-0.1316	-0.1800	-0.0881	-0.2260
$D°\rho°$	2	0	7	-0.0017	-0.0003	-0.0021	-0.0007
$f°\rho°$	10/3	2	-3	-0.0083	-0.0065	-0.0075	-0.0100
$A_1\pm\pi\mp$	2	6	0	+0.0267	-0.0255	+0.0266	-0.0172
$B\pm\rho\mp$	8	0	3	-0.0015	-0.0004	-0.0017	-0.0009
total				-0.1776	-0.2447	-0.1412	-0.3099

Table XIIc $N_i(S\to ps)$, $Q_i^{(1)}(S\to ps)$, $Q_i^{(2)}(S\to ps)$ and $I^{S\to ps}(E_{CM}, II_z JLS, \alpha\beta)$ in $(I=0, {}^1S_0)$ channel.

Channel	N_i	$Q_i^{(1)}$	$Q_i^{(2)}$	T_{lab}= 100 MeV Re I	Im I	T_{lab}= 300 MeV Re I	Im I
$\delta^\circ\pi^\circ$	2/3	6	0	+0.0088	-0.0015	+0.0074	-0.0007
$\delta^\pm\pi^\mp$	4/3	6	0	+0.0176	-0.0030	+0.0148	-0.0014
$B^\circ\rho^\circ$	6	0	2	-0.0005	-0.0001	-0.0006	-0.0003
$B^\pm\rho^\mp$	12	0	2	-0.0010	-0.0003	-0.0011	-0.0006
$\varepsilon^\circ\eta^\circ$	2/3	18	0	-0.0268	-0.1721	+0.0351	-0.1716
$H^\circ\omega^\circ$	6	0	6	-0.0047	-0.0018	-0.0050	-0.0035
total				-0.0066	-0.1788	+0.0505	-0.1782

Table XIId $N_i(S\to ps)$, $Q_i^{(1)}(S\to ps)$, $Q_i^{(2)}(S\to ps)$ and $I^{S\to ps}(E_{CM}, II_z JLS, \alpha\beta)$ in $(I=1, {}^1S_0)$ channel.

Channel	N_i	$Q_i^{(1)}$	$Q_i^{(2)}$	T_{lab}= 100 MeV Re I	Im I	T_{lab}= 300 MeV Re I	Im I
$A_1^\pm\rho^\mp$	6	6	6	-0.0638	-0.0931	-0.0390	-0.1194
$\delta^\circ\eta^\circ$	2/3	6	0	+0.0211	-0.0122	+0.0178	-0.0061
$H^\circ\rho^\circ$	6	0	2	-0.0005	-0.0003	-0.0005	-0.0005
$\varepsilon^\circ\pi^\circ$	2/3	30	0	+0.1808	-0.2020	+0.1889	-0.1456
$B^\circ\omega^\circ$	6	0	10	-0.0109	-0.0015	-0.0137	-0.0044
total				+0.1268	-0.3090	+0.1534	-0.2760

Table XIIIa $N_i(P\to ss)$, $Q_i^{(1)}(P\to ss)$, $Q_i^{(2)}(P\to ss)$ and $I^{P\to ss}(E_{CM}, II_z JLS, \alpha\beta)$ in $(I=0, {}^3P_2)$ channel.

Channel	N_i	$Q_i^{(1)}$	$Q_i^{(2)}$	T_{lab}= 100 MeV Re I	Im I	T_{lab}= 300 MeV Re I	Im I
$\omega^\circ\omega^\circ$	1	9	9	+0.1133	-0.1009	+0.1088	-0.0568
$\rho^\circ\rho^\circ$	1	3	3	+0.0121	-0.0090	+0.0193	-0.0052
$\rho^\pm\rho^\mp$	2	3	3	+0.0242	-0.0181	+0.0227	-0.0103
total				+0.1496	-0.1280	+0.1428	-0.0723

Table XIIIb $N_i(P\to ss)$, $Q_i^{(1)}(P\to ss)$, $Q_i^{(2)}(P\to ss)$ and $I^{P\to ss}(E_{CM}, II_z JLS, \alpha\beta)$ in $(I=0, {}^3P_1)$ channel.

Table XIIIc $N_i(P\to ss)$, $Q_i^{(1)}(P\to ss)$, $Q_i^{(2)}(P\to ss)$ and $I^{P\to ss}(E_{CM}, II_z JLS, \alpha\beta)$ in $(I=0, {}^3P_0)$ channel.

Table XIIId $N_i(P\to ss)$, $Q_i^{(1)}(P\to ss)$, $Q_i^{(2)}(P\to ss)$ and $I^{P\to ss}(E_{CM}, II_z JLS, \alpha\beta)$ in $(I=1, {}^3P_2)$ channel.

Channel	N_i	$Q_i^{(1)}$	$Q_i^{(2)}$	T_{lab}= 100 MeV Re I	Im I	T_{lab}= 300 MeV Re I	Im I
$\omega^\circ\rho^\circ$	2	9	3	+0.0985	-0.0807	+0.0936	-0.0457
total				+0.0985	-0.0807	+0.0936	-0.0457

Table XIIIe $N_i(P\to ss)$, $Q_i^{(1)}(P\to ss)$, $Q_i^{(2)}(P\to ss)$ and $I^{P\to ss}(E_{CM}, II_z JLS, \alpha\beta)$ in $(I=1, {}^3P_1)$ channel.

Channel	N_i	$Q_i^{(1)}$	$Q_i^{(2)}$	T_{lab}= 100 MeV Re I	Im I	T_{lab}= 300 MeV Re I	Im I
$\omega^\circ\rho^\circ$	2	7	-1	+0.0246	-0.0202	+0.0224	-0.0114
$\rho^\pm\pi^\mp$	2	6	0	+0.0193	-0.0005	+0.0168	-0.0002
total				+0.0440	-0.0206	+0.0401	-0.0116

Table XIIIf $N_i(P\to ss)$, $Q_i^{(1)}(P\to ss)$, $Q_i^{(2)}(P\to ss)$ and $I^{P\to ss}(E_{CM}, II_z JLS, \alpha\beta)$ in $(I=1, {}^3P_0)$ channel.

Table XIIIg $N_i(P\to ss)$, $Q_i^{(1)}(P\to ss)$, $Q_i^{(2)}(P\to ss)$ and $I^{P\to ss}(E_{CM}, II_z JLS, \alpha\beta)$ in ($I=0$, $^1P_1$) channel.

Channel	N_i	$Q_i^{(1)}$	$Q_i^{(2)}$	T_{lab}= 100 MeV Re I	Im I	T_{lab}= 300 MeV Re I	Im I
$\omega^\circ\eta^\circ$	2	6	0	+0.0253	-0.0065	+0.0207	-0.0030
$\rho^\circ\pi^\circ$	2	2	0	+0.0011	-0.0001	+0.0010	-0.
$\rho^\pm\pi^\mp$	4	2	0	+0.0022	-0.0001	+0.0019	-0.
total				+0.0287	-0.0066	+0.0236	-0.0031

Table XIIIh $N_i(P\to ss)$, $Q_i^{(1)}(P\to ss)$, $Q_i^{(2)}(P\to ss)$ and $I^{P\to ss}(E_{CM}, II_z JLS, \alpha\beta)$ in ($I=1$, $^1P_1$) channel.

Channel	N_i	$Q_i^{(1)}$	$Q_i^{(2)}$	T_{lab}= 100 MeV Re I	Im I	T_{lab}= 300 MeV Re I	Im I
$\omega^\circ\pi^\circ$	2	10	0	+0.0280	-0.0014	+0.0242	-0.0007
$\rho^\circ\eta^\circ$	2	2	0	+0.0028	-0.0007	+0.0023	-0.0003
$\rho^+\rho^-$	4	3	3	+0.0484	-0.0362	+0.0453	-0.0206
total				+0.0792	-0.0382	+0.0717	-0.0216

Table XIVa $N_i(P\to ps)$, $Q_i^{(1)}(P\to ps)$, $Q_i^{(2)}(P\to ps)$ and $I^{P\to ps}(E_{CM}, II_z JLS, \alpha\beta)$ in $(I=0, {}^3P_2)$ channel.

Channel	N_i	$Q_i^{(1)}$	$Q_i^{(2)}$	T_{lab}= 100 MeV Re I	Im I	T_{lab}= 300 MeV Re I	Im I
$A_1{}^\circ\pi^\circ$	1	5	-6	+0.0083	-0.0162	+0.0106	-0.0122
$A_1{}^\pm\pi^\mp$	2	5	-6	+0.0166	-0.0324	+0.0212	-0.0245
$A_2{}^\circ\pi^\circ$	3	5	-6	+0.0287	-0.0563	+0.0376	-0.0394
$A_2{}^\pm\pi^\mp$	6	5	-6	+0.0574	-0.1126	+0.0752	-0.0788
$B^\circ\rho^\circ$	4	6	-5	-0.0411	-0.0269	-0.0379	-0.0468
$B^\pm\rho^\mp$	8	6	-5	-0.0823	-0.0538	-0.0759	-0.0936
$D^\circ\eta^\circ$	1	3	0	-0.0015	-0.0018	-0.0001	-0.0023
$f^\circ\eta^\circ$	3	3	0	-0.0025	-0.0044	-0.0003	-0.0053
$H^\circ\omega^\circ$	4	0	3	-0.0025	-0.0020	-0.0019	-0.0031
total				-0.0190	-0.3065	+0.0284	-0.3061

Table XIVb $N_i(P\to ps)$, $Q_i^{(1)}(P\to ps)$, $Q_i^{(2)}(P\to ps)$ and $I^{P\to ps}(E_{CM}, II_z JLS, \alpha\beta)$ in $(I=0, {}^3P_1)$ channel.

Channel	N_i	$Q_i^{(1)}$	$Q_i^{(2)}$	T_{lab}= 100 MeV		T_{lab}= 300 MeV	
				Re I	Im I	Re I	Im I
$\delta^\circ\pi^\circ$	4/3	5	-6	+0.0187	-0.0066	+0.0159	-0.0034
$\delta^\pm\pi^\mp$	8/3	5	-6	+0.0374	-0.0131	+0.0318	-0.0068
$A_1{}^\circ\pi^\circ$	1	5	-6	+0.0083	-0.0162	+0.0106	-0.0122
$A_1{}^\pm\pi^\mp$	2	5	-6	+0.0166	-0.0324	+0.0212	-0.0245
$A_2{}^\circ\pi^\circ$	5/3	5	-6	+0.0159	-0.0313	+0.0209	-0.0220
$A_2{}^\pm\pi^\mp$	10/3	5	-6	+0.0319	-0.0626	+0.0418	-0.0438
$B^\circ\rho^\circ$	4	6	-5	-0.0411	-0.0269	-0.0379	-0.0468
$B^\pm\rho^\mp$	8	6	-5	-0.0823	-0.0538	-0.0759	-0.0936
$\varepsilon^\circ\eta^\circ$	4/3	3	0	-0.0007	-0.0014	-0.0002	-0.0016
$D^\circ\eta^\circ$	1	3	0	-0.0015	-0.0018	-0.0001	-0.0023
$f^\circ\eta^\circ$	5/3	3	0	-0.0014	-0.0025	-0.0002	-0.0029
$H^\circ\omega^\circ$	4	0	3	-0.0025	-0.0020	-0.0019	-0.0031
total				-0.0006	-0.2505	+0.0258	-0.2629

Table XIVc $N_i(P\to ps)$, $Q_i^{(1)}(P\to ps)$, $Q_i^{(2)}(P\to ps)$ and $I^{P\to ps}(E_{CM}, II_z JLS, \alpha\beta)$ in $(I=0, {}^3P_0)$ channel.

Channel	N_i	$Q_i^{(1)}$	$Q_i^{(2)}$	T_{lab}= 100 MeV Re I	Im I	T_{lab}= 300 MeV Re I	Im I
$A_1{}^\circ\pi^\circ$	4	5	-6	+0.0332	-0.0647	+0.0424	-0.0490
$A_1{}^\pm\pi^\mp$	8	5	-6	+0.0663	-0.1295	+0.0849	-0.0979
$B^\circ\rho^\circ$	4	6	-5	-0.0411	-0.0269	-0.0379	-0.0468
$B^\pm\rho^\mp$	8	6	-5	-0.0823	-0.0538	-0.0759	-0.0936
$D^\circ\eta^\circ$	4	3	0	-0.0061	-0.0074	-0.0006	-0.0092
$H^\circ\omega^\circ$	4	0	3	+0.0025	-0.0020	-0.0019	-0.0031
total				-0.0325	-0.2843	+0.0109	-0.2996

Table XIVd $N_i(P\to ps)$, $Q_i^{(1)}(P\to ps)$, $Q_i^{(2)}(P\to ps)$ and $I^{P\to ps}(E_{CM}, II_z JLS, \alpha\beta)$ in $(I=1, {}^3P_2)$ channel.

Channel	N_i	$Q_i^{(1)}$	$Q_i^{(2)}$	T_{lab}= 100 MeV Re I	Im I	T_{lab}= 300 MeV Re I	Im I
$\delta\pm\rho\mp$	4/3	3	0	-0.0002	-0.0024	+0.0007	-0.0021
$A_1\pm\rho\mp$	2	0	3				
	2	3	0	-0.0070	-0.0056	-0.0061	-0.0083
	2	3	-3				
$A_2\pm\rho\mp$	6	0	3				
	14/3	3	0	-0.0213	-0.0089	-0.0231	-0.0171
	6	3	-3				
$A_1{}^\circ\eta^\circ$	1	1	0	-0.0001	-0.0002	-0.	-0.0002
$A_2{}^\circ\eta^\circ$	3	1	0	-0.0005	-0.0004	-0.0002	-0.0007
$H^\circ\rho^\circ$	4	0	1	-0.0002	-0.0003	-0.0002	-0.0004
$D^\circ\pi^\circ$	1	1	-6	+0.0056	-0.0080	+0.0064	-0.0052
$f^\circ\pi^\circ$	3	1	-6	+0.0142	-0.0222	+0.0168	-0.0155
$B^\circ\omega^\circ$	4	6	-1	-0.0188	-0.0057	-0.0224	-0.0154
$B\pm\pi\mp$	4	6	-6	+0.0613	-0.0748	+0.0658	-0.0485
total				+0.0331	-0.1285	+0.0377	-0.1132

Table XIVe $N_i(P\to ps)$, $Q_i^{(1)}(P\to ps)$, $Q_i^{(2)}(P\to ps)$ and $I^{P\to ps}(E_{CM}, II_z JLS, \alpha\beta)$ in $(I=1, {}^3P_1)$ channel.

Channel	N_i	$Q_i^{(1)}$	$Q_i^{(2)}$	T_{lab}= 100 MeV Re I	T_{lab}= 100 MeV Im I	T_{lab}= 300 MeV Re I	T_{lab}= 300 MeV Im I
$\delta\pm\rho\mp$	4/3	3	-6	-0.0011	-0.0176	+0.0057	-0.0153
$A_1\pm\rho\mp$	1	3	3				
	1	0	3				
	2	3	0	-0.0097	-0.0078	-0.0084	-0.0115
	1	3	-3				
	1	6	-3				
$A_2\pm\rho\mp$	3	3	-3				
	1/3	6	-3				
	2	3	0	-0.0108	-0.0045	-0.0117	-0.0086
	1/3	3	3				
	3	0	3				
$\delta°\eta°$	4/3	1	0	+0.0002	-0.0002	+0.0002	-0.0001
$A_1°\eta°$	1	1	0	-0.0001	-0.0002	-0.	-0.0002
$A_2°\eta°$	5/3	1	0	-0.0003	-0.0002	-0.0001	-0.0004
$H°\rho°$	4	0	1	-0.0002	-0.0003	-0.0002	-0.0004
$\varepsilon°\pi°$	4/3	1	-6	+0.0039	-0.0088	+0.0052	-0.0070
$D°\pi°$	1	1	-6	+0.0056	-0.0080	+0.0064	-0.0052
$f°\pi°$	4/3	1	-6	+0.0079	-0.0123	+0.0094	-0.0086
$B°\omega°$	4	6	-1	-0.0188	-0.0057	-0.0224	-0.0154
$B\pm\pi\mp$	4	6	-6	+0.0613	-0.0748	+0.0658	-0.0485
total				+0.0379	-0.1405	+0.0498	-0.1212

Table XIVf $N_i(P\to ps)$, $Q_i^{(1)}(P\to ps)$, $Q_i^{(2)}(P\to ps)$ and $I^{P\to ps}(E_{CM}, II_z JLS, \alpha\beta)$ in $(I=1, {}^3P_0)$ channel.

Channel	N_i	$Q_i^{(1)}$	$Q_i^{(2)}$	T_{lab}= 100 MeV		T_{lab}= 300 MeV	
				Re I	Im I	Re I	Im I
$\delta\pm\rho\mp$	16/3	3	0	-0.0002	-0.0024	+0.0008	-0.0021
$A_1\pm\rho\mp$	4	3	-6	-0.0198	-0.0160	-0.0172	-0.0235
$A_2\pm\rho\mp$	20/3	3	0	-0.0048	-0.0020	-0.0052	-0.0038
$A_1{}^\circ\eta^\circ$	12/3	1	0	-0.0003	-0.0006	-0.0001	-0.0007
$H^\circ\rho^\circ$	12/3	0	1	-0.0002	-0.0003	-0.0002	-0.0004
$D^\circ\pi^\circ$	12/3	1	-6	+0.0225	-0.0321	+0.0254	-0.0208
$B^\circ\omega^\circ$	12/3	6	-1	-0.0188	-0.0057	-0.0224	-0.0154
$B\pm\pi\mp$	12/3	6	-6	+0.0613	-0.0748	+0.0658	-0.0485
total				+0.0397	-0.1339	+0.0469	-0.1152

Table XIVg $N_i(P\to ps)$, $Q_i^{(1)}(P\to ps)$, $Q_i^{(2)}(P\to ps)$ and $I^{P\to ps}(E_{CM}, II_z JLS, \alpha\beta)$ in $(I=0, {}^1P_1)$ channel.

Channel	N_i	$Q_i^{(1)}$	$Q_i^{(2)}$	T_{lab}= 100 MeV Re I	Im I	T_{lab}= 300 MeV Re I	Im I
$\varepsilon°\omega°$	4/3	3	-3	-0.0023	-0.0018	-0.0023	-0.0026
$D°\omega°$	4	3	-3	-0.0096	-0.0012	-0.0132	-0.0038
$f°\omega°$	20/3	3	-3	-0.0155	-0.0064	-0.0180	-0.0128
$\delta°\rho°$	4/3	1	-1	-0.	-0.0009	+0.0003	-0.0008
$\delta\pm\rho\mp$	8/3	1	-1	-0.0001	-0.0018	+0.0006	-0.0016
$A_1°\rho°$	4	1	-1	-0.0010	-0.0008	-0.0009	-0.0012
$A_1\pm\rho\mp$	8	1	-1	-0.0021	-0.0017	-0.0018	-0.0024
$A_2°\rho°$	20/3	1	-1	-0.0018	-0.0008	-0.0020	-0.0015
$A_2\pm\rho\mp$	40/3	1	-1	-0.0036	-0.0015	-0.0040	-0.0029
total				-0.0362	-0.0170	-0.0413	-0.0296

Table XIVh $N_i(P\to ps)$, $Q_i^{(1)}(P\to ps)$, $Q_i^{(2)}(P\to ps)$ and $I^{P\to ps}(E_{CM}, II_z JLS, \alpha\beta)$ in $(I=1, {}^1P_1)$ channel.

Channel	N_i	$Q_i^{(1)}$	$Q_i^{(2)}$	T_{lab}= 100 MeV Re I	T_{lab}= 100 MeV Im I	T_{lab}= 300 MeV Re I	T_{lab}= 300 MeV Im I
$\delta^\circ\omega^\circ$	4/3	5	1	-0.0011	-0.0051	+0.0012	-0.0046
$A_1{}^\circ\omega^\circ$	4	5	1	-0.0053	-0.0028	-0.0054	-0.0049
$A_2{}^\circ\omega^\circ$	20/3	5	1	-0.0080	-0.0014	-0.0104	-0.0037
$\varepsilon^\circ\rho^\circ$	4/3	1	5	-0.0008	-0.0008	-0.0007	-0.0011
$D^\circ\rho^\circ$	4	1	5	-0.0038	-0.0016	-0.0042	-0.0032
$f^\circ\rho^\circ$	20/3	1	5	-0.0054	-0.0039	-0.0051	-0.0062
$\delta^\pm\pi^\mp$	4/3	0	6	+0.0068	-0.0024	+0.0058	-0.0012
$A_1{}^\pm\pi^\mp$	4	0	6	+0.0119	-0.0235	+0.0153	-0.0178
$A_2{}^\pm\pi^\mp$	20/3	0	6	+0.0229	-0.0454	+0.0302	-0.0318
$B^\pm\rho^\mp$	12	6	0	-0.0421	-0.0273	-0.0390	-0.0476
total				-0.0250	-0.1142	-0.0124	-0.1221

Table XVa $N_i(D\to ps)$, $Q_i^{(1)}(D\to ps)$, $Q_i^{(2)}(D\to ps)$ and $I^{D\to ps}(E_{CM}, II_z JLS, \alpha\beta)$ in $(I=0, {}^3D_3)$ channel.

Channel	N_i	$Q_i^{(1)}$	$Q_i^{(2)}$	T_{lab}= 100 MeV Re I	Im I	T_{lab}= 300 MeV Re I	Im I
$f^\circ\omega^\circ$	6/5	9	9	-0.0481	-0.0270	-0.0514	-0.0521
$A_2{}^\circ\rho^\circ$	6/5	3	3	-0.0054	-0.0034	-0.0053	-0.0058
$A_2{}^\pm\rho^\mp$	12/5	3	3	-0.0108	-0.0068	-0.0106	-0.0115
total				-0.0642	-0.0371	-0.0674	-0.0694

Table XVb $N_i(D\to ps)$, $Q_i^{(1)}(D\to ps)$, $Q_i^{(2)}(D\to ps)$ and $I^{D\to ps}(E_{CM}, II_z JLS, \alpha\beta)$ in $(I=0, {}^3D_2)$ channel.

Channel	N_i	$Q_i^{(1)}$	$Q_i^{(2)}$	T_{lab}= 100 MeV Re I	Im I	T_{lab}= 300 MeV Re I	Im I
$D^\circ\omega^\circ$	1/10	9	-36	-0.0199	-0.0042	-0.0281	-0.0113
$f^\circ\omega^\circ$	3/10	27	-18	-0.	-0.0001	-0.0002	-0.0001
$A_1{}^\circ\rho^\circ$	1/10	15	-6	-0.0001	-0.0002	-0.0001	-0.0002
$A_1{}^\pm\rho^\mp$	1/5	15	-6	-0.0003	-0.0004	-0.0002	-0.0005
$A_2{}^\circ\rho^\circ$	3/10	9	-12	-0.0015	-0.0015	-0.0025	-0.0026
$A_2{}^\pm\rho^\mp$	3/5	9	-12	-0.0029	-0.0030	-0.0050	-0.0051
total				-0.0279	-0.0093	-0.0360	-0.0199

Table XVc $N_i(D\to ps)$, $Q_i^{(1)}(D\to ps)$, $Q_i^{(2)}(D\to ps)$ and $I^{D\to ps}(E_{CM}, II_z JLS, \alpha\beta)$ in $(I=0, {}^3D_1)$ channel.

Channel	N_i	$Q_i^{(1)}$	$Q_i^{(2)}$	T_{lab}= 100 MeV Re I	Im I	T_{lab}= 300 MeV Re I	Im I
$\varepsilon^\circ\omega^\circ$	1/150	60	-90	-0.0026	-0.0024	-0.0022	-0.0033
$D^\circ\omega^\circ$	1/50	45	-30	-0.	-0.	-0.	-0.
$f^\circ\omega^\circ$	1/30	39	-36	-0.0010	-0.0005	-0.0011	-0.0010
$\delta^\circ\rho^\circ$	1/150	40	18	+0.0016	-0.0052	+0.0029	-0.0037
$\delta^\pm\rho^\mp$	1/75	40	18	+0.0031	-0.0106	+0.0058	-0.0073
$A_1{}^\circ\rho^\circ$	1/50	15	-20	-0.0004	-0.0004	-0.0003	-0.0006
$A_1{}^\pm\rho^\mp$	1/25	15	-20	-0.0008	-0.0008	-0.0006	-0.0012
$A_2{}^\circ\rho^\circ$	1/30	17	-18	-0.0004	-0.0002	-0.0004	-0.0004
$A_2{}^\pm\rho^\mp$	1/15	17	-18	-0.0008	-0.0004	-0.0008	-0.0008
total				-0.0012	-0.0207	+0.0034	-0.0182

Table XVd $N_i(D\to ps)$, $Q_i^{(1)}(D\to ps)$, $Q_i^{(2)}(D\to ps)$ and $I^{D\to ps}(E_{CM}, II_z JLS, \alpha\beta)$ in $(I=1, {}^3D_3)$ channel.

Channel	N_i	$Q_i^{(1)}$	$Q_i^{(2)}$	T_{lab}= 100 MeV Re I	Im I	T_{lab}= 300 MeV Re I	Im I
$f^\circ\rho^\circ$	6/5	9	3	-0.0148	-0.0148	-0.0115	-0.0217
$A_2{}^\circ\omega^\circ$	6/5	3	9	-0.0266	-0.0071	-0.0335	-0.0175
total				-0.0414	-0.0219	-0.0450	-0.0392

Table XVe $N_i(D\to ps)$, $Q_i^{(1)}(D\to ps)$, $Q_i^{(2)}(D\to ps)$ and $I^{D\to ps}(E_{CM}, II_z JLS, \alpha\beta)$ in $(I=1, {}^3D_2)$ channel.

Channel	N_i	$Q_i^{(1)}$	$Q_i^{(2)}$	T_{lab}= 100 MeV Re I	Im I	T_{lab}= 300 MeV Re I	Im I
$D^\circ\rho^\circ$	1/10	3	6	-0.0013	-0.0008	-0.0014	-0.0015
$f^\circ\rho^\circ$	3/10	15	0	-0.0043	-0.0043	-0.0033	-0.0063
$A_1{}^\circ\omega^\circ$	1/10	3	24	-0.0121	-0.0091	-0.0109	-0.0144
$A_2{}^\circ\omega^\circ$	3/10	3	-6	-0.0010	-0.0003	-0.0012	-0.0006
$A_2{}^\pm\pi^\mp$	2/5	9	0	+0.0040	-0.0032	+0.0038	-0.0019
$B^\pm\rho^\mp$	2/5	0	9	-0.0073	-0.0069	-0.0050	-0.0107
total				-0.0219	-0.0245	-0.0181	-0.0355

Table XVf $N_i(D\to ps)$, $Q_i^{(1)}(D\to ps)$, $Q_i^{(2)}(D\to ps)$ and $I^{D\to ps}(E_{CM}, II_z JLS, \alpha\beta)$ in $(I=1, {}^3D_1)$ channel.

Channel	N_i	$Q_i^{(1)}$	$Q_i^{(2)}$	T_{lab}= 100 MeV Re I	Im I	T_{lab}= 300 MeV Re I	Im I
$\varepsilon°\rho°$	1/150	20	-30	-0.0003	-0.0003	-0.0002	-0.0004
$D°\rho°$	1/50	15	-40	-0.0042	-0.0025	-0.0043	-0.0046
$f°\rho°$	1/30	59	-42	-0.0002	-0.0002	-0.0002	-0.0003
$\delta°\omega°$	1/150	40	-90	+0.0027	-0.0150	+0.0069	-0.0104
$A_1°\omega°$	1/50	45	-50	-0.0019	-0.0014	-0.0017	-0.0022
$A_2°\omega°$	1/30	37	-24	-0.	-0.	-0.	-0.
$A_1^{\pm}\pi^{\mp}$	1/50	30	0	+0.0019	-0.0018	+0.0019	-0.0012
$B^{\pm}\pi^{\mp}$	2/25	0	15	+0.0023	-0.0015	+0.0021	-0.0009
total				+0.0003	-0.0227	+0.0045	-0.0199

Table XVg $N_i(D\to ps)$, $Q_i^{(1)}(D\to ps)$, $Q_i^{(2)}(D\to ps)$ and $I^{D\to ps}(E_{CM}, II_z JLS, \alpha\beta)$ in $(I=0, {}^1D_2)$ channel.

Channel	N_i	$Q_i^{(1)}$	$Q_i^{(2)}$	T_{lab}= 100 MeV Re I	Im I	T_{lab}= 300 MeV Re I	Im I
$f°\eta°$	6/5	6	0	-0.0009	-0.0080	+0.0022	-0.0068
$H°\omega°$	6/5	0	6	-0.0087	-0.0103	-0.0050	-0.0141
$A_2°\pi°$	6/5	2	0	+0.0006	-0.0005	+0.0006	-0.0003
$A_2\pm\pi\mp$	12/5	2	0	+0.0012	-0.0009	+0.0011	-0.0006
$B°\rho°$	6/5	0	2	-0.0011	-0.0010	-0.0007	-0.0016
$B\pm\rho\mp$	12/5	0	2	-0.0021	-0.0020	-0.0015	-0.0032
total				-0.0110	-0.0227	-0.0033	-0.0265

Table XVh $N_i(D\to ps)$, $Q_i^{(1)}(D\to ps)$, $Q_i^{(2)}(D\to ps)$ and $I^{D\to ps}(E_{CM}, II_z JLS, \alpha\beta)$ in $(I=1, {}^1D_2)$ channel.

Channel	N_i	$Q_i^{(1)}$	$Q_i^{(2)}$	T_{lab}= 100 MeV Re I	Im I	T_{lab}= 300 MeV Re I	Im I
$A_1\pm\rho\mp$	6/5	3	3	-0.0044	-0.0051	-0.0032	-0.0069
$A_2\pm\rho\mp$	18/5	3	3	-0.0161	-0.0102	-0.0160	-0.0173
$f°\pi°$	6/5	10	0	+0.0140	-0.0100	+0.0130	-0.0059
$B°\omega°$	6/5	0	10	-0.0320	-0.0151	-0.0321	-0.0361
$A_2°\eta°$	6/5	2	0	-0.0005	-0.0010	0.	-0.0010
$H°\rho°$	6/5	0	2	-0.0007	-0.0013	+0.0002	-0.0016
total				-0.0397	-0.0426	-0.0384	-0.0688

Table XVI Annihilation branching ratios at rest (T_{lab} = 0 MeV). b(I,S) are taken as b(0,1):b(1,1):b(0,0):b(1,0) = 0.80:0.86:1.00:0.68. The numbers below are given in units of %.

channel	experiment[33]	theory
$\pi^\circ\pi^\circ\pi^\circ$	1.03 ± 0.34	1.6
$m\pi^\circ (m\geq 4)$	2.2 ± 0.5	2.1
$\pi^+\pi^-\pi^\circ$	7.8 ± 0.6 (6.9 ± 0.35)	5.1
$\pi^+\pi^-2\pi^\circ$	9.3 ± 3.0	9.7
$\pi^+\pi^-3\pi^\circ$	23.3 ± 3.0	19.1
$\pi^+\pi^-m\pi^\circ (m\geq 4)$	2.8 ± 0.7	5.2
$2\pi^+2\pi^-$	5.8 ± 0.3 (6.9 ± 0.6)	6.8
$2\pi^+2\pi^-\pi^\circ$	18.1 ± 0.9 (19.6± 0.7)	21.5
$\omega^\circ\pi^+\pi^-$	3.4 ± 0.4	3.4
$\rho^\circ\pi^+\pi^-\pi^\circ$	7.3 ± 1.7	7.2
$\rho^\pm\pi^\mp\pi^+\pi^-$	6.4 ± 1.8	6.2
$\eta^\circ\pi^+\pi^-$	0.28 ± 0.07 (0.35± 0.04)	0.36
$2\pi^+2\pi^-2\pi^\circ$	16.6 ± 1.0	15.9
$2\pi^+2\pi^-m\pi^\circ (m\geq 3)$	4.2 ± 1.0	6.1
$3\pi^+3\pi^-$	1.9 ± 0.2	0.8
$3\pi^+3\pi^-\pi^\circ$	1.3 ± 0.3	0.8
$3\pi^+3\pi^-m\pi^\circ (m\geq 2)$	0.3 ± 0.1	0.3

Table XVIIa Two s-wave meson annihilation at rest (T_{lab}= 0 MEV) and in flight (T_{lab}= 100 MeV). Branching ratios are shown in units of % for the cases of the $^3s_1$ and $^3p_0$ $\bar{q}q$ annihilation. Δ indicates the deviations from the data.

channel	experiment	T_{lab}= 0 MeV				T_{lab}= 100 MeV
		S → ss		P → ss		$\bar{P}P$ → ss($^3s_1$)
		theory($^3s_1$)	Δ	theory($^3p_0$)	Δ	
$\pi^\circ\ \pi^\circ$	0.048± 0.01	0.	0.04	0.004	0.04	0.
$\pi+\ \pi-$	0.33 ± 0.04	0.03	0.30	0.009	0.33	0.01
$\eta^\circ\ \pi^\circ$	0.02 ± 0.005	0.	0.02	0.001	0.02	0.
$\omega^\circ\ \pi^\circ$	0.9 ± 0.45	0.5	0.4	0.06	0.8	0.1
$\rho^\circ\ \pi^\circ$	1.4 ± 0.2	0.8	0.6	0.002	1.4	0.1
$\rho^\pm\ \pi^\mp$	2.9 ± 0.4	1.9	1.0	0.09	2.8	0.3
$\eta^\circ\ \eta^\circ$		0.		0.01		0.
$\eta^\circ\ \omega^\circ$		0.3		0.07		0.8
$\eta^\circ\ \rho^\circ$	0.22 ± 0.17	0.03	0.2	0.007	0.21	0.02
$\omega^\circ\ \omega^\circ$	1.4 ± 0.6	1.4	0.0	1.4	0.0	2.5
$\omega^\circ\ \rho^\circ$	0.7 ± 0.3	0.8	-0.1	1.2	-0.5	4.0
$\rho^\circ\ \rho^\circ$	0.4 ± 0.3	0.1	0.3	0.6	-0.2	0.2
$\rho+\ \rho-$		3.3		1.5		1.8

Table XVIIb One p- and one s-wave meson annihilation at rest (T_{lab}= 0 MeV) and in flight (T_{lab}= 100 MeV). The numbers below are in units of %.

Channel	Predictions		
	T_{lab}= 0 MeV	T_{lab}= 100 MeV	
	$S \to ps(^3s_1)$	$\bar{N}N \to ps(^3s_1)$	
		Case A	Case B
$B^\circ\pi^\circ$	0.	0.	0.
$B^\pm\pi^\mp$	0.	6.2	6.3
$H^\circ\pi^\circ$	0.	0.	0.
$\delta^\circ\pi^\circ$	0.03	0.1	0.1
$\delta^\pm\pi^\mp$	0.06	0.3	0.3
$A_1{}^\circ\pi^\circ$	0.	1.1	1.1
$A_1{}^\pm\pi^\mp$	0.7	2.9	3.0
$A_2{}^\circ\pi^\circ$	0.	1.9	1.9
$A_2{}^\pm\pi^\mp$	0.	4.8	5.1
$\varepsilon^\circ\pi^\circ$	2.3	0.6	0.6
$D^\circ\pi^\circ$	0.	1.0	1.0
$f^\circ\pi^\circ$	0.	1.5	1.9
$B^\circ\eta^\circ$	0.	0.	0.
$H^\circ\eta^\circ$	0.	0.	0.
$\delta^\circ\eta^\circ$	0.2	0.03	0.03
$A_1{}^\circ\eta^\circ$	0.	0.02	0.02
$A_2{}^\circ\eta^\circ$	0.	0.05	0.08
$\varepsilon^\circ\eta^\circ$	2.3	0.5	0.5
$D^\circ\eta^\circ$	0.	0.1	0.1
$f^\circ\eta^\circ$	0.	0.5	1.1
$B^\circ\rho^\circ$	0.	1.3	1.4
$B^\pm\rho^\mp$	0.01	3.5	4.1
$H^\circ\rho^\circ$	0.	0.06	0.1
$\delta^\circ\rho^\circ$	0.3	0.3	0.6
$\delta^\pm\rho^\mp$	0.6	1.3	1.8
$A_1{}^\circ\rho^\circ$	1.0	0.3	0.4
$A_1{}^\pm\rho^\mp$	2.7	1.6	1.9

(continued)

$A_2 \circ \rho \circ$	0.4	0.5	1.0
$A_2 \pm \rho \mp$	0.8	1.8	3.2
$\varepsilon \circ \rho \circ$	3.4	1.6	1.6
$D \circ \rho \circ$	0.	0.2	0.4
$f \circ \rho \circ$	0.1	1.4	3.3
$B \circ \omega \circ$	0.01	0.9	1.4
$H \circ \omega \circ$	0.02	0.6	1.3
$\delta \circ \omega \circ$	0.06	0.6	1.2
$A_1 \circ \omega \circ$	0.4	0.7	1.4
$A_2 \circ \omega \circ$	0.1	0.6	1.4
$\varepsilon \circ \omega \circ$	5.4	1.4	1.5
$D \circ \omega \circ$	0.01	0.6	1.4
$f \circ \omega \circ$	0.8	2.1	3.8
Total	21.4 %	38.6 %	62.2 %

Table XVIII Annihilation branching ratios are predicted at T_{lab}= 100 MeV and compared with data[50,51,56,57]. The numbers are in the units of %.

#	channel	L = 0			L = 1			L = 2			Total		Data
		sss	ss	ps	ssp	ss	ps	sss	A ps	B ps	A	B	
1	$m\pi^\circ$	0.3	0.0	0.3	0.5	0.1	0.9	0.3	0.2	0.6	2.6	2.7	
2	$\pi+\pi-$	-	0.01	-	-	-	-	-	-	-	0.01	0.01	0.3∿ 0.5
3	$\pi+\pi-\pi^\circ$	0.1	0.5	0.4	0.0	0.0	1.3	0.0	0.3	0.6	2.5	2.9	4.9∿ 6.5
3a	$\rho^\circ\pi^\circ$	-	0.1	-	-	0.0	-	-	-	-	0.1	0.1	0.7∿ 1.1
3b	$\rho\pm\pi\mp$	-	0.3	-	-	0.0	-	-	-	-	0.3	0.3	1.0∿ 1.6
3c	$f^\circ\pi^\circ$	-	-	0.0	-	-	0.7	-	0.2	0.4	0.9	1.1	0.2∿ 0.5
4	$\pi+\pi-m\pi^\circ$	5.0	0.8	2.2	5.8	2.4	9.6	4.6	2.7	6.8	33.1	32.6	33.7∿35.3
5	$2\pi+2\pi-$	0.4	0.0	1.2	0.7	0.3	3.2	0.4	0.9	2.2	6.9	7.9	4.7∿ 6.4
5a	$\rho^\circ\pi+\pi-$	0.4	-	0.5	-	-	-	0.4	-	-	1.2	0.9	0.2∿ 0.5
5b	$\rho^\circ\rho^\circ$	-	0.0	-	-	0.2	-	-	-	-	0.2	0.2	0.6∿ 1.0
5c	$f^\circ\pi+\pi-$	-	-	-	0.7	-	-	-	-	-	0.7	0.7	1.1∿ 1.7
5d	$f^\circ\rho^\circ$	-	-	0.5	-	-	0.0	-	0.8	1.9	1.3	2.5	1.1∿ 1.7
5e	$A_2\pm\pi\mp$	-	-	0.0	-	-	1.7	-	0.1	0.2	1.8	1.9	0.3∿ 0.8
6	$2\pi+2\pi-\pi^\circ$	3.2	0.1	2.0	4.5	3.6	7.8	3.3	1.6	4.1	26.0	25.3	19.2∿22.5
6a	$\omega^\circ\pi+\pi-$	0.4	-	0.6	-	-	-	0.4	-	-	1.3	0.9	1.2∿ 1.7
6b	$\rho^\circ\rho\pm\pi\mp$	1.6	-	0.5	-	-	0.3	1.7	0.1	0.2	4.1	2.5	2.8∿ 3.7
6c	$\rho\pm\pi\mp\pi+\pi-$	0.8	-	0.2	-	-	0.1	0.8	0.0	0.1	2.1	1.3	1.6∿ 2.9
6d	$\omega^\circ\rho^\circ$	-	0.1	-	-	3.5	-	-	-	-	3.6	3.6	2.5∿ 3.0
6e	$f^\circ\omega^\circ$	-	-	0.4	-	-	0.4	-	0.7	1.6	1.5	2.5	1.1∿ 1.4
6f	$A_2^\circ\pi+\pi-$	-	-	0.2	1.2	-	0.3	-	0.4	0.3	2.0	2.5	1.8∿ 2.3
7	$2\pi+2\pi-m\pi^\circ$	5.2	0.2	0.4	3.6	2.0	5.9	4.6	2.8	6.9	24.6	24.2	20.6∿25.6
8	$3\pi+3\pi-$	0.3	0.0	0.0	0.2	0.0	0.0	0.2	0.1	0.1	0.8	0.6	1.3∿ 1.6
9	$3\pi+3\pi-\pi^\circ$	0.2	0.0	0.0	0.8	0.0	0.1	0.1	0.1	0.4	1.5	1.5	1.7∿ 2.0
10	$3\pi+3\pi-m\pi^\circ$	0.1	0.0	0.0	0.3	0.0	0.0	0.1	0.1	0.2	0.6	0.6	1.0∿ 1.6
	total	14.8	1.6	6.5	16.4	8.4	28.8	13.6	8.8	21.9	98.5	98.5	

Table XIX Annihilation branching ratios are predicted at T_{lab}= 300 MeV and compared with data[50,51,56,57]. The numbers are in the units of %.

#	channel	L = 0			L = 1			L = 2 A		L = 2 B	Total A	Total B
		sss	ss	ps	ssp	ss	ps	sss	ps	ps		
1	$m\pi^\circ$	0.1	0.0	0.1	0.3	0.0	0.5	0.3	0.3	0.7	1.6	1.8
2	$\pi^+\pi^-$	-	0.0	-	-	-	-	-	-	-	0.0	0.0
3	$\pi^+\pi^-\pi^\circ$	0.0	0.1	0.2	0.0	0.0	0.7	0.0	0.2	0.5	1.2	1.5
3a	$\rho^\circ\pi^\circ$	-	0.03	-	-	0.0	-	-	-	-	0.0	0.0
3b	$\rho^\pm\pi^\mp$	-	0.07	-	-	0.0	-	-	-	-	0.1	0.1
3c	$f^\circ\pi^\circ$	-	-	0.0	-	-	0.4	-	0.1	0.2	0.5	0.6
4	$\pi^+\pi^-m\pi^\circ$	2.8	0.2	1.4	4.2	0.8	5.6	7.7	4.5	11.3	27.1	26.2
5	$2\pi^+2\pi^-$	0.1	0.0	0.7	0.4	0.1	1.5	0.3	1.3	3.2	4.4	6.0
5a	$\rho^\circ\pi^+\pi^-$	0.1	-	0.3	-	-	-	0.3	-	-	0.7	0.4
5b	$\rho^\circ\rho^\circ$	-	0.0	-	-	0.1	-	-	-	-	0.1	0.1
5c	$f^\circ\pi^+\pi^-$	-	-	-	0.4	-	-	-	-	-	0.4	0.4
5d	$f^\circ\rho^\circ$	-	-	0.3	-	-	0.0	-	1.2	2.9	1.5	3.2
5e	$A_2^\pm\pi^\mp$	-	-	0.0	-	-	0.8	-	0.1	0.1	0.8	0.9
6	$2\pi^+2\pi^-\pi^\circ$	1.5	0.0	1.4	2.7	1.5	4.2	5.0	2.9	7.1	19.1	18.4
6a	$\omega^\circ\pi^+\pi^-$	0.4	-	0.4	-	-	-	0.4	-	-	0.8	0.5
6b	$\rho^\circ\rho^\pm\pi^\mp$	1.6	-	0.3	-	-	0.3	2.6	0.1	0.3	4.0	1.6
6c	$\rho^\pm\pi^+\pi^+\pi^-$	0.8	-	0.1	-	-	0.1	1.3	0.1	0.1	2.0	0.8
6d	$\omega^\circ\rho^\circ$	-	0.0	-	-	1.5	-	-	-	-	1.5	1.5
6e	$f^\circ\omega^\circ$	-	-	0.3	-	-	0.3	-	1.2	3.1	1.9	3.7
6f	$A_2^\circ\pi^+\pi^-$	-	-	0.2	0.9	-	0.3	-	0.6	1.5	2.0	2.6
7	$2\pi^+2\pi^-m\pi^\circ$	3.3	0.1	0.3	3.8	0.8	6.3	8.8	5.9	14.8	29.2	29.3
8	$3\pi^+3\pi^-$	0.2	0.0	0.0	0.2	0.0	0.0	0.6	0.1	0.3	1.1	0.7
9	$3\pi^+3\pi^-\pi^\circ$	0.2	0.0	0.0	1.2	0.0	0.1	0.7	0.3	0.8	2.4	2.2
10	$3\pi^+3\pi^-m\pi^\circ$	0.1	0.0	0.0	0.5	0.0	0.0	0.3	0.2	0.5	1.1	1.1
	total	8.3	0.4	4.0	13.1	3.2	18.9	23.6	15.7	39.3	87.4	87.4

Table XXa The numerical list of $\sum_{F_K} I^{L\to F_K}(E_{CM}, II_z JLS, F_K)$ and ranges X_o in the case of r_P= 0.62 fm and D_π/D_s= 2.3. The number of terms for separable potentials in each $^{2I+1}\,^{2S+1}L_J$ state is that of rows in it. The practical values are multiplied by λ^2 = 328.8 except those with asterisk * which is multiplied by λ_D^2 = 40.96. The resulting values for potentials are in units of nucleon mass.

T_{lab}(MeV)=		0		100		200		300		X_o
State		Re	Im	Re	Im	Re	Im	Re	Im	(fm)
$^{11}S_0$	sss	-0.94	-0.86	-0.93	-1.04	-0.97	-1.21	-1.08	-1.39	0.58
	ss	0.02	-0.10	0.03	-0.09	0.05	-0.08	0.05	-0.07	0.44
	ps	-0.04	-0.15	-0.01	-0.17	0.00	-0.17	0.03	-0.17	0.41
$^{31}S_0$	sss	-1.24	-1.41	-0.96	-1.53	-0.64	-1.60	-0.32	-1.63	0.58
	ss	0.14	-0.11	0.14	-0.10	0.14	-0.08	0.14	-0.07	0.44
	ps	0.10	-0.39	0.13	-0.37	0.15	-0.35	0.17	-0.32	0.41
$^{13}P_0$	ssp	-0.35	-0.12	-0.35	-0.14	-0.35	-0.16	-0.35	-0.18	0.46
	ps	-0.08	-0.26	-0.06	-0.27	-0.04	-0.28	-0.01	-0.29	0.35
$^{33}P_0$	ssp	-0.26	-0.12	-0.27	-0.12	-0.29	-0.12	-0.31	-0.13	0.46
	ps	0.00	-0.15	0.01	-0.14	0.03	-0.13	0.03	-0.12	0.35

(continued)

$^{11}P_1$	ssp	-0.33	-0.06	-0.35	-0.07	-0.38	-0.08	-0.40	-0.10	0.46
	ss	0.03	-0.01	0.02	-0.01	0.02	-0.01	0.02	-0.01	0.44
	ps	-0.03	-0.01	-0.03	-0.01	-0.03	-0.02	-0.04	-0.02	0.35
$^{31}P_1$	ssp	-0.42	-0.29	-0.42	-0.32	-0.41	-0.35	-0.41	-0.37	0.46
	ss	0.07	-0.05	0.07	-0.04	0.07	-0.03	0.06	-0.02	0.44
	ps	-0.04	-0.10	-0.03	-0.11	-0.02	-0.11	-0.02	-0.11	0.35
$^{13}P_1$	ssp	-0.39	-0.17	-0.41	-0.20	-0.42	-0.23	-0.42	-0.26	0.46
	ps	-0.04	-0.24	-0.02	-0.25	-0.01	-0.25	0.01	-0.26	0.35
$^{33}P_1$	ssp	-0.34	-0.11	-0.35	-0.13	-0.36	-0.15	-0.37	-0.17	0.46
	ss	0.04	-0.03	0.04	-0.02	0.04	-0.02	0.04	-0.01	0.44
	ps	-0.00	-0.15	0.01	-0.14	0.03	-0.14	0.03	-0.13	0.35
$^{13}S_1$	sss	-0.59	-0.93	-0.50	-0.95	-0.39	-0.96	-0.28	-0.98	0.58
	ss	0.33	-0.14	0.32	-0.11	0.30	-0.08	0.28	-0.06	0.44
	ps	-0.45	-0.29	-0.46	-0.36	-0.45	-0.44	-0.43	-0.53	0.41
$^{33}S_1$	sss	-0.68	-0.81	-0.71	-0.91	-0.67	-1.02	-0.60	-1.12	0.58
	ss	0.13	-0.09	0.13	-0.08	0.13	-0.07	0.13	-0.06	0.44
	ps	-0.17	-0.22	-0.17	-0.24	-0.16	-0.27	-0.14	-0.30	0.41
$^{11}D_2$	ps	-0.01	-0.02	-0.01	-0.02	-0.01	-0.02	-0.01	-0.03	0.41
	*sss	-0.94	-0.86	-0.93	-1.04	-0.97	-1.21	-1.08	-1.39	0.58
$^{31}D_2$	ps	-0.04	-0.04	-0.04	-0.04	-0.04	-0.05	-0.04	-0.07	0.41
	*sss	-1.24	-1.41	-0.96	-1.53	-0.64	-1.60	-0.32	-1.63	0.58

(continued)

$^{13}D_2$	ps	-0.02	-0.01	-0.02	-0.01	-0.03	-0.01	-0.03	-0.02	0.41
	*sss	-0.59	-0.93	-0.50	-0.95	-0.39	-0.96	-0.28	-0.98	0.58
$^{33}D_2$	ps	-0.02	-0.02	-0.02	-0.03	-0.02	-0.03	-0.02	-0.03	0.41
	*sss	-0.68	-0.81	-0.71	-0.91	-0.67	-1.02	-0.60	-1.12	0.58
$^{13}P_2$	ssp	-0.31	-0.12	-0.30	-0.13	-0.30	-0.14	-0.30	-0.15	0.46
	ss	0.09	-0.14	0.10	-0.12	0.11	-0.10	0.11	-0.08	0.44
	ps	-0.09	-0.28	-0.06	-0.29	-0.03	-0.29	-0.00	-0.30	0.35
$^{33}P_2$	ssp	-0.33	-0.10	-0.34	-0.12	-0.34	-0.14	-0.35	-0.16	0.46
	ss	0.06	-0.09	0.07	-0.07	0.07	-0.06	0.07	-0.05	0.44
	ps	-0.00	-0.14	0.01	-0.13	0.02	-0.13	0.03	-0.12	0.35
$^{13}D_3$	ps	-0.06	-0.03	-0.07	-0.04	-0.07	-0.05	-0.07	-0.07	0.41
	*sss	-0.59	-0.93	-0.50	-0.95	-0.39	-0.96	-0.28	-0.98	0.58
$^{33}D_3$	ps	-0.04	-0.02	-0.04	-0.02	-0.04	-0.03	-0.04	-0.04	0.41
	*sss	-0.68	-0.81	-0.71	-0.91	-0.67	-1.02	-0.60	-1.12	0.58

Table XXb The numerical list of $\sum_{F_K} I^{L\to F_K}(E_{CM}, II_z JLS, F_K)$ and ranges X_o in the case of r_P= 0.7 fm and D_π/D_s= 3.0. The resulting values for potentials are in units of nucleon mass.

T_{lab}(MeV)=		0		100		200		30		X_o
State		Re	Im	Re	Im	Re	Im	Re	Im	(fm)
$^{11}S_0$	sss	-0.77	-0.75	-0.75	-0.88	-0.78	-1.01	-0.88	-1.14	0.75
	ss	+0.05	-0.13	+0.07	-0.11	+0.08	-0.09	+0.08	-0.07	0.50
	ps	-0.04	-0.17	-0.01	-0.18	+0.01	-0.18	+0.05	-0.18	0.44
$^{31}S_0$	sss	-0.81	-1.03	-0.51	-1.11	-0.22	-1.14	+0.04	-1.13	0.64
	ss	+0.18	-0.11	+0.18	-0.09	+0.17	-0.07	+0.16	-0.05	0.50
	ps	+0.11	-0.33	+0.13	-0.31	+0.14	-0.29	+0.15	-0.28	0.35
$^{13}P_0$	ssp	-0.18	-0.06	-0.18	-0.07	-0.18	-0.08	-0.18	-0.10	0.46
	ps	-0.05	-0.28	-0.03	-0.28	-0.01	-0.29	+0.01	-0.30	0.35
$^{33}P_0$	ssp	-0.14	-0.05	-0.15	-0.05	-0.17	-0.05	-0.19	-0.06	0.46
	ps	+0.03	-0.15	+0.04	-0.13	+0.04	-0.12	+0.05	-0.12	0.35

(continued)

$^{11}P_1$	ssp	-0.19	-0.03	-0.20	-0.03	-0.22	-0.05	-0.24	-0.06	0.46
	ss	+0.03	-0.01	+0.03	-0.01	+0.03	-0.00	+0.02	-0.00	0.50
	ps	-0.03	-0.01	-0.04	-0.02	-0.04	-0.02	-0.04	-0.03	0.44
$^{31}P_1$	ssp	-0.20	-0.15	-0.20	-0.16	-0.20	-0.17	-0.20	-0.18	0.46
	ss	+0.08	-0.05	+0.08	-0.04	+0.08	-0.03	+0.07	-0.02	0.50
	ps	-0.03	-0.11	-0.03	-0.11	-0.02	-0.12	-0.01	-0.12	0.35
$^{13}P_1$	ssp	-0.20	-0.09	-0.22	-0.11	-0.22	-0.12	-0.22	-0.13	0.46
	ps	-0.01	-0.25	-0.00	-0.25	+0.01	-0.25	+0.03	-0.26	0.35
$^{33}P_1$	ssp	-0.18	-0.06	-0.18	-0.06	-0.19	-0.08	-0.20	-0.09	0.46
	ss	+0.04	-0.03	+0.04	-0.02	+0.04	-0.02	+0.04	-0.01	0.50
	ps	+0.03	-0.15	+0.04	-0.14	+0.05	-0.13	+0.05	-0.12	0.35
$^{13}S_1$	sss	-0.44	-0.58	-0.36	-0.60	-0.27	-0.62	-0.18	-0.64	0.64
	ss	+0.36	-0.08	+0.33	-0.06	+0.31	-0.04	+0.28	-0.03	0.42
	ps	-0.46	-0.32	-0.48	-0.41	-0.45	-0.50	-0.42	-0.59	0.44
$^{33}S_1$	sss	-0.60	-0.55	-0.62	-0.65	-0.56	-0.74	-0.49	-0.83	0.64
	ss	+0.15	-0.10	+0.15	-0.08	+0.15	-0.06	+0.14	-0.05	0.50
	ps	-0.18	-0.22	-0.18	-0.24	-0.16	-0.28	-0.14	-0.31	0.44
$^{11}D_2$	ps	-0.01	-0.02	-0.01	-0.02	-0.01	-0.03	-0.00	-0.03	0.44
$^{31}D_2$	ps	-0.04	-0.03	-0.04	-0.04	-0.04	-0.05	-0.04	-0.07	0.44

(continued)

$^{13}D_2$	ps	-0.02	-0.01	-0.02	-0.01	-0.03	-0.01	-0.03	-0.02	0.44
$^{33}D_2$	ps	-0.02	-0.02	-0.02	-0.02	-0.02	-0.03	-0.02	-0.04	0.44
$^{13}P_2$	ssp	-0.16	-0.06	-0.16	-0.07	-0.16	-0.07	-0.16	-0.07	0.46
	ss	+0.14	-0.16	+0.15	-0.13	+0.15	-0.10	+0.14	-0.07	0.50
	ps	-0.05	-0.31	-0.02	-0.31	+0.00	-0.30	+0.03	-0.31	0.35
$^{33}P_2$	ssp	-0.18	-0.06	-0.18	-0.06	-0.18	-0.07	-0.18	-0.08	0.46
	ss	+0.10	-0.10	+0.10	-0.08	+0.10	-0.06	+0.09	-0.05	0.50
	ps	+0.03	-0.14	+0.03	-0.13	+0.04	-0.12	+0.04	-0.11	0.35
$^{13}D_3$	ps	-0.06	-0.03	-0.06	-0.04	-0.07	-0.05	-0.07	-0.07	0.44
$^{33}D_3$	ps	-0.04	-0.02	-0.04	-0.02	-0.04	-0.03	-0.04	-0.04	0.44

Table XXI The effect of the repulsive components in eq. (5-7) on the magnitudes, R, of the S matrix of the partial waves at T_{lab}= 120 MeV. $\sigma = (2J+1)(1-R^2)$. $\Delta\sigma$ indicates the differences between the σ's with and without the repulsive components.

	$V_c(0)=14.6, V_c(1)=11.0$		$V_c(0)=V_c(1)=0$		
	R	σ	R	σ	$\Delta\sigma$
$^{11}S_0$	0.61	0.63	0.26	0.93	-0.30
$^{11}P_1$	0.51	2.20	0.95	0.31	1.89
$^{11}D_2$	0.82	1.65	0.93	0.67	0.98
$^{13}P_1$	0.82	0.97	0.88	0.68	0.29
$^{13}D_2$	0.97	0.27	0.96	0.43	-0.16
$^{13}S_1$	0.27	2.78	0.93	0.42	2.36
$^{13}P_2$	0.22	4.76	0.75	2.20	2.56
$^{13}P_0$	0.39	0.84	0.93	0.13	0.71
$^{13}D_1$	0.91	0.53	0.94	0.33	0.30
$^{31}S_0$	0.52	0.72	0.46	0.79	-0.07
$^{31}P_1$	0.56	2.07	0.23	2.83	-0.76
$^{31}D_2$	0.87	1.23	0.95	0.53	0.70
$^{33}P_1$	0.31	2.72	0.45	2.39	0.33
$^{33}D_2$	0.76	2.15	0.96	0.41	1.74
$^{33}S_1$	0.48	2.31	0.74	1.38	0.92
$^{33}P_2$	0.37	4.30	0.56	3.41	0.89
$^{33}P_0$	0.81	0.35	0.85	0.28	0.07
$^{33}D_1$	0.99	0.06	0.99	0.06	0.00
Total		30.5		18.2	

Table XXIIa Comparison between approximated $b(I,{}^{2S+1}L_J,E_{CM})$ used in calculating branching ratios and the one estimated by the result given in Table XXI at T_{lab}= 100 MeV. The numbers are fractions of the total annihilation cross section, which are in units of %.

State	Calculation	Approximation	Ratio
$^{13}S_1$	9.08	8.58	1.06
$^{33}S_1$	7.52	8.58	0.88
$^{11}S_0$	2.02	2.86	0.71
$^{31}S_0$	2.36	2.86	0.82
$^{13}P_2$	15.72	11.17	1.41
$^{13}P_1$	2.50	6.70	0.37
$^{13}P_0$	2.81	2.23	1.26
$^{33}P_2$	13.32	11.17	1.19
$^{33}P_1$	8.66	6.70	1.29
$^{33}P_0$	0.91	2.23	0.41
$^{11}P_1$	7.22	6.70	1.08
$^{31}P_1$	6.26	6.70	0.93
$^{13}D_3$	1.83	3.85	0.48
$^{13}D_2$	0.56	2.75	0.20
$^{13}D_1$	1.44	1.65	0.87
$^{33}D_3$	3.96	3.85	1.03
$^{33}D_2$	5.29	2.75	1.92
$^{33}D_1$	0.17	1.65	0.10
$^{11}D_2$	3.92	2.75	1.43
$^{31}D_2$	2.95	2.75	1.07

Table XXIIb Comparison between approximated $b(I, {}^{2S+1}L_J, E_{CM})$ used in calculating branching ratios and the one estimated by the result given in Table XXI at T_{lab}= 300 MeV. The numbers are fractions of the total annihilation cross section, which are in units of %.

State	Calculation	Approximation	Ratio
$^{13}S_1$	4.78	4.77	1.00
$^{33}S_1$	3.91	4.77	0.82
$^{11}S_0$	1.12	1.59	0.70
$^{31}S_0$	1.22	1.59	0.77
$^{13}P_2$	7.15	7.35	0.97
$^{13}P_1$	3.69	4.41	0.84
$^{13}P_0$	1.41	1.47	0.96
$^{33}P_2$	8.21	7.35	1.12
$^{33}P_1$	4.93	4.41	1.12
$^{33}P_0$	1.38	1.47	0.94
$^{11}P_1$	3.97	4.41	0.90
$^{31}P_1$	4.30	4.41	0.98
$^{13}D_3$	4.38	6.88	0.64
$^{13}D_2$	2.86	4.91	0.58
$^{13}D_1$	2.30	2.95	0.78
$^{33}D_3$	9.12	6.88	1.33
$^{33}D_2$	7.42	4.91	1.51
$^{33}D_1$	0.28	2.95	0.09
$^{11}D_2$	7.03	4.91	1.43
$^{31}D_2$	5.57	4.91	1.13

Figure Captions

Fig. 1 The quark rearrangement and annihilation diagrams. (a) The quark rearrangement process into three mesons, (b) the one $\bar{q}q$-pair annihilation process into two mesons and (c) the two $\bar{q}q$-pair annihilation process into two mesons.

Fig. 2 Mass distribution functions of (a) ρ meson and (b) ω meson.

Fig. 3 The one $\bar{q}q$-pair annihilation process.

Fig. 4 The $\bar{N}\Delta$, $N\bar{\Delta}$ and $\bar{\Delta}\Delta$ annihilation into mesons due to π or ρ meson exchange.

Fig. 5 Partial cross sections predicted by case A and compared with data[51,56,57]: (a) $\sigma(\pi^+\pi^-)$, (b) $\sigma(\pi^+\pi^-\pi^\circ)$, (c) $\sigma(\pi^+\pi^- m\pi^\circ)$ $(m \geq 2)$, (d) $\sigma(2\pi^+2\pi^-)$, (e) $\sigma(2\pi^+2\pi^-\pi^\circ)$, (f) $\sigma(2\pi^+2\pi^- m\pi^\circ)$ $(m \geq 2)$, (g) $\sigma(3\pi^+3\pi^-)$, (h) $\sigma(3\pi^+3\pi^-\pi^\circ)$ and (i) $\sigma(3\pi^+3\pi^- m\pi^\circ)$ $(m \geq 2)$. The abscissas indicate incident laboratory momenta.

Fig. 6 (a) Fractions of $\rho^\circ\pi^\circ$, $\rho^\pm\pi^\mp$ and $f^\circ\pi^\circ$ in the final state $\pi^+\pi^-\pi^\circ$, (b) those of $\rho^\circ\pi^+\pi^-$, $f^\circ\pi^+\pi^-$, $\rho^\circ\rho^\circ$, $\rho^\circ f^\circ$ and $A_2^\pm\pi^\mp$ in the final state $2\pi^+2\pi^-$ and (c) those of $\rho^\pm\pi^\mp\pi^+\pi^-$, $\rho^\circ\rho^\pm\pi^\mp$, $\omega^\circ\rho^\circ$, $\omega^\circ f^\circ$, $A_2^\circ\pi^+\pi^-$ and $\omega^\circ\pi^+\pi^-$ in the final state $2\pi^+2\pi^-\pi^\circ$ as function of incident momentum[29,36,51,57~59]. The solid and the broken curves indicate case A and case B respectively.

Fig. 7 Energy dependence of $\sum_{\alpha\beta\gamma} I^{S\to sss}(E_{CM}, II_z J\ L=0\ S, \alpha\beta\gamma)$ due to the three s-wave meson annihilation from the S-wave $\bar{N}N$ states.

Fig. 8 Energy dependence of $\sum_{\alpha\beta\gamma} I^{P\to ssp}(E_{CM}, II_z J\ L=1\ S, \alpha\beta\gamma)$ due to the two s-wave and one p-wave meson annihilation from the P-wave $\bar{N}N$ states.

Fig. 9 Energy dependence of $\sum_{\alpha\beta} I^{S\to ss}(E_{CM}, II_z J\ L=0\ S, \alpha\beta)$ due to the two s-wave meson annihilation from the S-wave $\bar{N}N$ states.

Fig. 10 Energy dependence of $\sum_{\alpha\beta} I^{S\to ps}(E_{CM}, II_z J\ L=0\ S, \alpha\beta)$ due to the one s-wave and one p-wave meson annihilation from the S-wave $\bar{N}N$ states.

Fig. 11 Energy dependence of $\sum_{\alpha\beta} I^{P\to ss}(E_{CM}, II_z J\ L=1\ S, \alpha\beta)$ due to the two s-wave meson annihilation from the P-wave $\bar{N}N$ states.

Fig. 12 Energy dependence of $\sum_{\alpha\beta} I^{P\to ps}(E_{CM}, II_z J\ L=1\ S, \alpha\beta)$ due to the one s-wave and one p-wave meson annihilation from the P-wave $\bar{N}N$ states.

Fig. 13 Energy dependence of $\sum_{\alpha\beta} I^{D\to ps}(E_{CM}, II_z J\ L=2\ S, \alpha\beta)$ due to the one s-wave and one p-wave meson annihilation from the D-wave $\bar{N}N$ states.

Fig. 14 The two meson annihilation process into $\pi\pi$, $\rho\pi$ and $\rho\rho$ via the exchange of N or Δ.

Fig. 15 The one-boson-exchange (OBE) contribution to the $\bar{N}N$ interaction.

Fig. 16 The $\bar{N}N$ optical potential generated by the intermediate meson state.

Fig. 17 The central components of $\bar{N}N$ OBEP[65] with (modified) and without (original) the phenomenological repulsion. The solid and the broken curves indicate the I=1 and I=0 components respectively.

Fig. 18 The $\bar{N}N$ optical potentials generated by the quark rearrangement and the quark annihilation processes.

Fig. 19 Fractions of main intermediate meson states of the optical potentials in the processes: (a) $^{33}S_1 \to sss$, (b) $^{33}P_2 \to ssp$, (c) $^{33}S_1 \to ss$ and (d) $^{33}S_1 \to ps$.

Fig. 20 Dependences of the predicted annihilation cross section on (a) λ^2 (the strength of the annihilation interaction), (b) $V_c(I)$ (the strength of the repulsive central components) and (c) λ_D^2 (the strength of the optical potential due to the process $D \to sss$ simulated by the one $S \to sss$). $V_c(I)= \lambda_D^2=0$ in (a). In (b), λ^2 is fixed as the value giving the maximum in (a) and $\lambda_D^2=0$. In (c), λ^2 and $V_c(I)$ are fixed as the values giving the maximum in (b).

Fig. 21 The total[66~69], the elastic[70] and the charge-exchange[63] cross sections at T_{lab}= 0 ~ 300 MeV. The one-boson-exchange part is employed from model II of Ueda, Riewe and Green[65].

Fig. 22 The differential cross section of the $\bar{P}P$ elastic scattering at T_{lab}= 120 MeV. The data are from ref. 63.

Fig. 23 The differential cross section of the $\bar{P}P$ charge-exchange scattering at T_{lab}= 120 MeV. The data are from ref. 70.

Fig. 24 The $\bar{P}P$ backward angle differential cross section[71]. We note that the prediction of this observable is sensitive to the parameters included in section 5.

Fig. 25 The equivalent local potential defined by eq. (5-8) in the text and the wave function in the $^{13}P_2$ state.

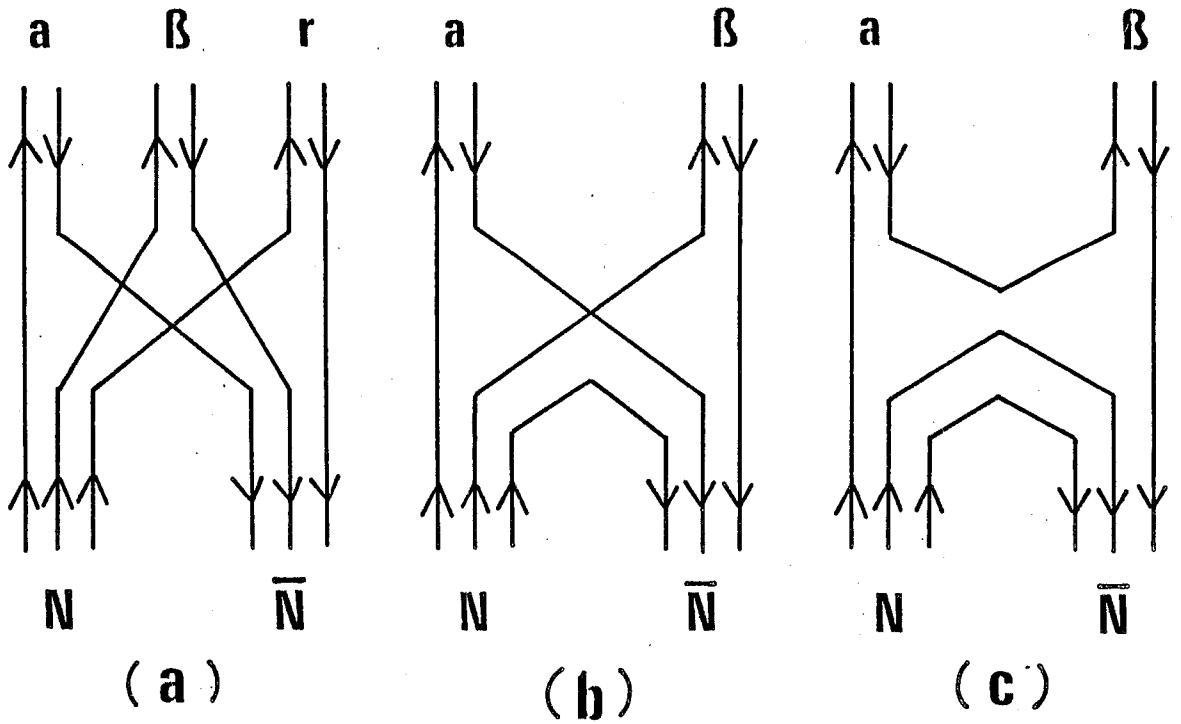

fig. 1

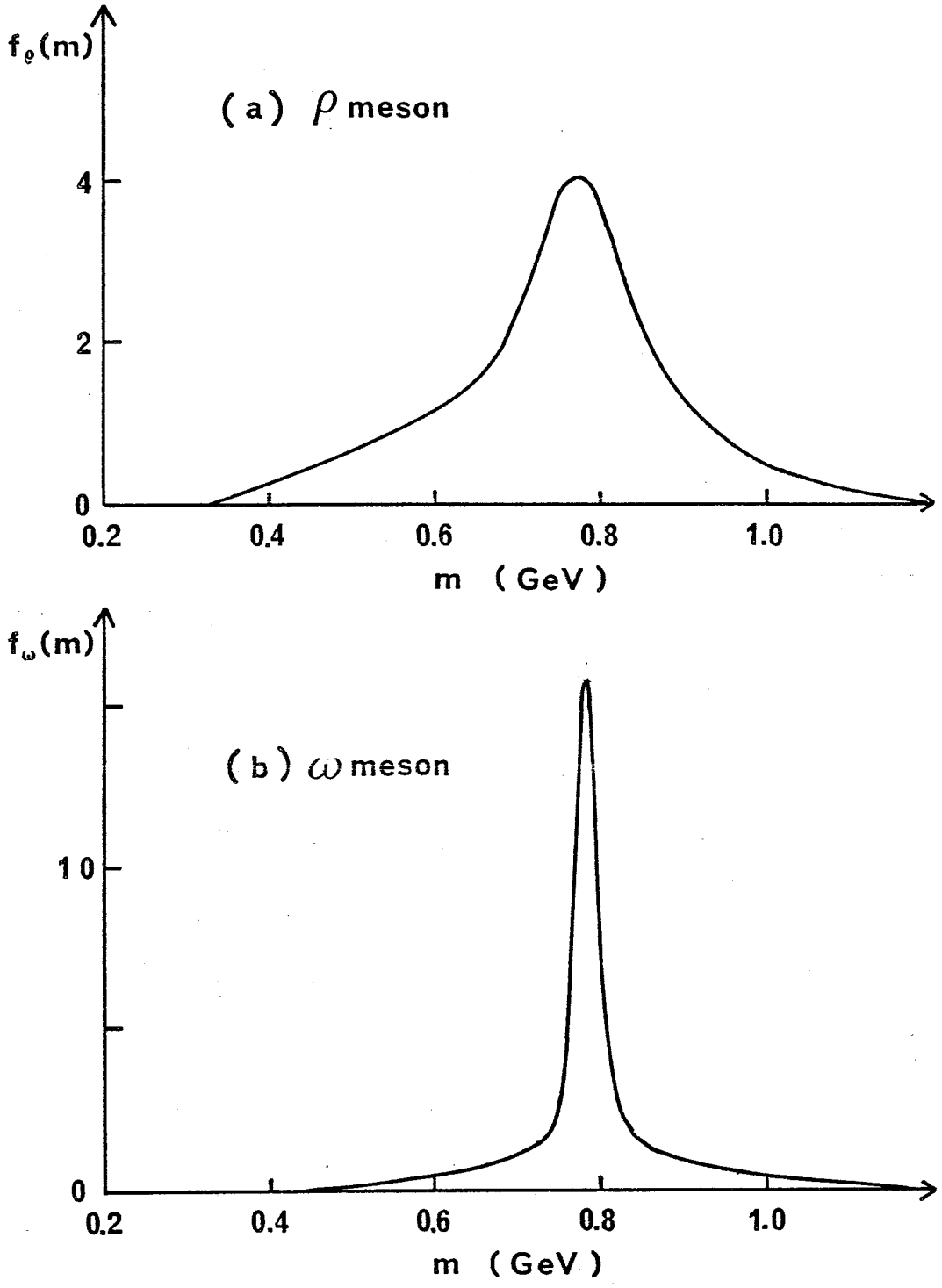
$f_\rho(m)$
(a) ρ meson
4
2
0
0.2
0.4
0.6
0.8
1.0
m (GeV)
$f_\omega(m)$
(b) ω meson
10
0
0.2
0.4
0.6
0.8
1.0
m (GeV)

fig. 2

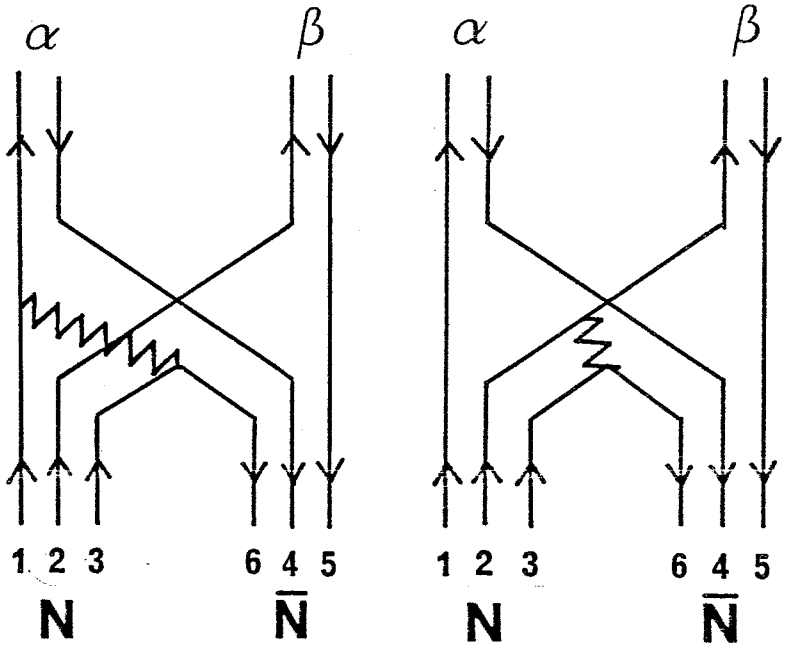

fig. 3

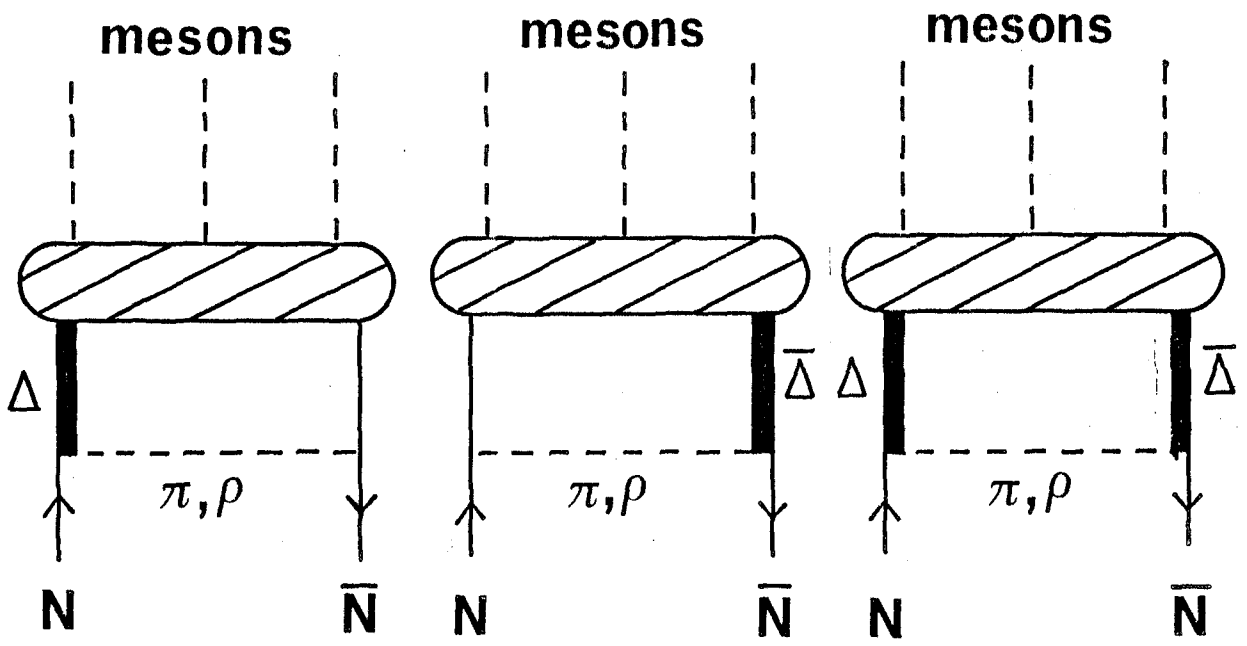
mesons
mesons
mesons
Δ
$\bar{\Delta}$
Δ
$\bar{\Delta}$
Δ
$\bar{\Delta}$
π,ρ
π,ρ
π,ρ
N
$\bar{N}$
N
$\bar{N}$
N
$\bar{N}$

fig. 4

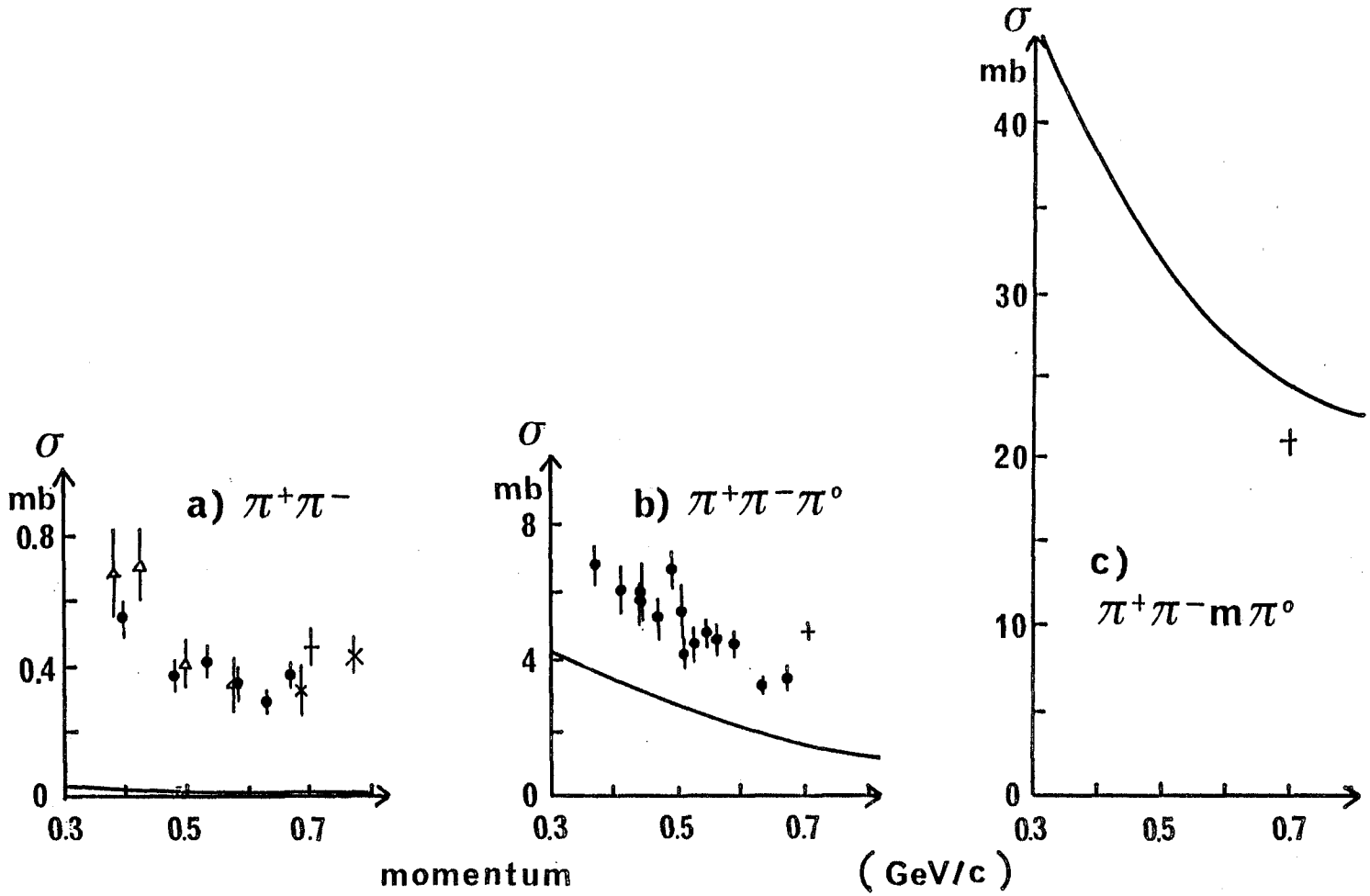
σ
mb
0.8
0.4
0
0.3
0.5
0.7
a) π⁺π⁻
σ
mb
8
4
0
0.3
0.5
0.7
b) π⁺π⁻π°
σ
mb
40
30
20
10
0
0.3
0.5
0.7
c)
π⁺π⁻mπ°
momentum
(GeV/c)

fig. 5

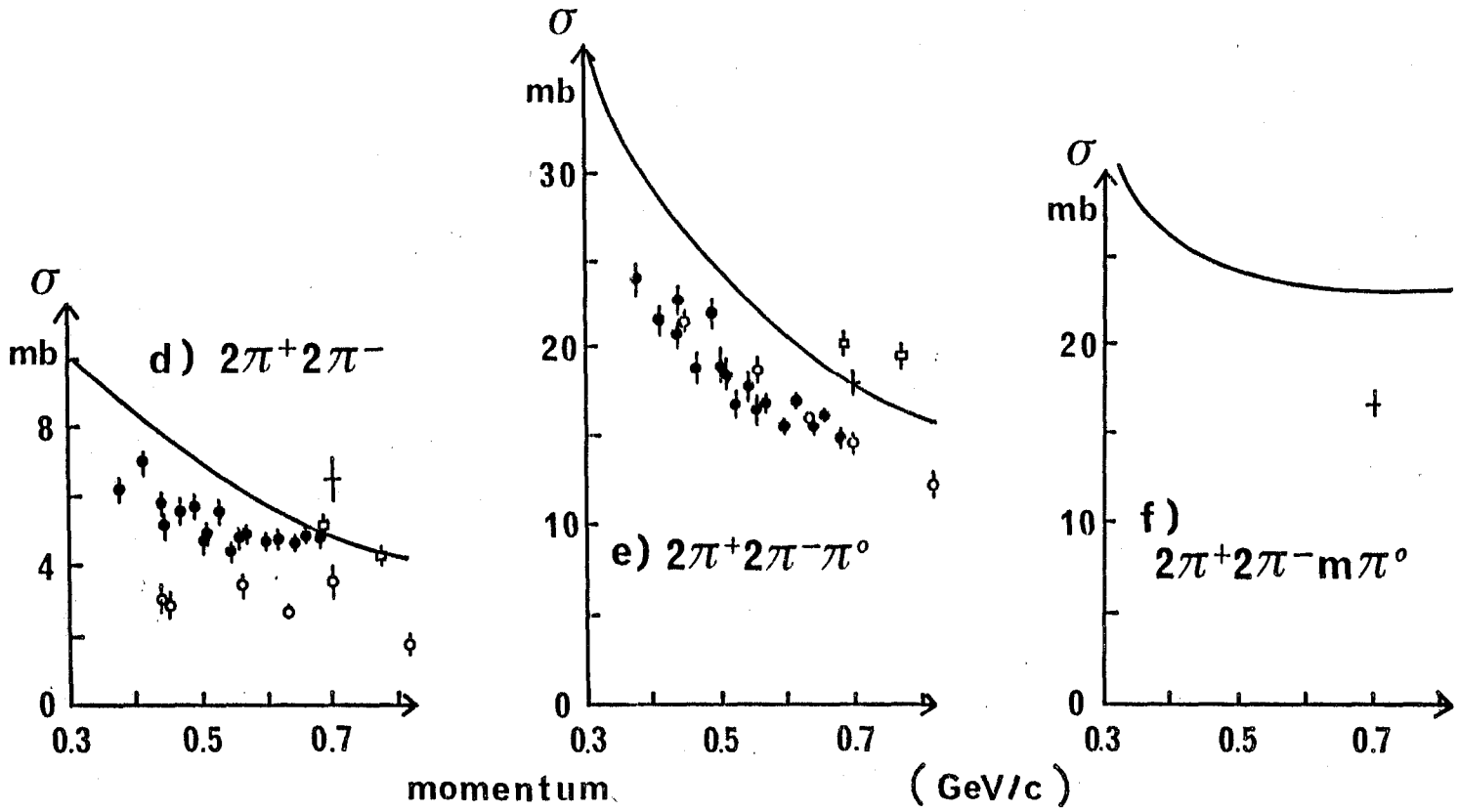
σ
mb
d) 2π+2π−
8
4
0
0.3
0.5
0.7
σ
mb
30
20
10
e) 2π+2π−π°
0
0.3
0.5
0.7
σ
mb
20
10
f)
2π+2π−mπ°
0
0.3
0.5
0.7
momentum
(GeV/c)

fig. 5

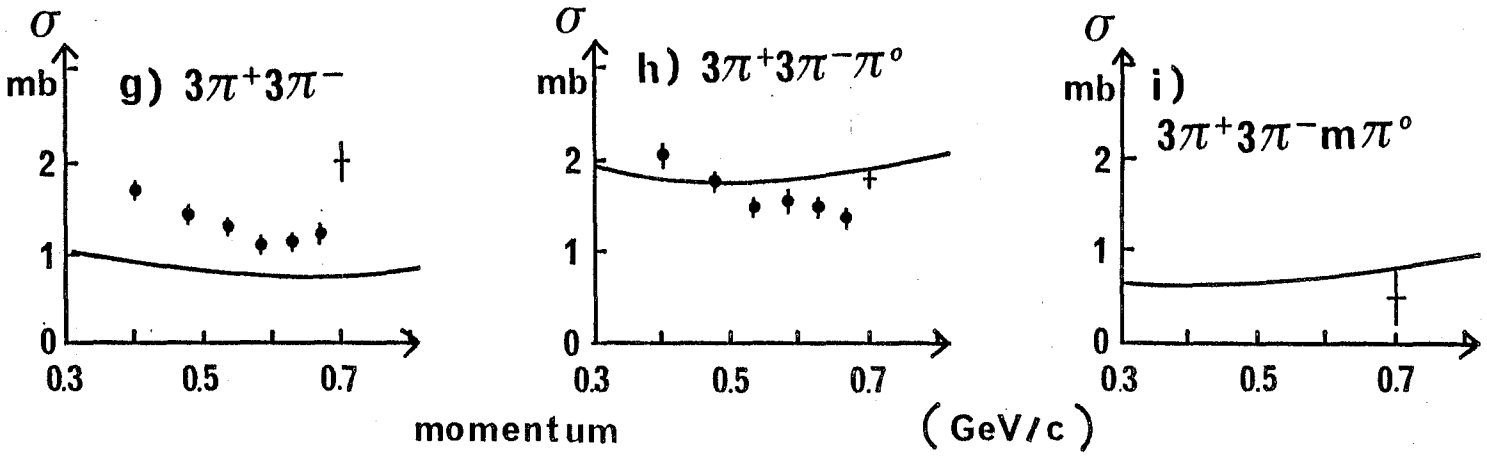
σ
mb
g) 3π+3π−
2
1
0
0.3
0.5
0.7
σ
mb
h) 3π+3π−π°
2
1
0
0.3
0.5
0.7
σ
mb
i)
3π+3π−mπ°
2
1
0
0.3
0.5
0.7
momentum
(GeV/c)

fig. 5

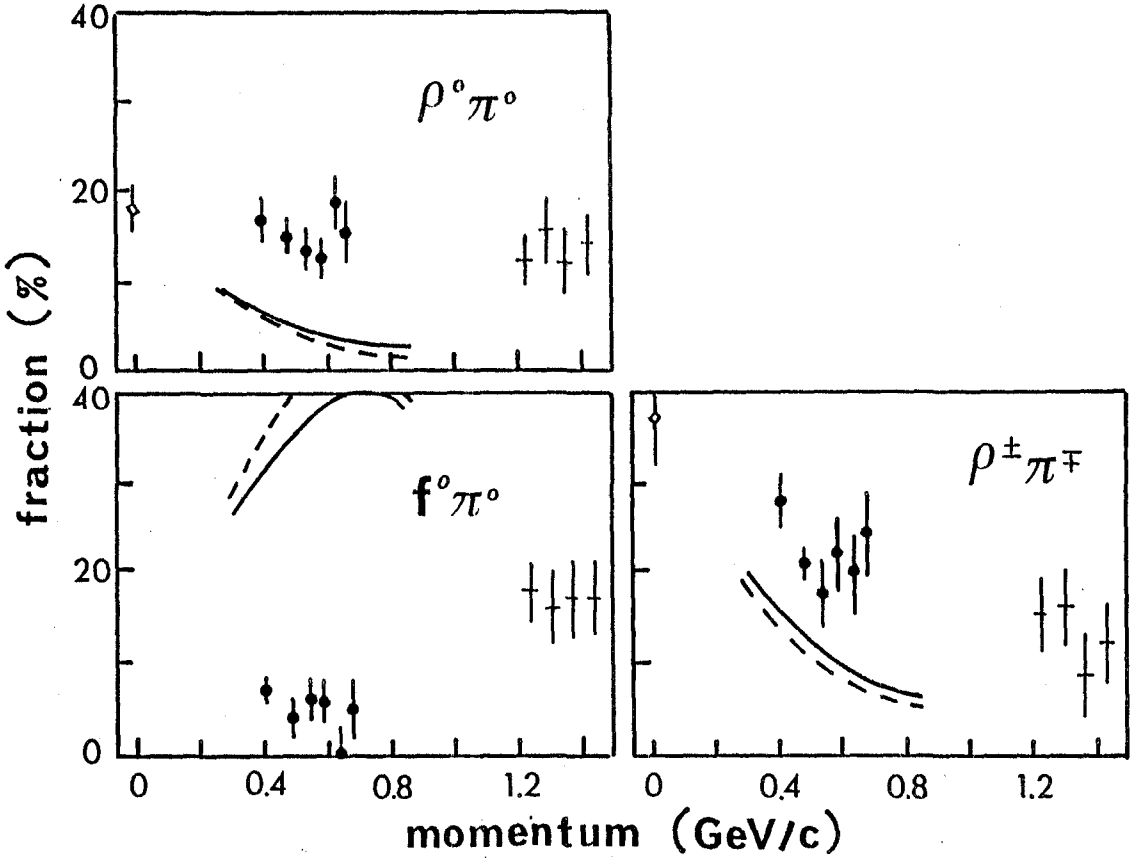
40
20
0
$\rho^0\pi^0$
40
20
0
$f^0\pi^0$
$\rho^\pm\pi^\mp$
fraction (%)
0
0.4
0.8
1.2
momentum (GeV/c)

fig. 6a

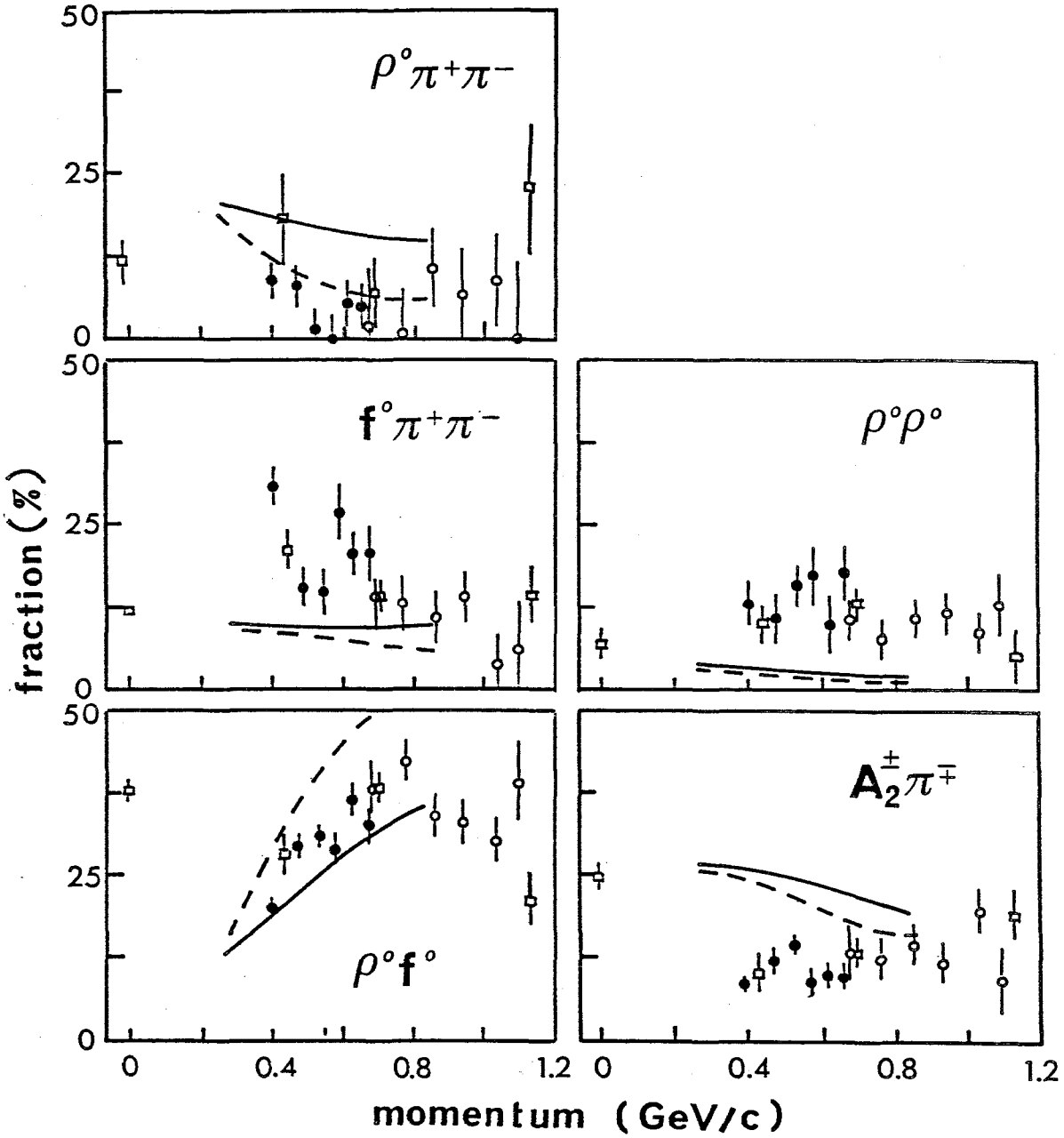
50
25
0
$\rho^0\pi^+\pi^-$
$f^0\pi^+\pi^-$
$\rho^0\rho^0$
$\rho^0 f^0$
$A_2^{\pm}\pi^{\mp}$
fraction (%)
0
0.4
0.8
1.2
momentum (GeV/c)

fig. 6b

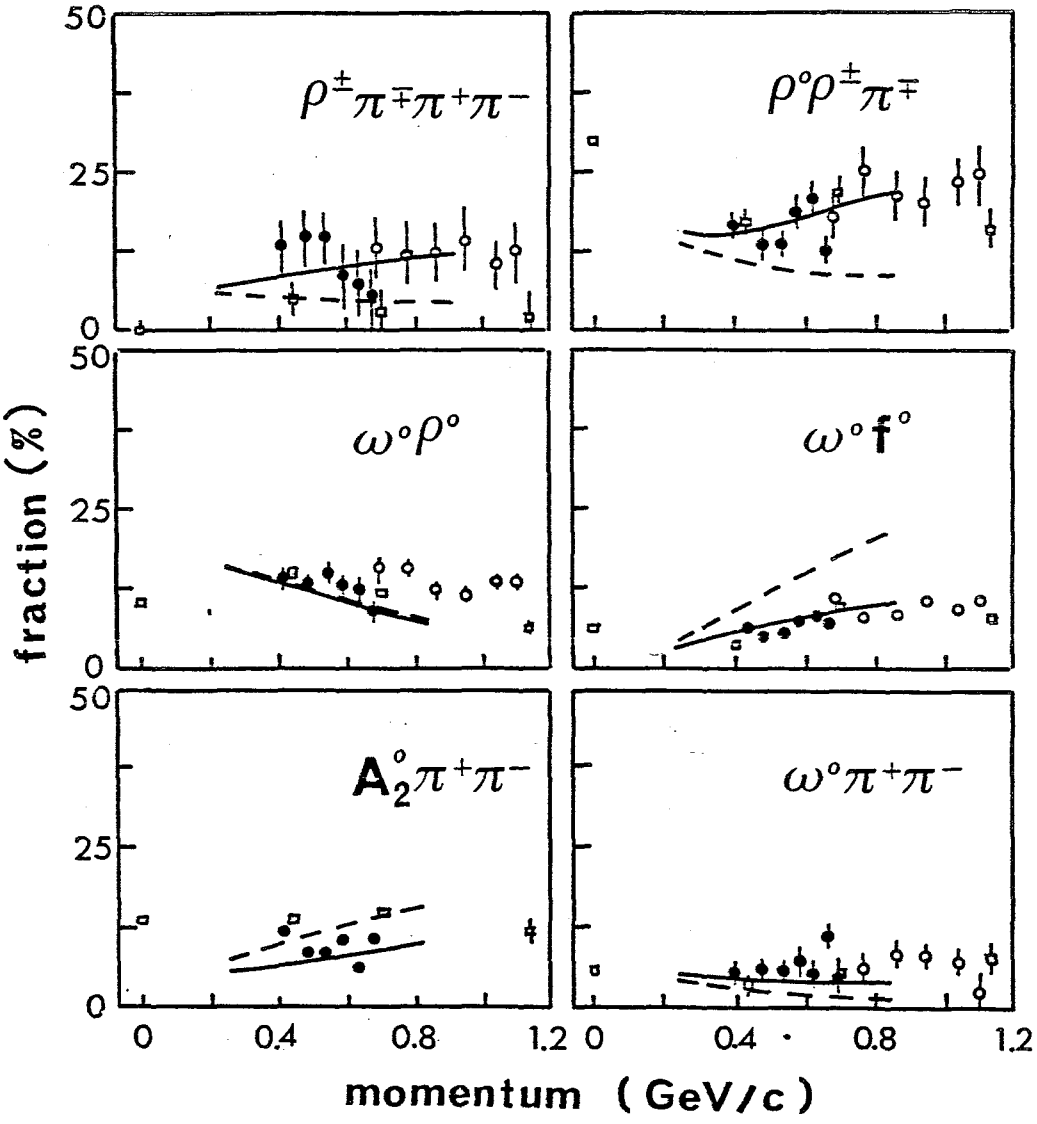
50
25
0
$\rho^{\pm}\pi^{\mp}\pi^{+}\pi^{-}$
$\rho^{o}\rho^{\pm}\pi^{\mp}$
$\omega^{o}\rho^{o}$
$\omega^{o}f^{o}$
$A_2^{o}\pi^{+}\pi^{-}$
$\omega^{o}\pi^{+}\pi^{-}$
fraction (%)
0
0.4
0.8
1.2
momentum (GeV/c)

fig. 6c

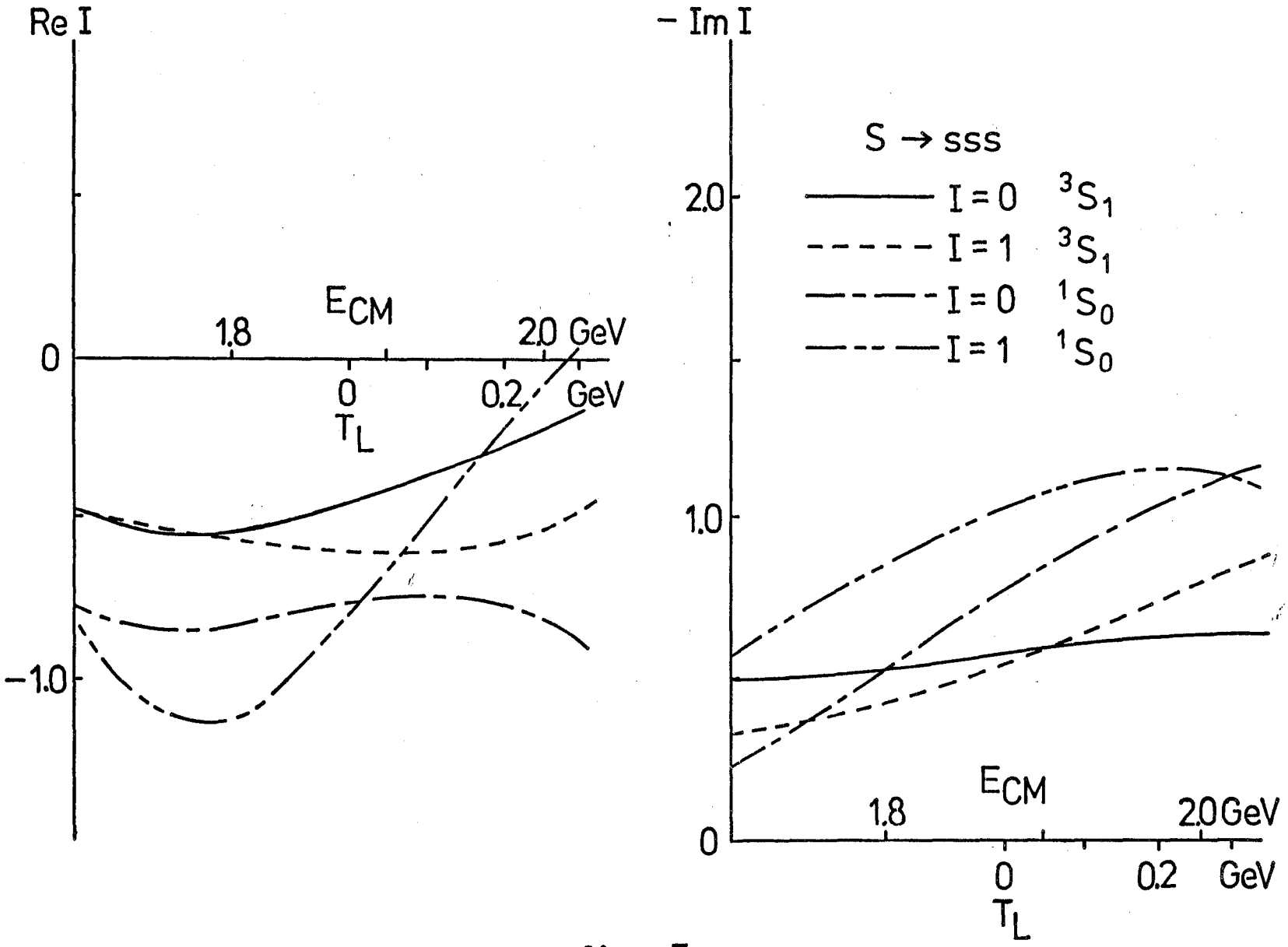
Re I
0
−1.0
1.8
E_{CM}
2.0 GeV
0
T_L
0.2
GeV
− Im I
2.0
1.0
0
S → sss
I = 0 $^3S_1$
I = 1 $^3S_1$
I = 0 $^1S_0$
I = 1 $^1S_0$
1.8
E_{CM}
2.0 GeV
0
T_L
0.2
GeV

fig. 7

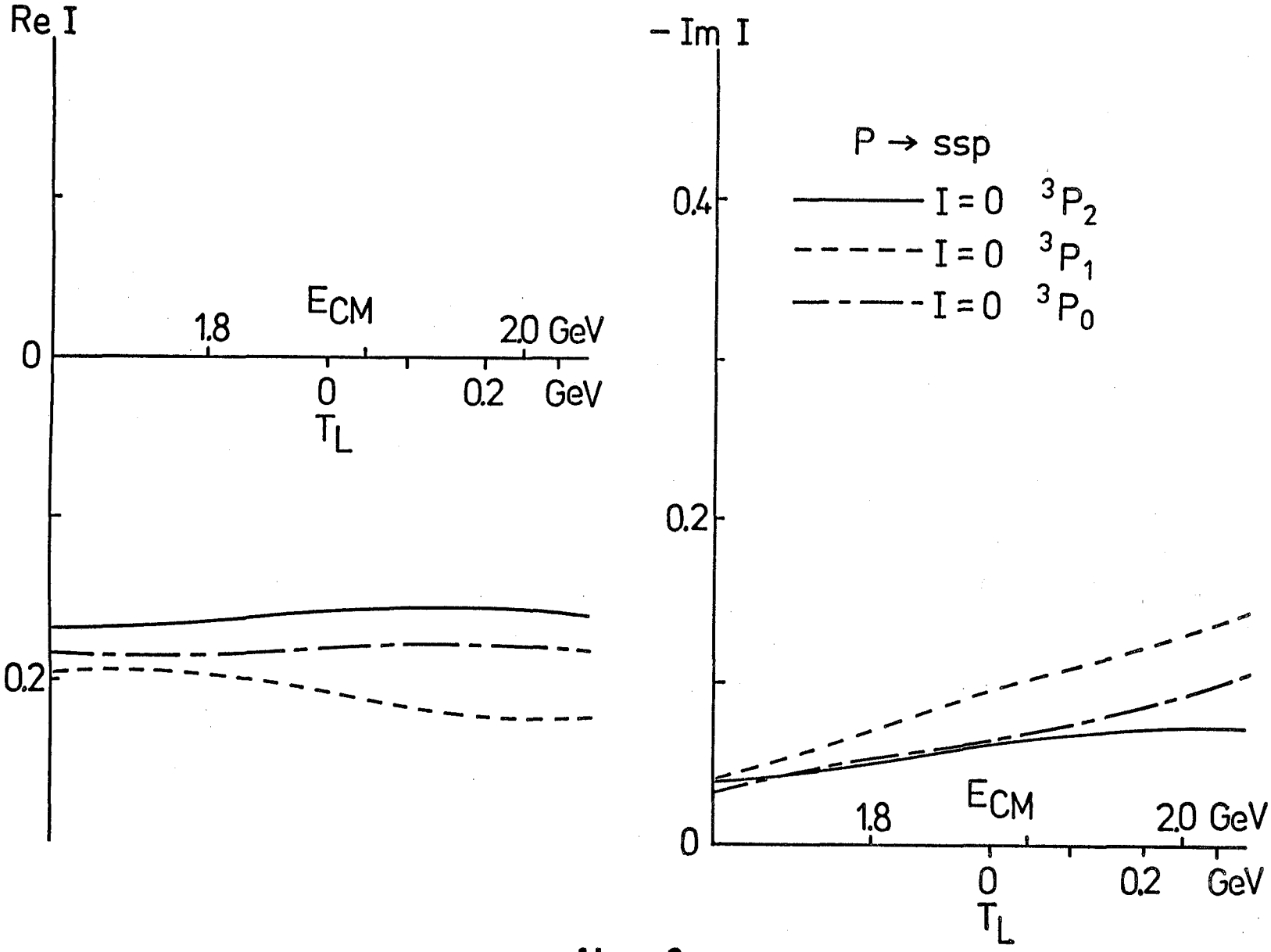
Re I
0
0.2
1.8
E_{CM}
2.0 GeV
0
T_L
0.2
GeV
- Im I
0.4
0.2
0
P → ssp
I = 0 $^3P_2$
I = 0 $^3P_1$
I = 0 $^3P_0$
1.8
E_{CM}
2.0 GeV
0
T_L
0.2
GeV

fig. 8a

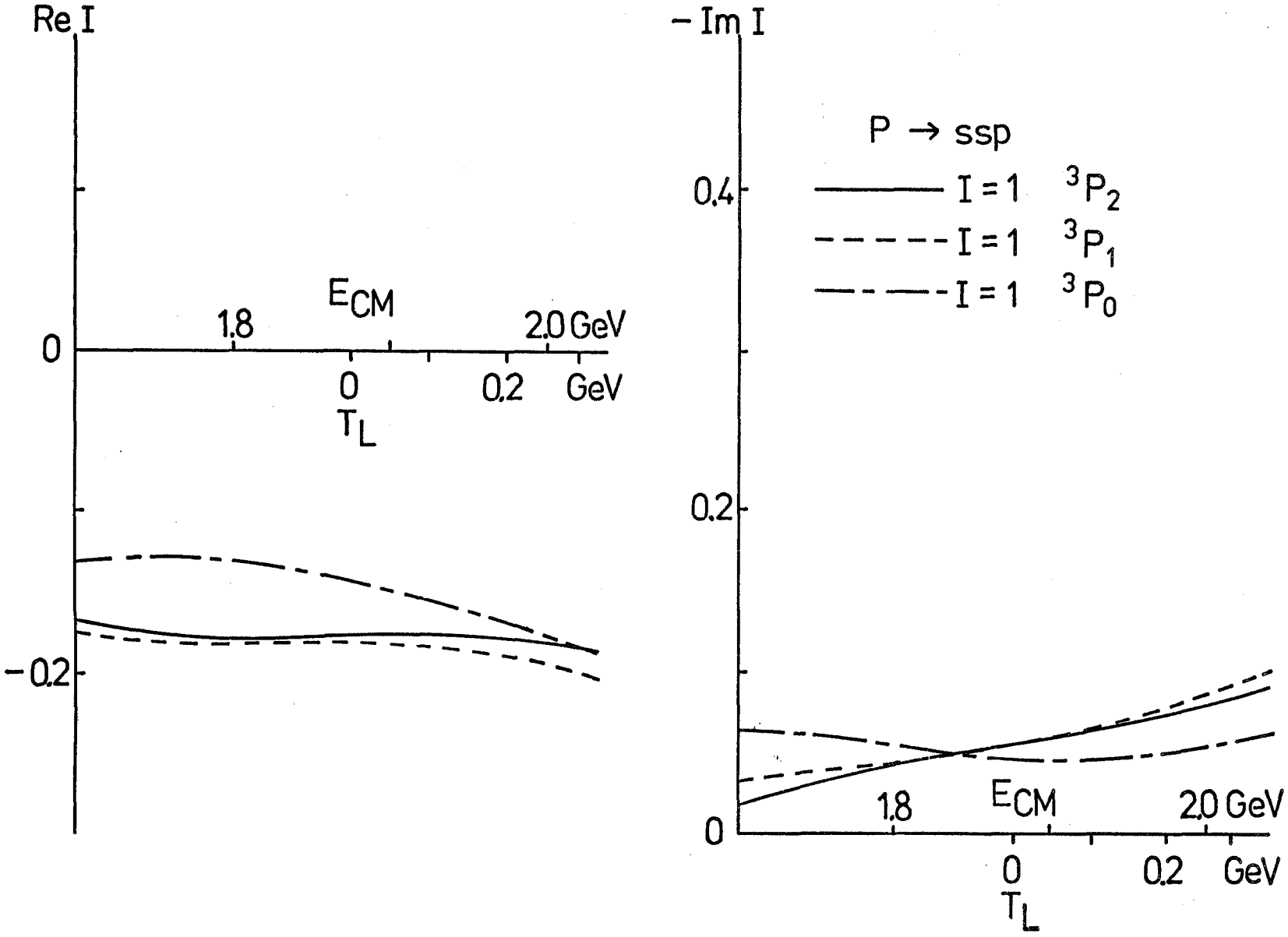
Re I
0
-0.2
1.8
E_{CM}
2.0 GeV
0
T_L
0.2
GeV
- Im I
0.4
0.2
0
P → ssp
I = 1 $^3P_2$
I = 1 $^3P_1$
I = 1 $^3P_0$
1.8
E_{CM}
2.0 GeV
0
T_L
0.2
GeV

fig. 8b

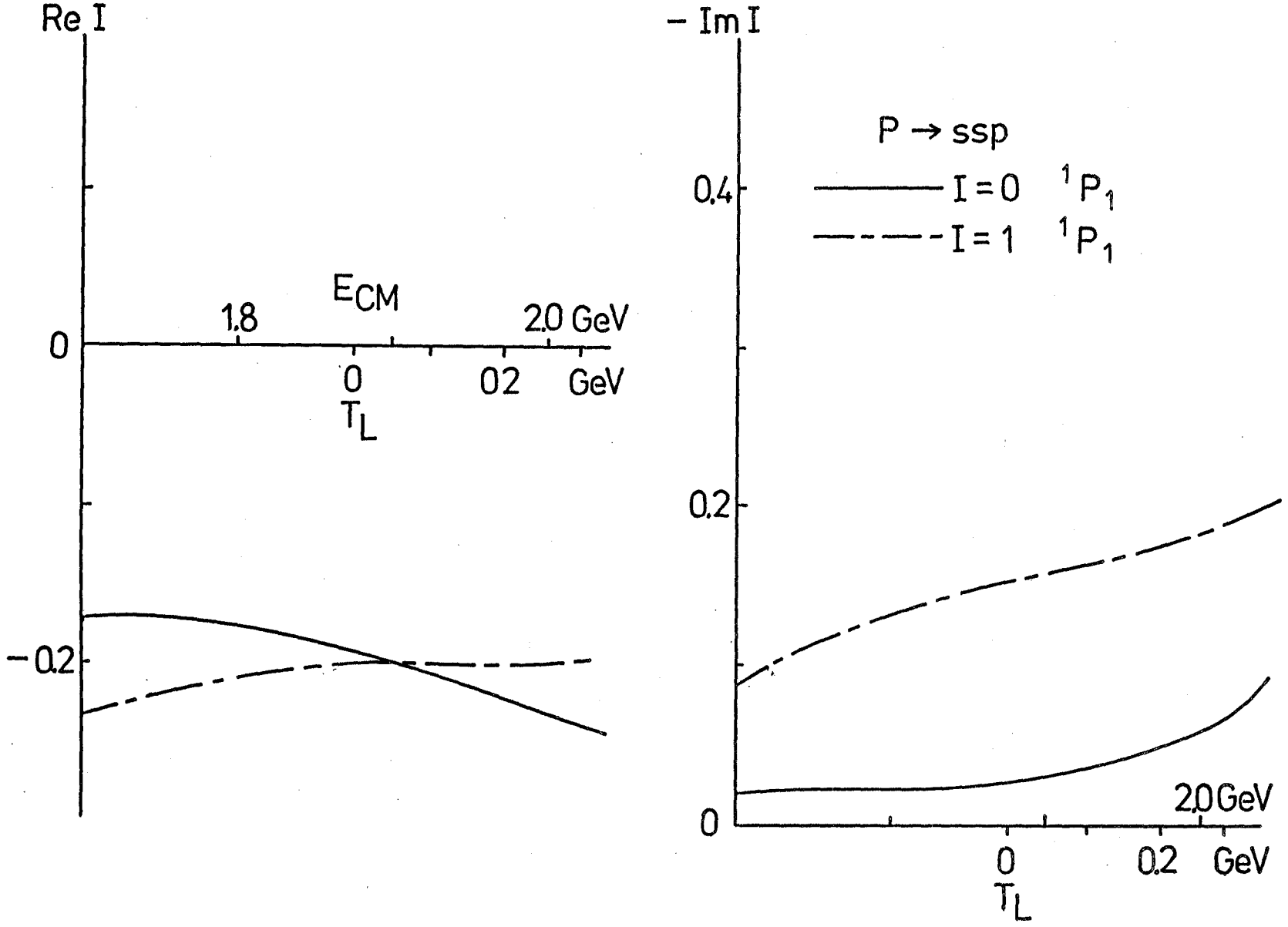
Re I
0
-0.2
1.8
E_{CM}
2.0 GeV
0
T_L
0.2
GeV
- Im I
P → ssp
I = 0 $^1P_1$
I = 1 $^1P_1$
0.4
0.2
0
2.0 GeV
0
T_L
0.2
GeV

fig. 8c

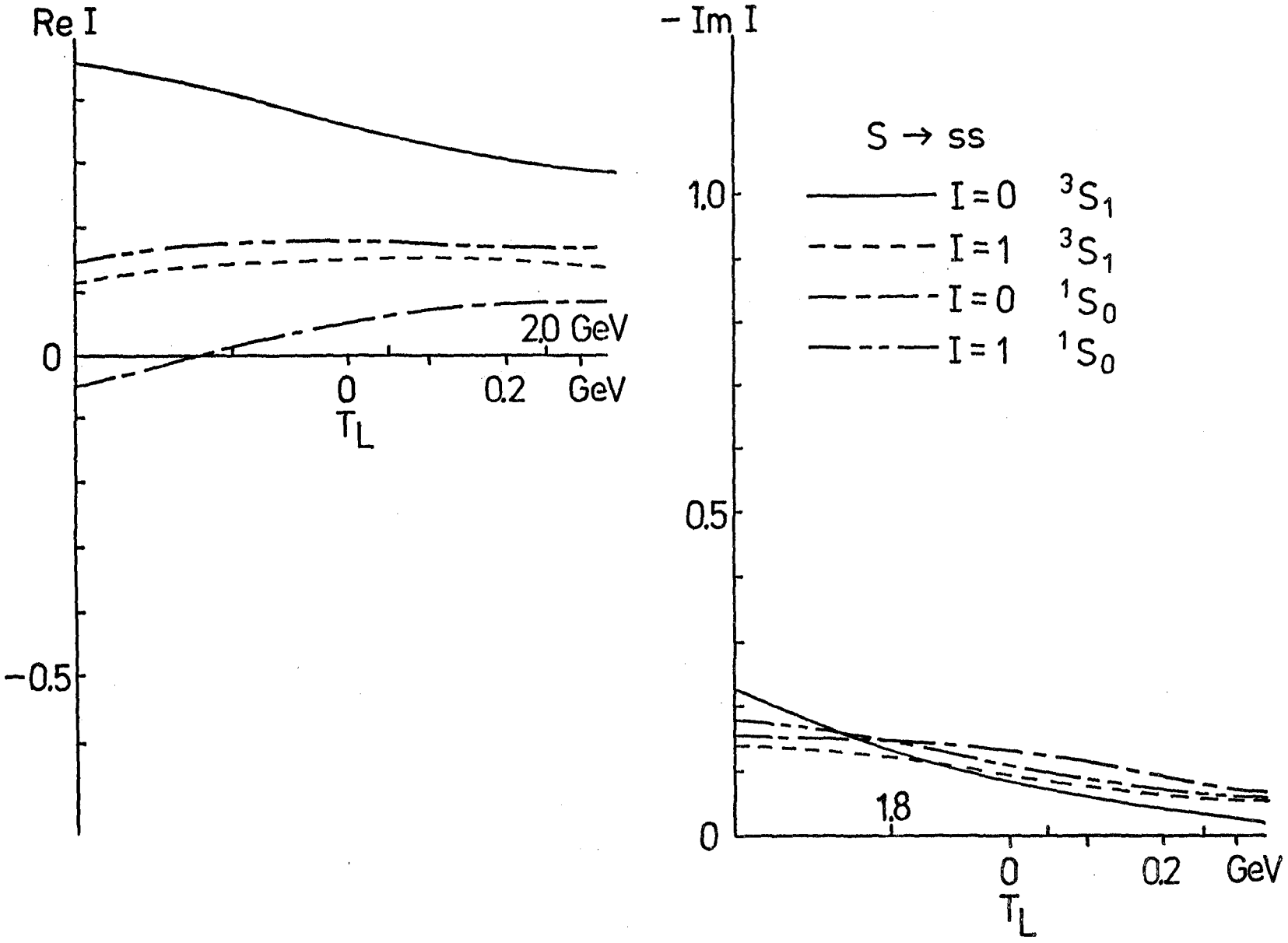
Re I
0
-0.5
2.0 GeV
0
0.2 GeV
T_L
- Im I
1.0
0.5
0
$S \rightarrow ss$
I = 0 $^3S_1$
I = 1 $^3S_1$
I = 0 $^1S_0$
I = 1 $^1S_0$
1.8
0
0.2 GeV
T_L

fig. 9

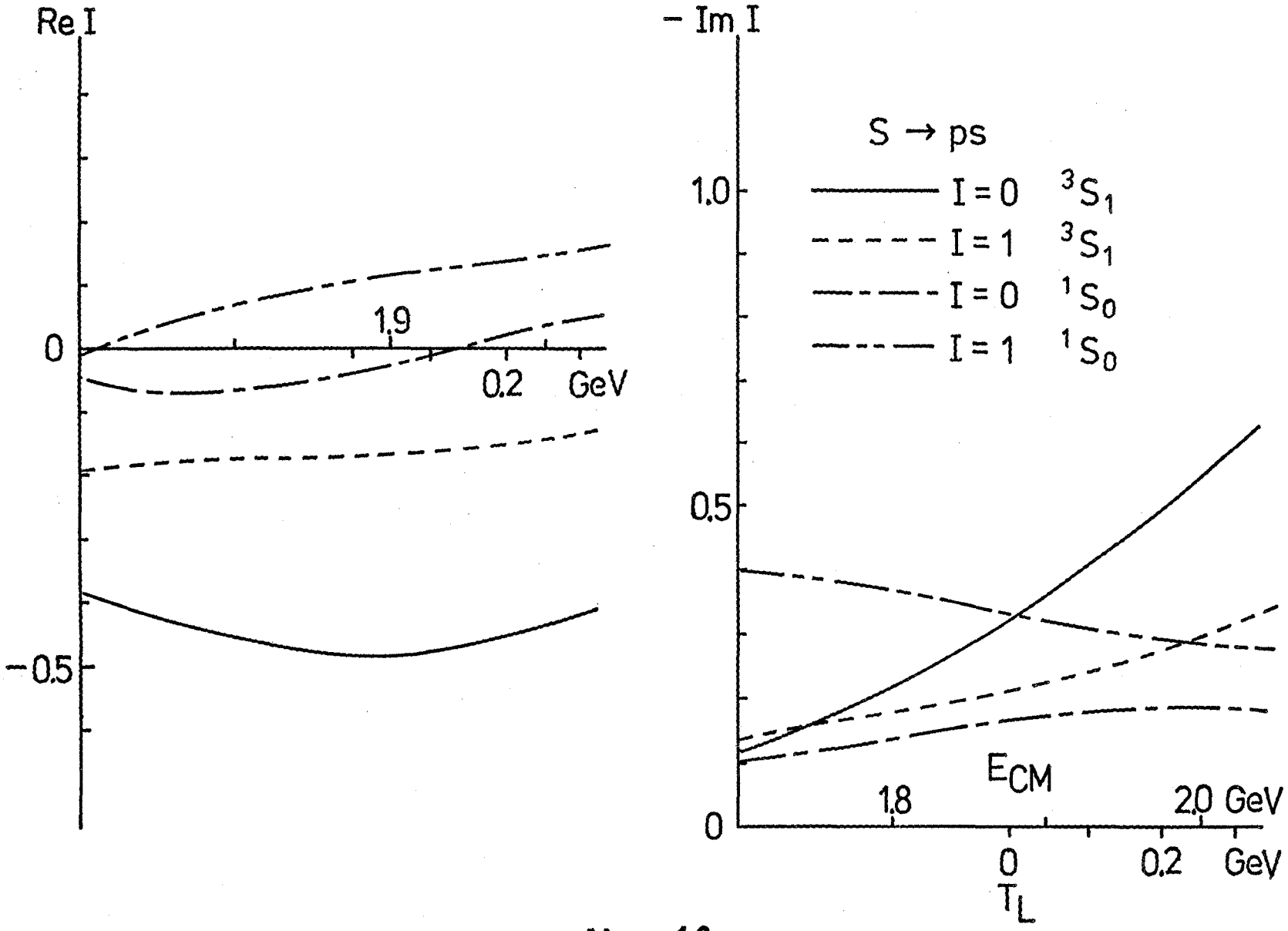
Re I
0
1.9
0.2 GeV
−0.5
− Im I
S → ps
1.0
I = 0 ³S₁
I = 1 ³S₁
I = 0 ¹S₀
I = 1 ¹S₀
0.5
0
1.8
E_CM
2.0 GeV
0
T_L
0.2 GeV

fig. 10

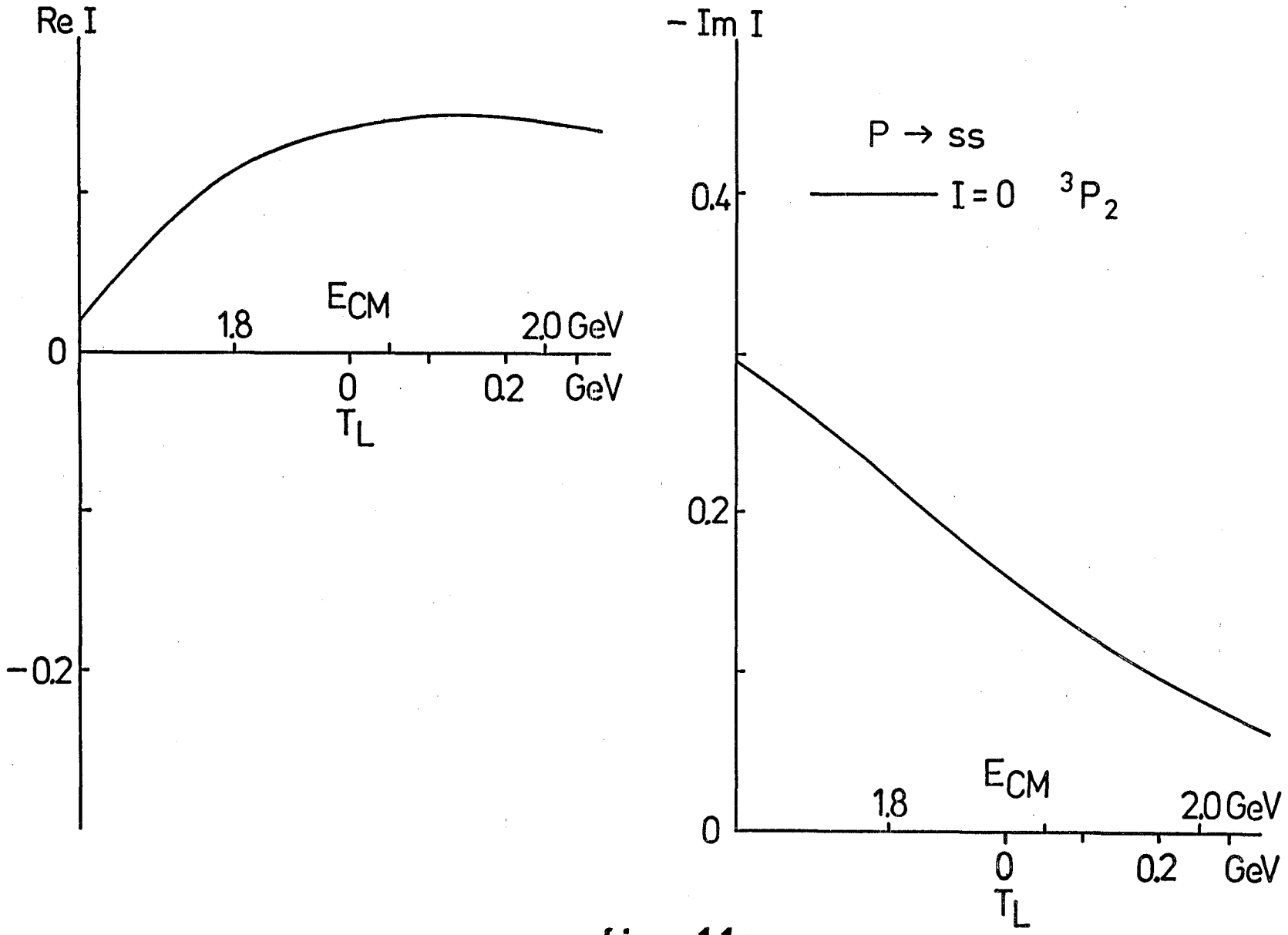
Re I
0
-0.2
1.8
E_{CM}
2.0 GeV
0
T_L
0.2
GeV
- Im I
P → ss
I = 0 $^3P_2$
0.4
0.2
0
1.8
E_{CM}
2.0 GeV
0
T_L
0.2
GeV

fig. 11a

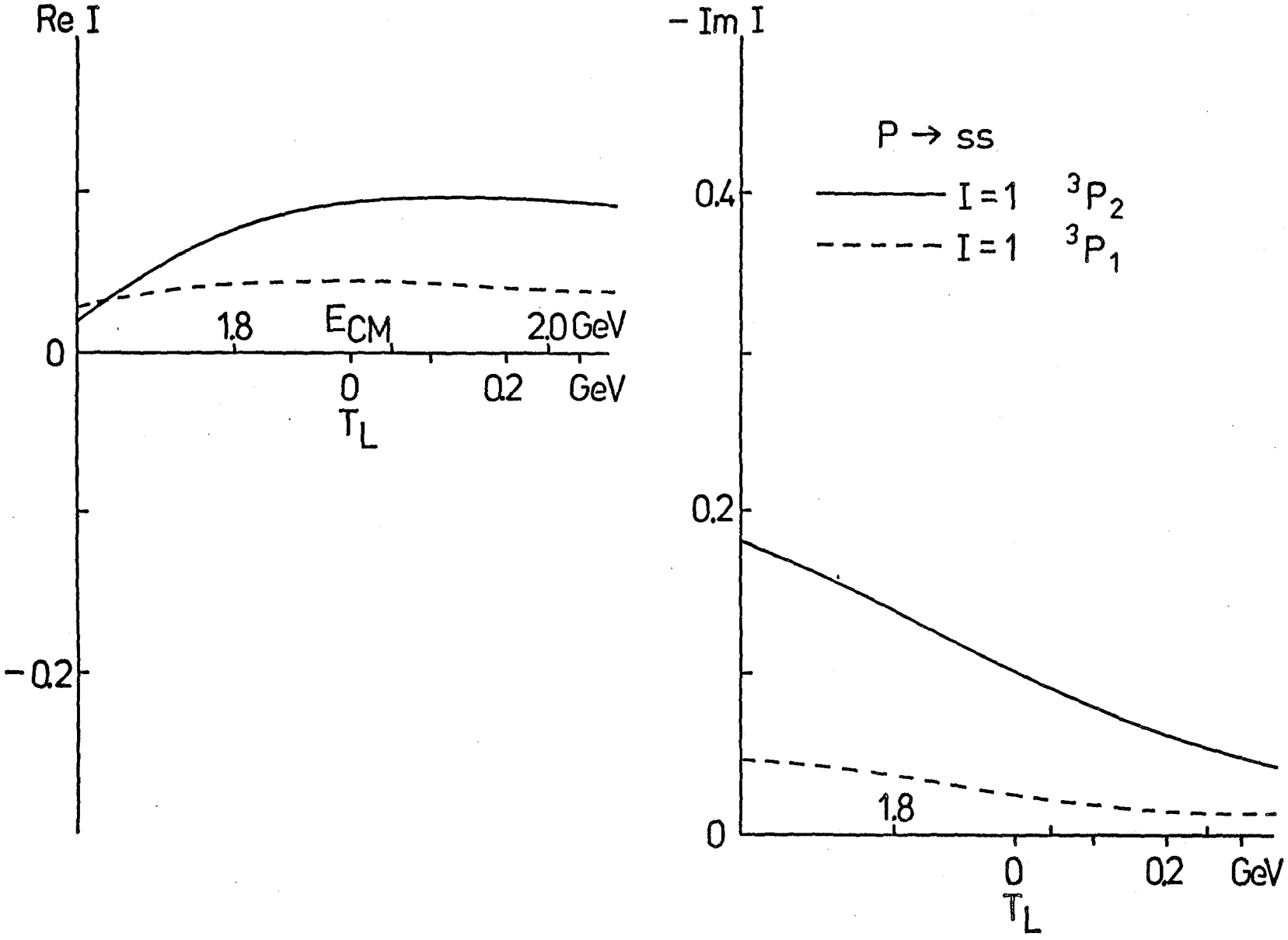
Re I
0
-0.2
1.8
E_{CM}
2.0 GeV
0
T_L
0.2
GeV
- Im I
P → ss
I = 1 $^3P_2$
I = 1 $^3P_1$
0.4
0.2
0
1.8
0
T_L
0.2
GeV

fig. 11b

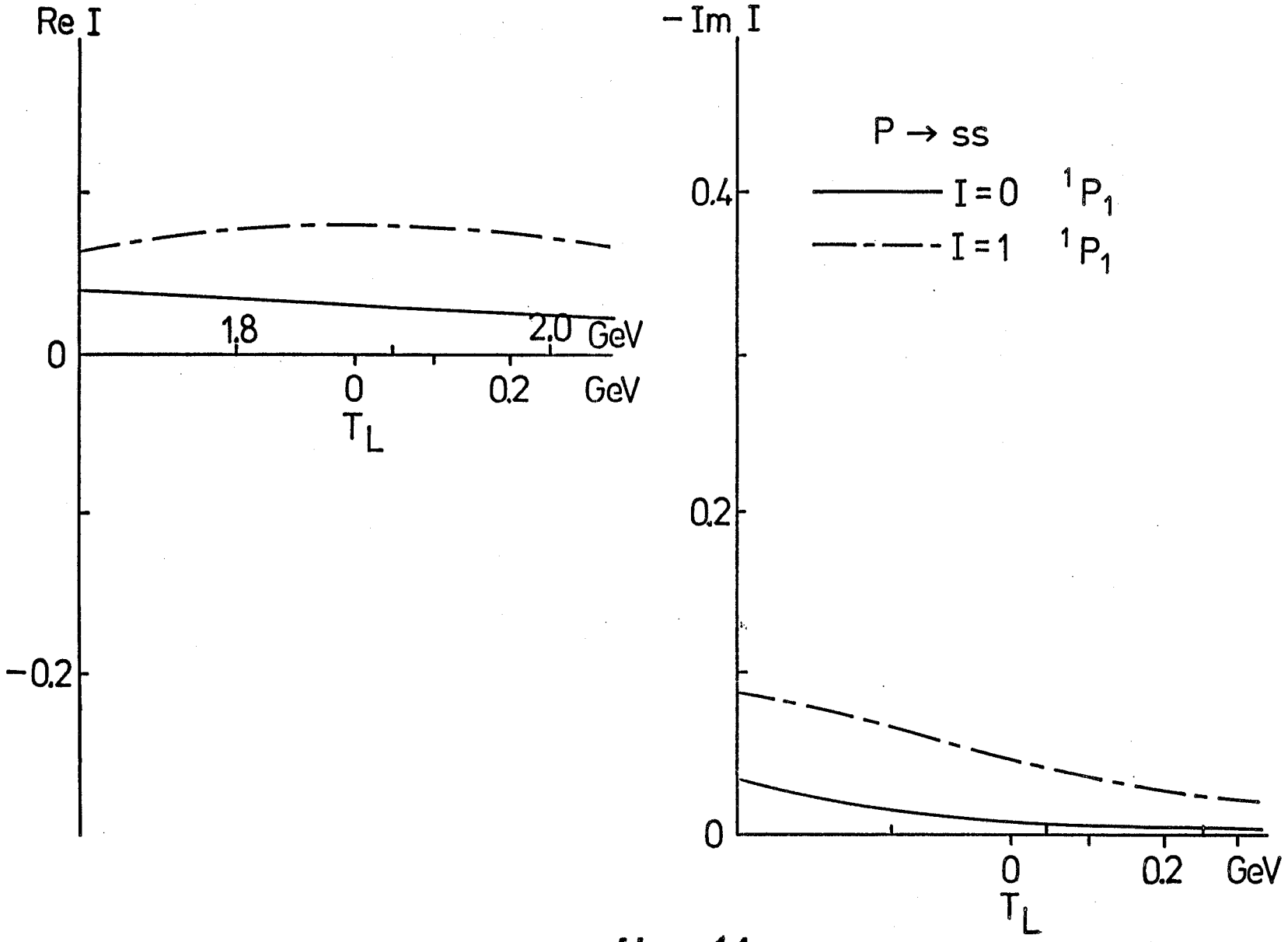
Re I
0
−0.2
1.8
2.0 GeV
0
0.2 GeV
T_L
− Im I
0.4
0.2
0
P → ss
I = 0 $^1P_1$
I = 1 $^1P_1$
0
0.2 GeV
T_L

fig. 11c

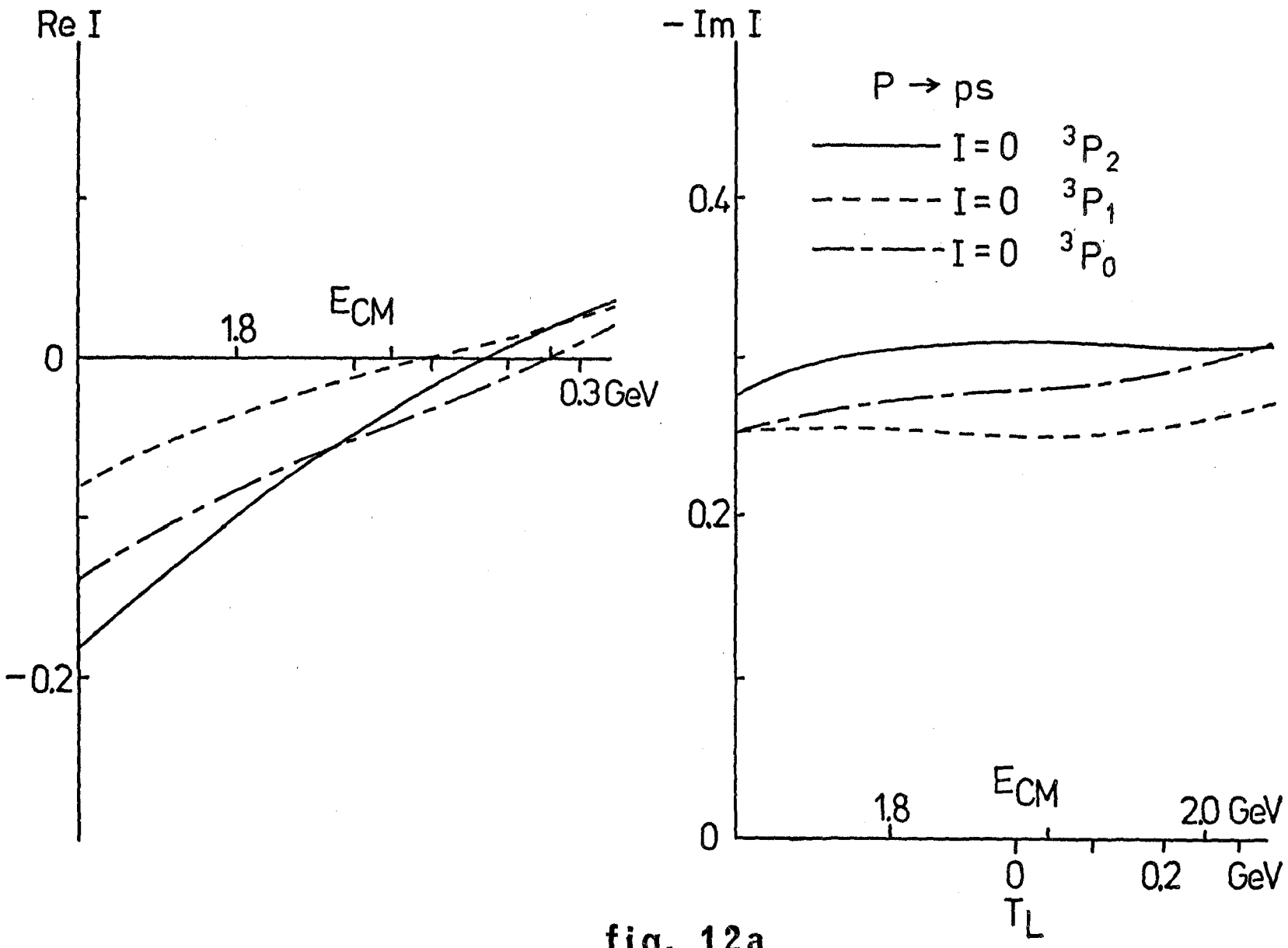
Re I
1.8
E_{CM}
0
0.3 GeV
−0.2
− Im I
P → ps
I = 0 $^3P_2$
I = 0 $^3P_1$
I = 0 $^3P_0$
0.4
0.2
0
1.8
E_{CM}
2.0 GeV
0
0.2
GeV
T_L

fig. 12a

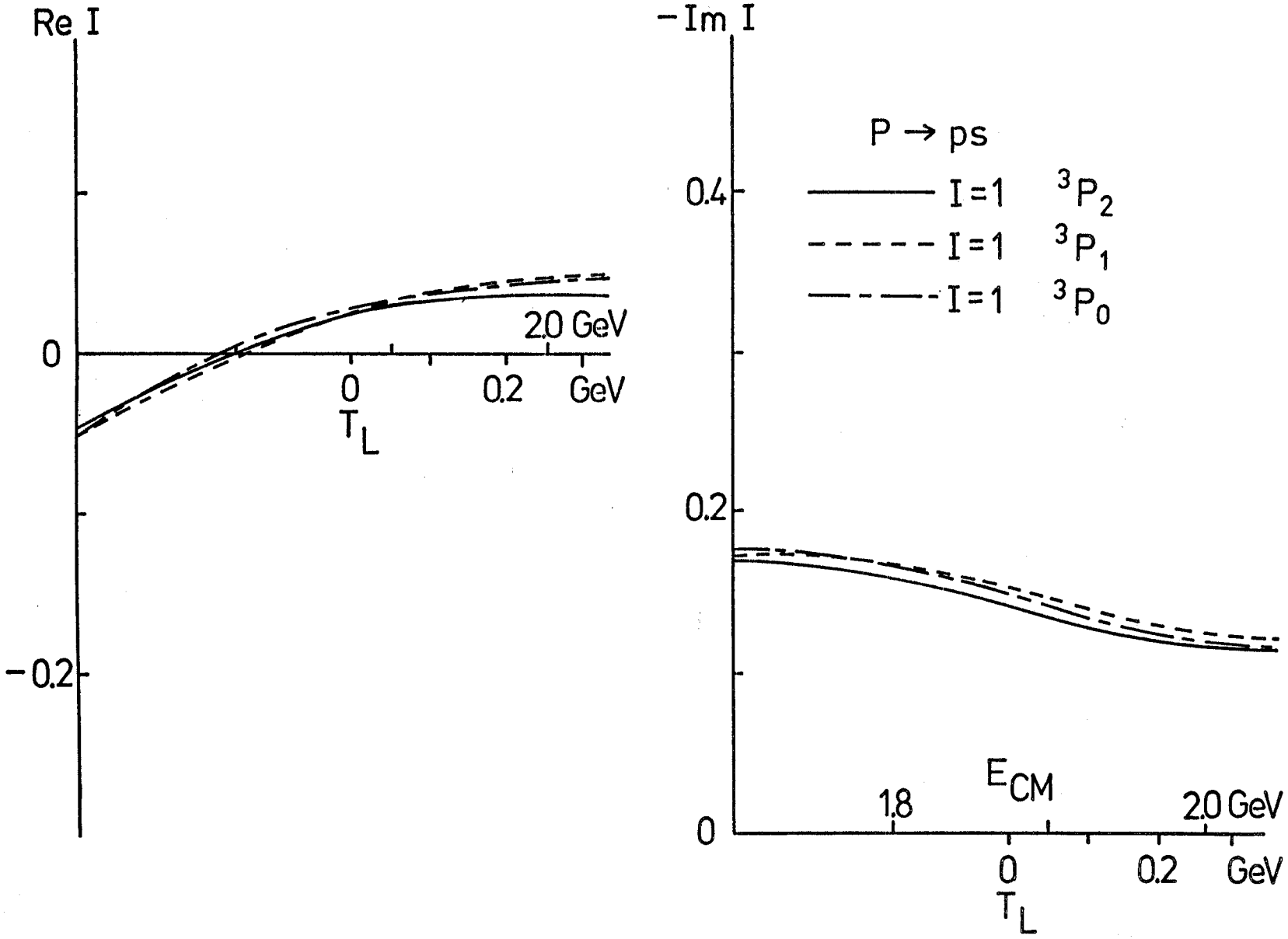
Re I
0
-0.2
0
T_L
0.2 GeV
2.0 GeV
-Im I
P → ps
I=1 $^3P_2$
I=1 $^3P_1$
I=1 $^3P_0$
0.4
0.2
0
1.8
E_{CM}
2.0 GeV
0
T_L
0.2 GeV

fig. 12b

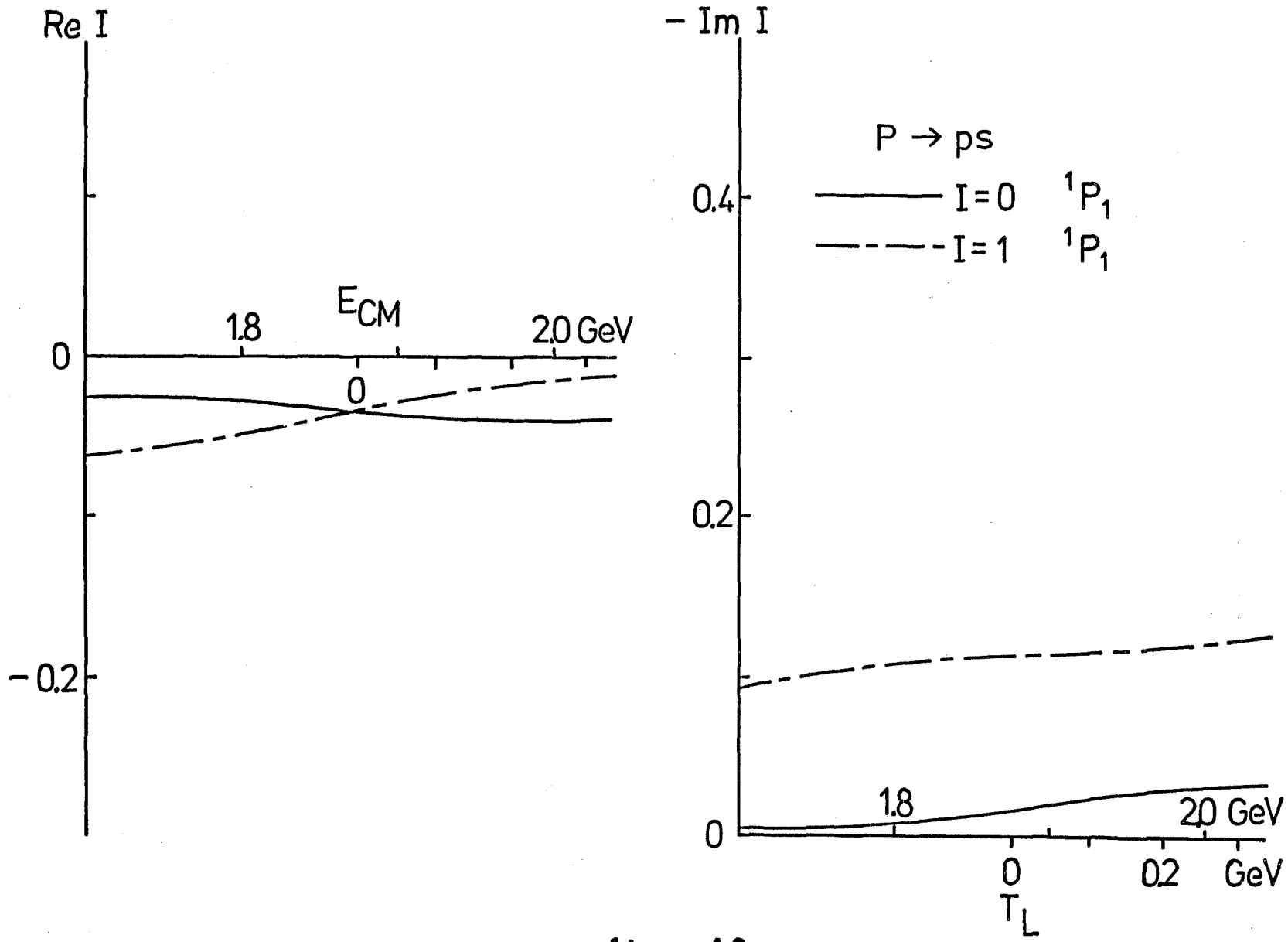
Re I
0
-0.2
1.8
E_{CM}
2.0 GeV
0
- Im I
P → ps
I=0 $^1P_1$
I=1 $^1P_1$
0.4
0.2
0
1.8
2.0 GeV
0
0.2
GeV
T_L

fig. 12c

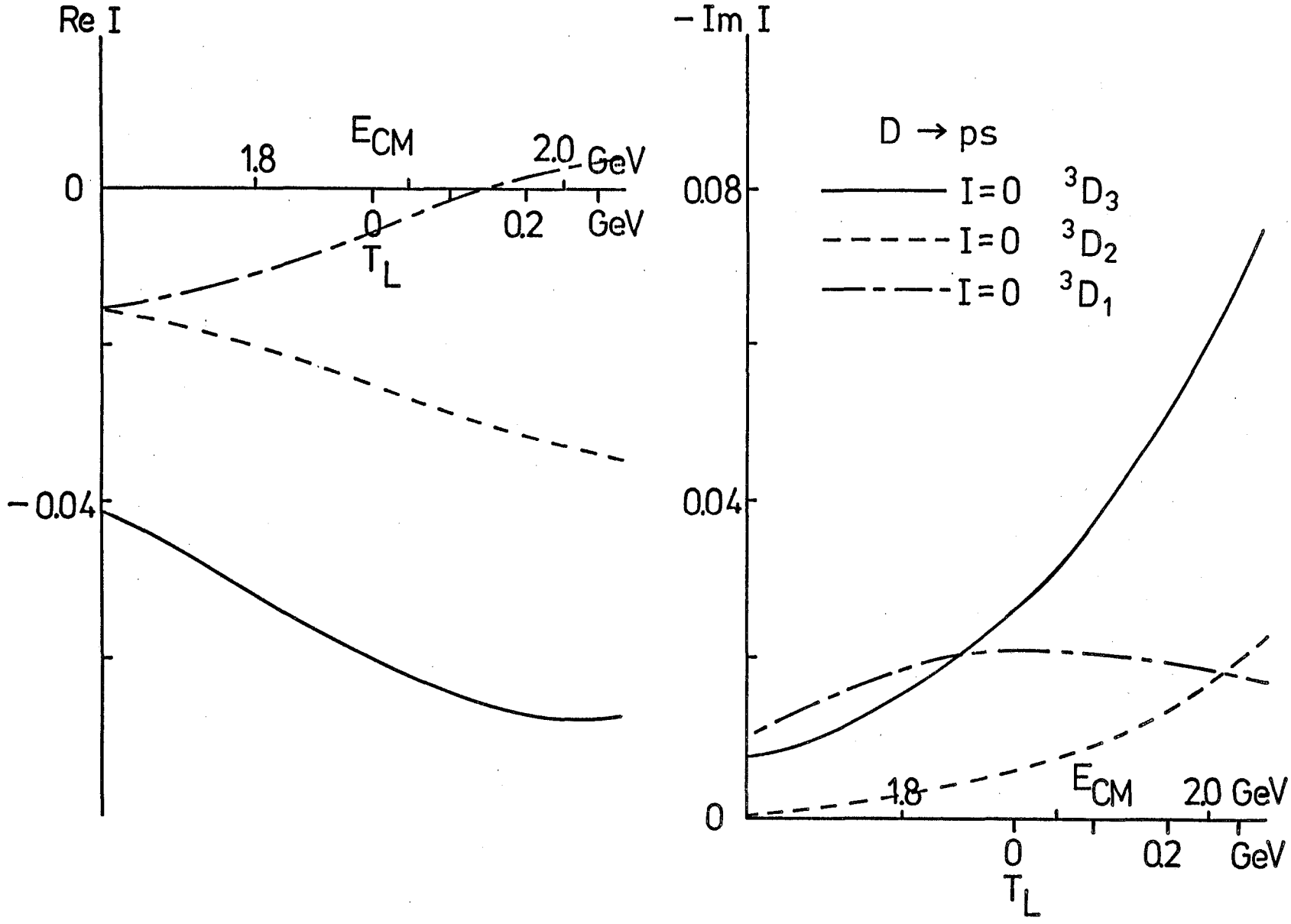
Re I
0
−0.04
1.8
E_{CM}
2.0 GeV
0
T_L
0.2 GeV
− Im I
0.08
0.04
0
D → ps
I=0 $^3D_3$
I=0 $^3D_2$
I=0 $^3D_1$
1.8
E_{CM}
2.0 GeV
0
T_L
0.2 GeV

fig. 13a

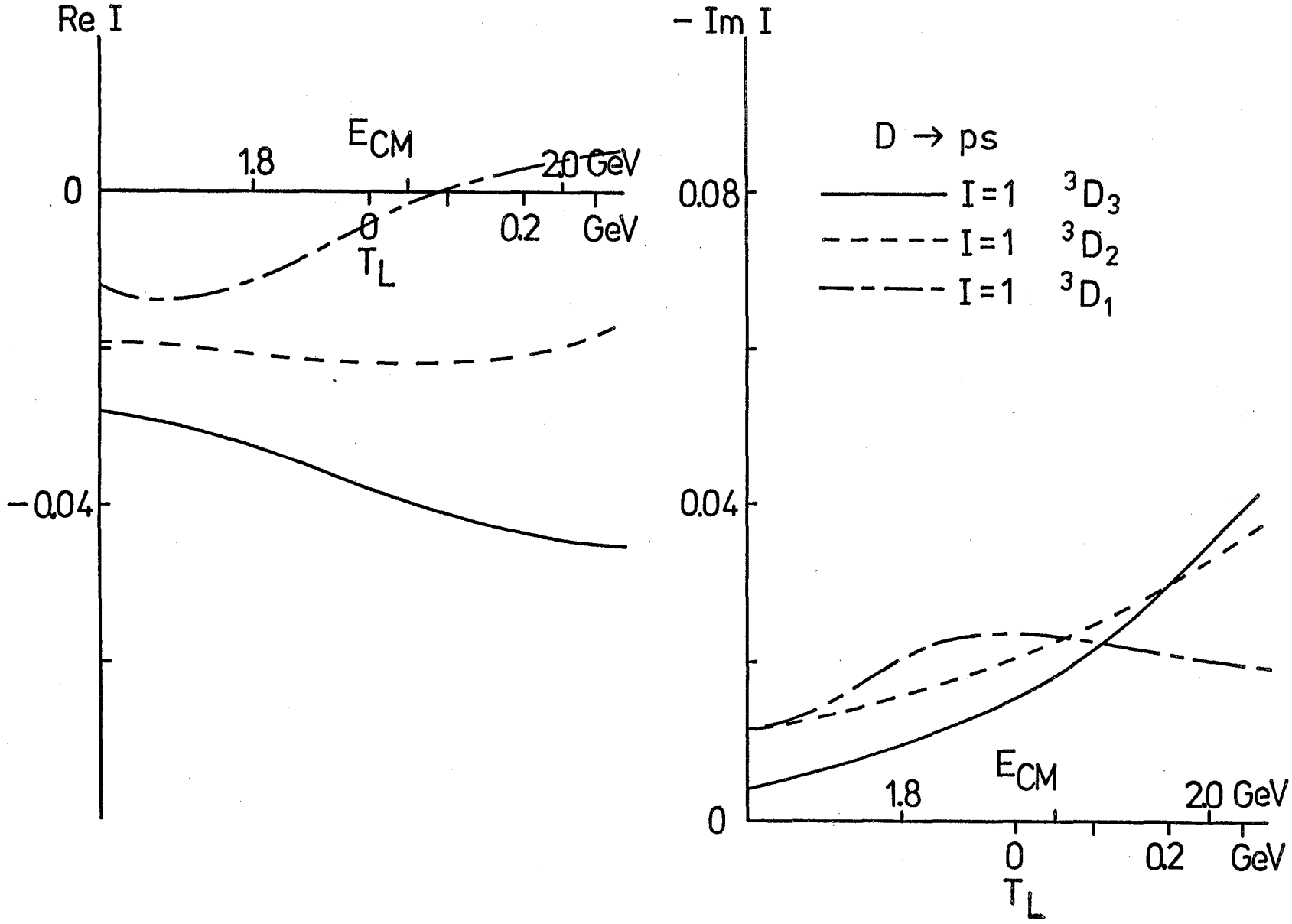
Re I
0
−0.04
1.8
E_{CM}
2.0 GeV
0
T_L
0.2
GeV
− Im I
0.08
0.04
0
D → ps
I=1 $^3D_3$
I=1 $^3D_2$
I=1 $^3D_1$
1.8
E_{CM}
2.0 GeV
0
T_L
0.2
GeV

fig. 13b

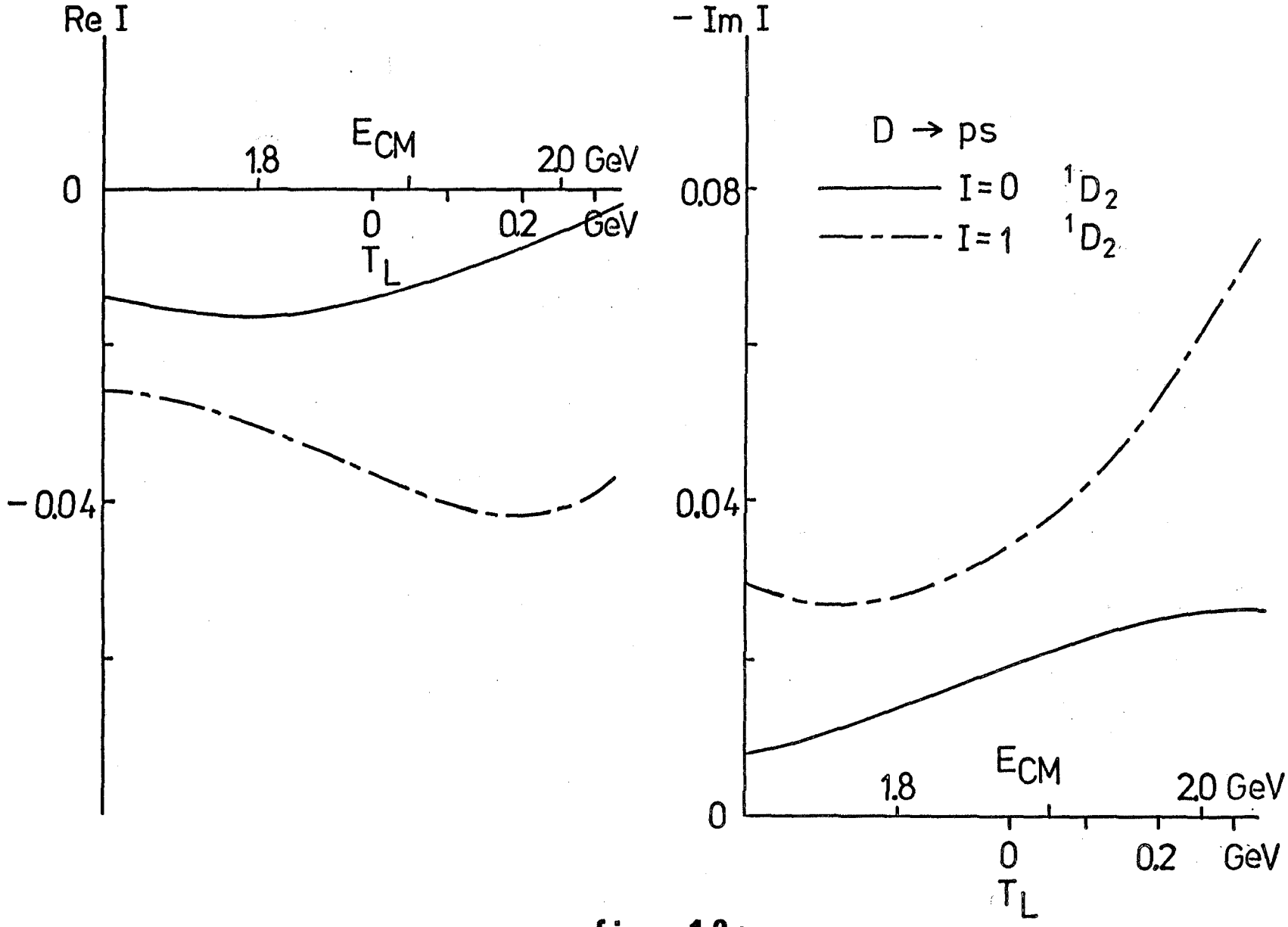
Re I
0
-0.04
1.8
E_{CM}
2.0 GeV
0
0.2
GeV
T_L
- Im I
0.08
0.04
0
D → ps
I = 0 $^1D_2$
I = 1 $^1D_2$
1.8
E_{CM}
2.0 GeV
0
0.2
GeV
T_L

fig. 13c

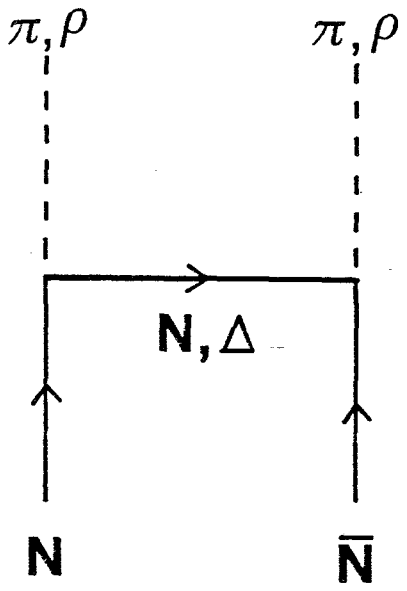

fig. 14

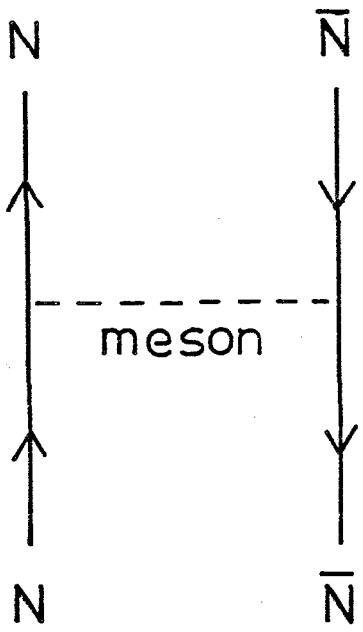

fig. 15

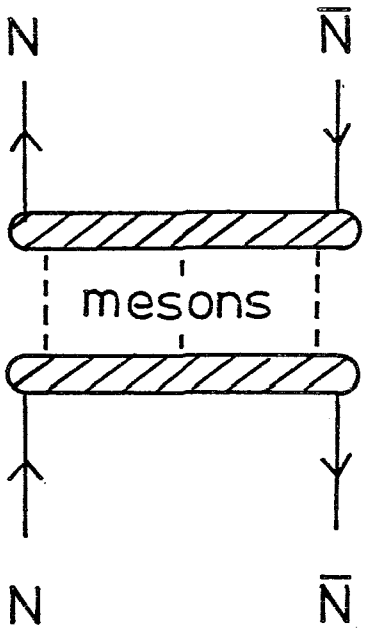

fig. 16

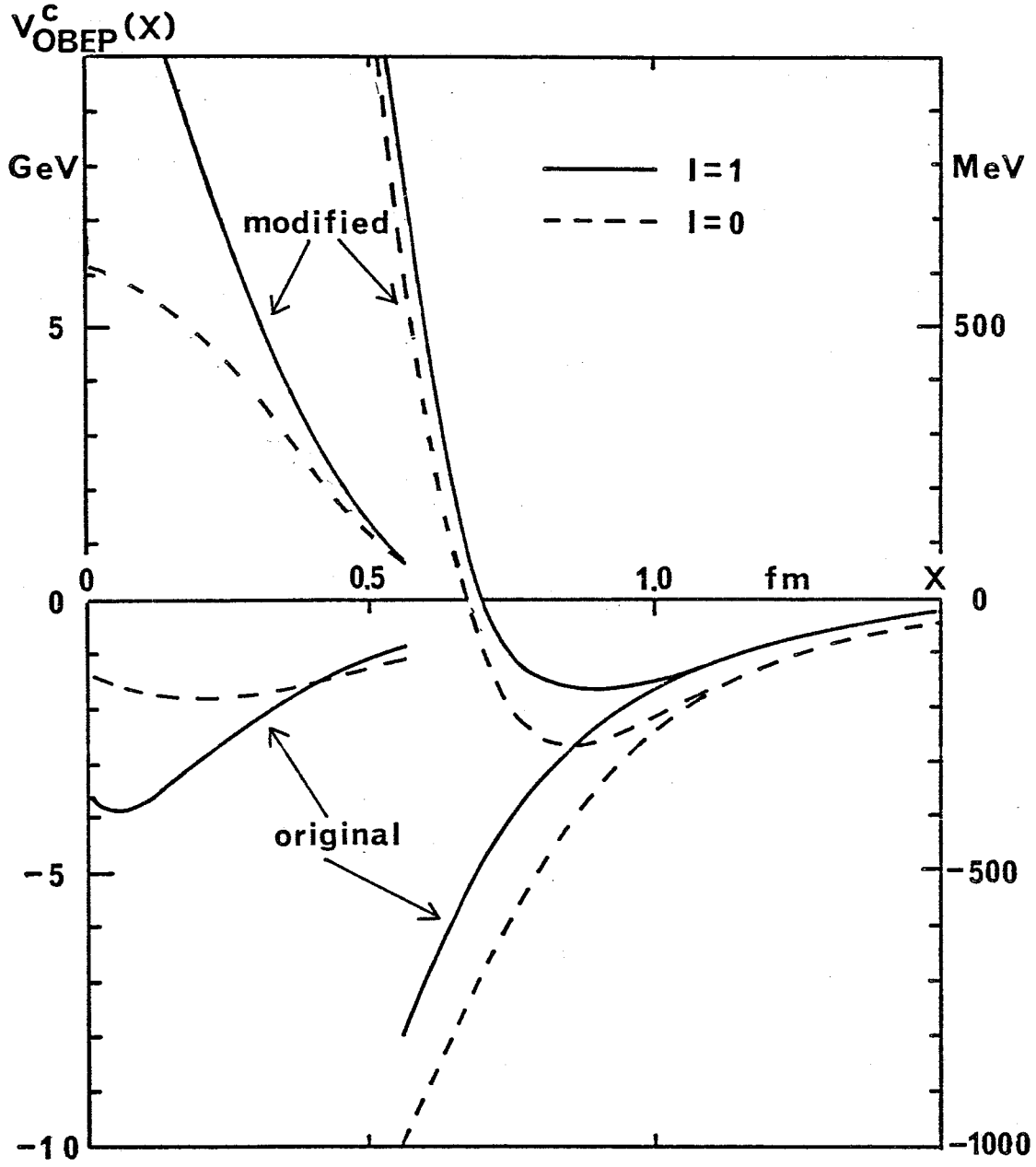
$V^c_{OBEP}(X)$
GeV
MeV
I=1
I=0
modified
5
500
0
0.5
1.0
fm
X
0
0
original
-5
-500
-10
-1000

fig. 17

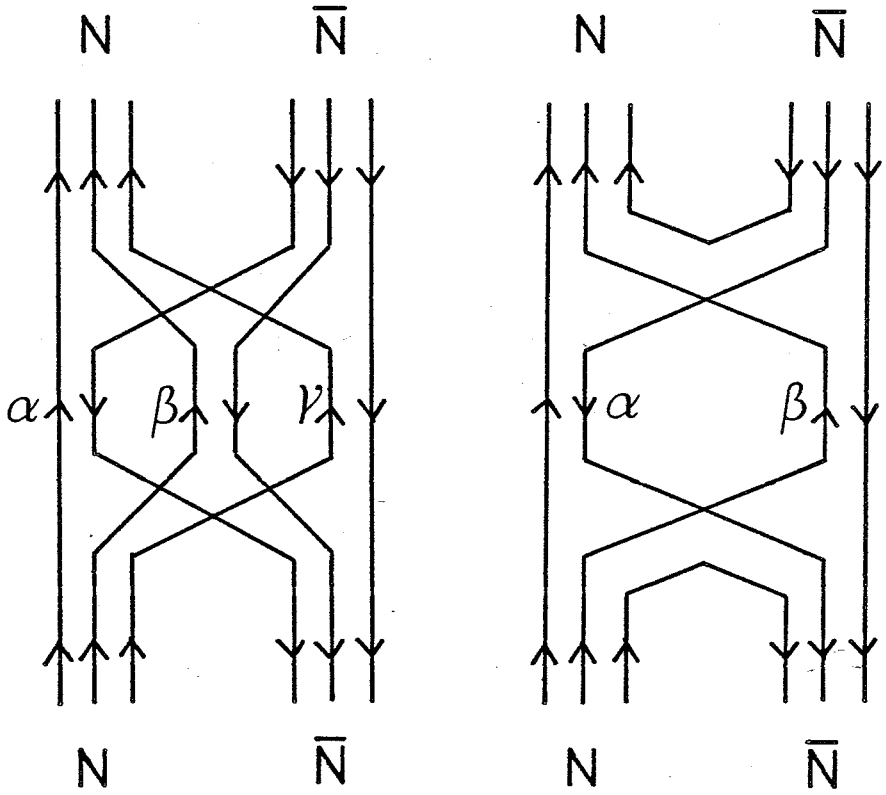

fig. 18

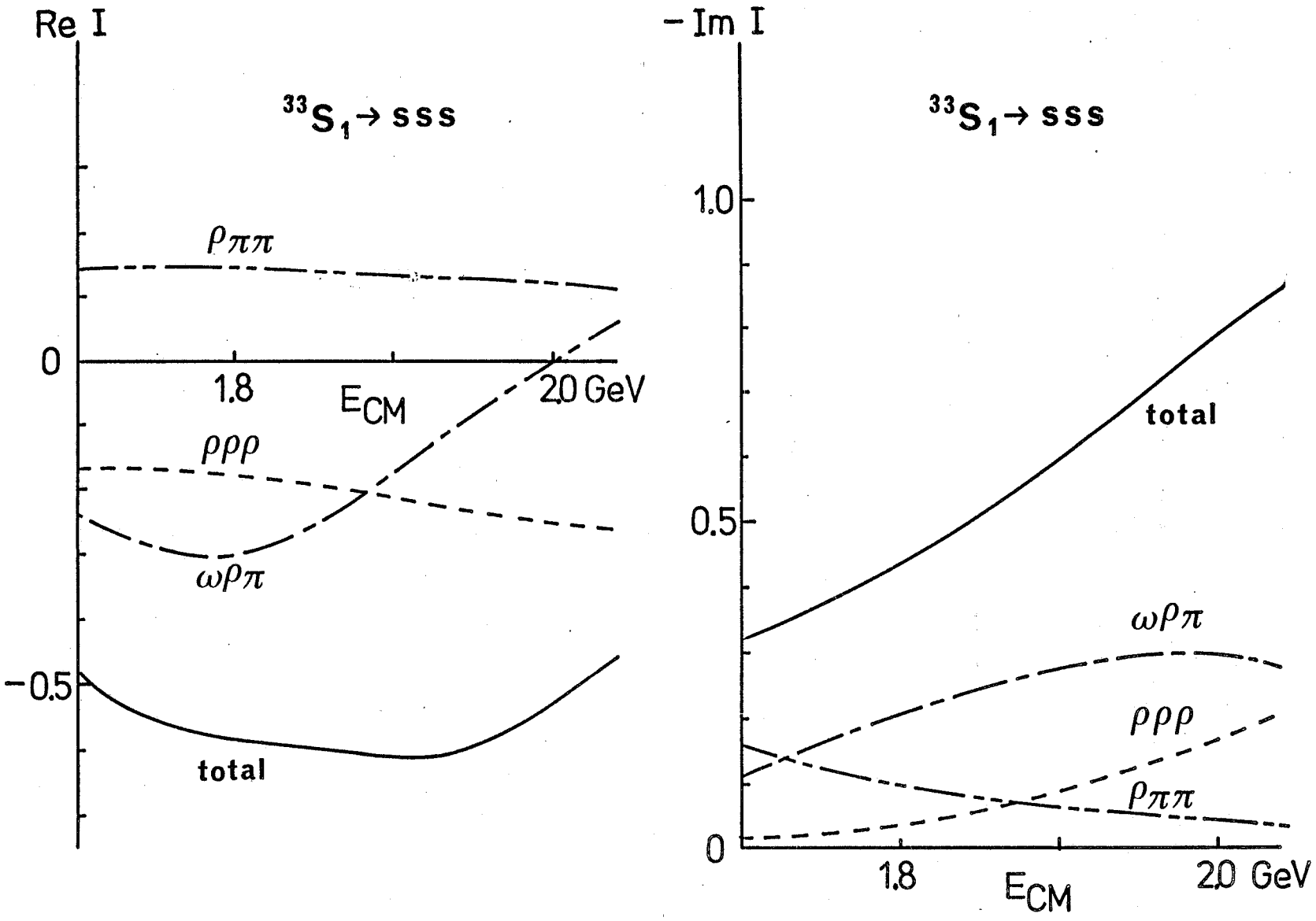
Re I
$^{33}S_1 \rightarrow sss$
$\rho\pi\pi$
0
1.8
E_{CM}
2.0 GeV
$\rho\rho\rho$
$\omega\rho\pi$
−0.5
total
− Im I
$^{33}S_1 \rightarrow sss$
1.0
0.5
total
$\omega\rho\pi$
$\rho\rho\rho$
$\rho\pi\pi$
0
1.8
E_{CM}
2.0 GeV

fig. 19a

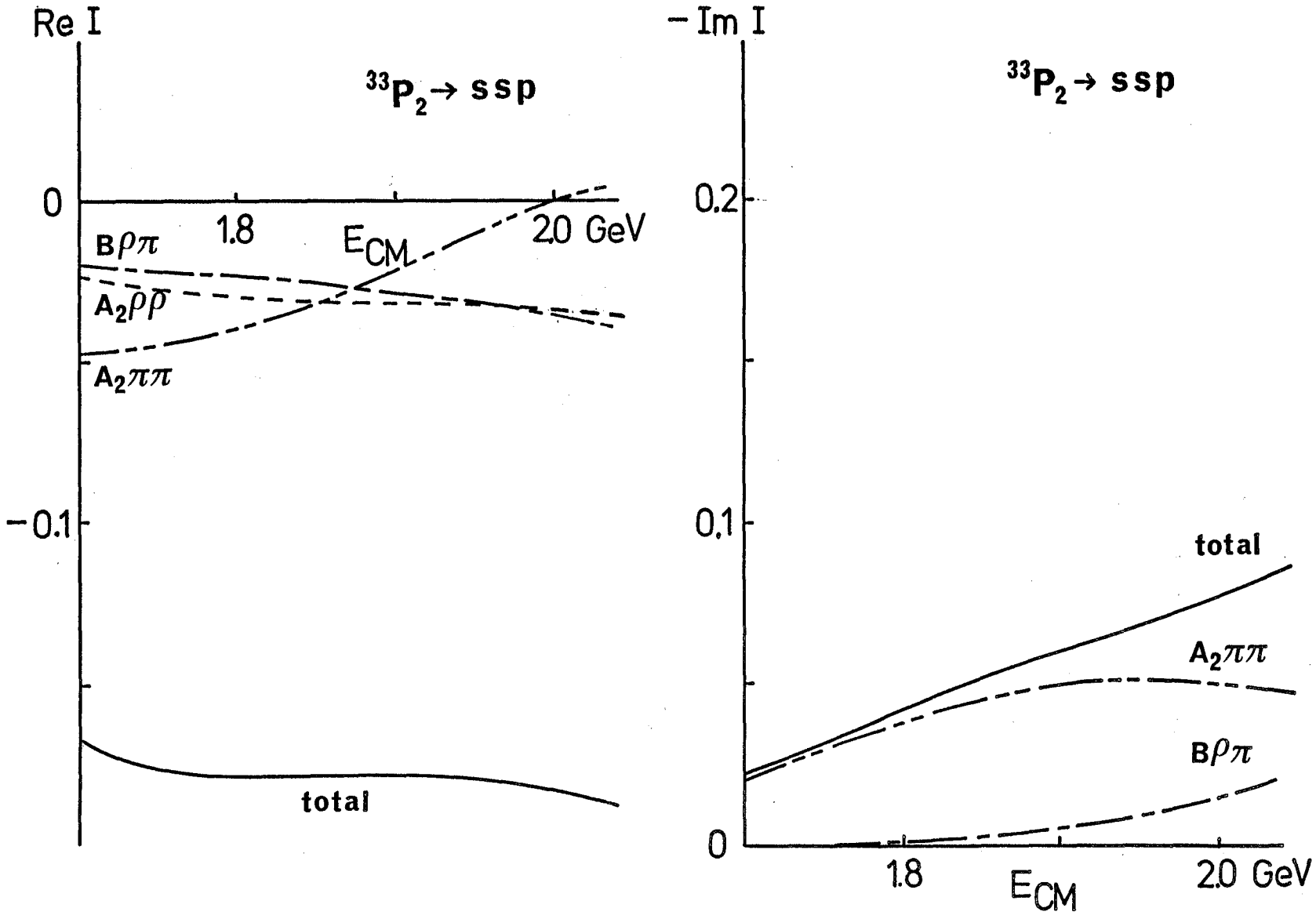
Re I
$^{33}P_2 \rightarrow ssp$
0
1.8
E_{CM}
2.0 GeV
$B\rho\pi$
$A_2\rho\rho$
$A_2\pi\pi$
−0.1
total
−Im I
$^{33}P_2 \rightarrow ssp$
0.2
0.1
total
$A_2\pi\pi$
$B\rho\pi$
0
1.8
E_{CM}
2.0 GeV

fig. 19b

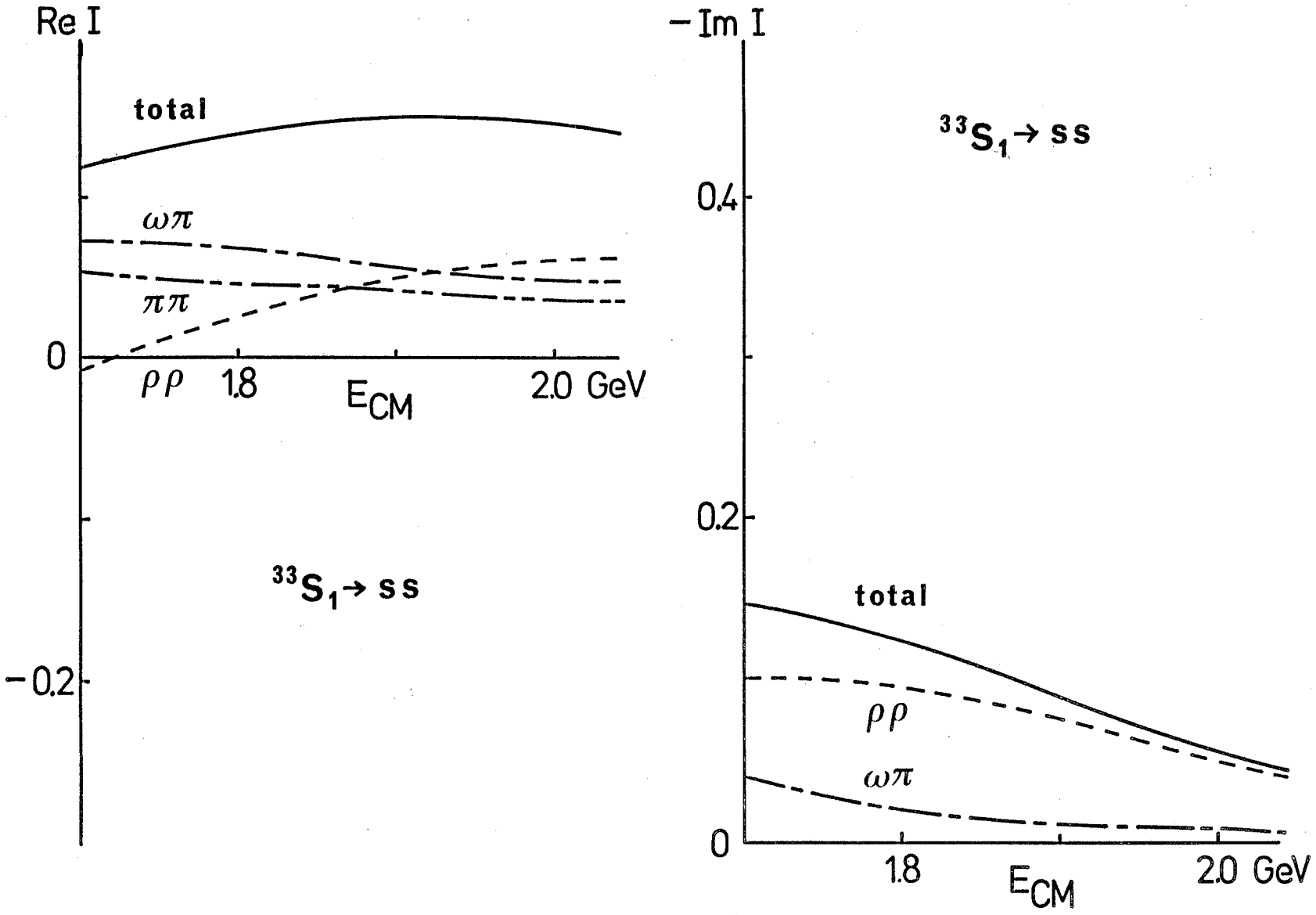
Re I
total
$\omega\pi$
$\pi\pi$
0
$\rho\rho$
1.8
E_{CM}
2.0 GeV
$^{33}S_1 \rightarrow ss$
−0.2
−Im I
$^{33}S_1 \rightarrow ss$
0.4
0.2
total
$\rho\rho$
$\omega\pi$
0
1.8
E_{CM}
2.0 GeV

fig. 19c

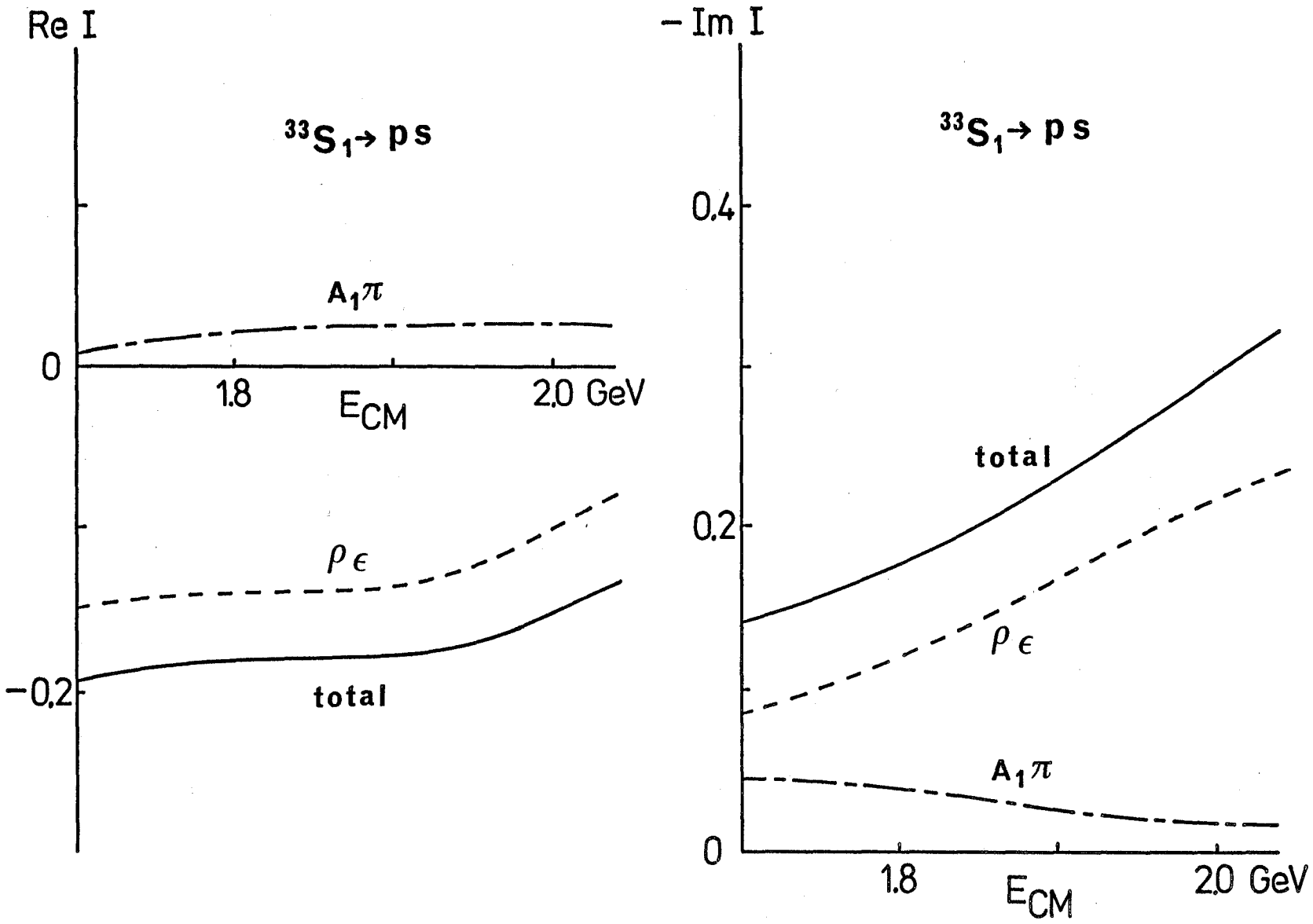
Re I
$^{33}S_1 \rightarrow ps$
$A_1\pi$
0
1.8
E_{CM}
2.0 GeV
$\rho\epsilon$
−0.2
total
− Im I
$^{33}S_1 \rightarrow ps$
0.4
total
0.2
$\rho\epsilon$
$A_1\pi$
0
1.8
E_{CM}
2.0 GeV

fig. 19d

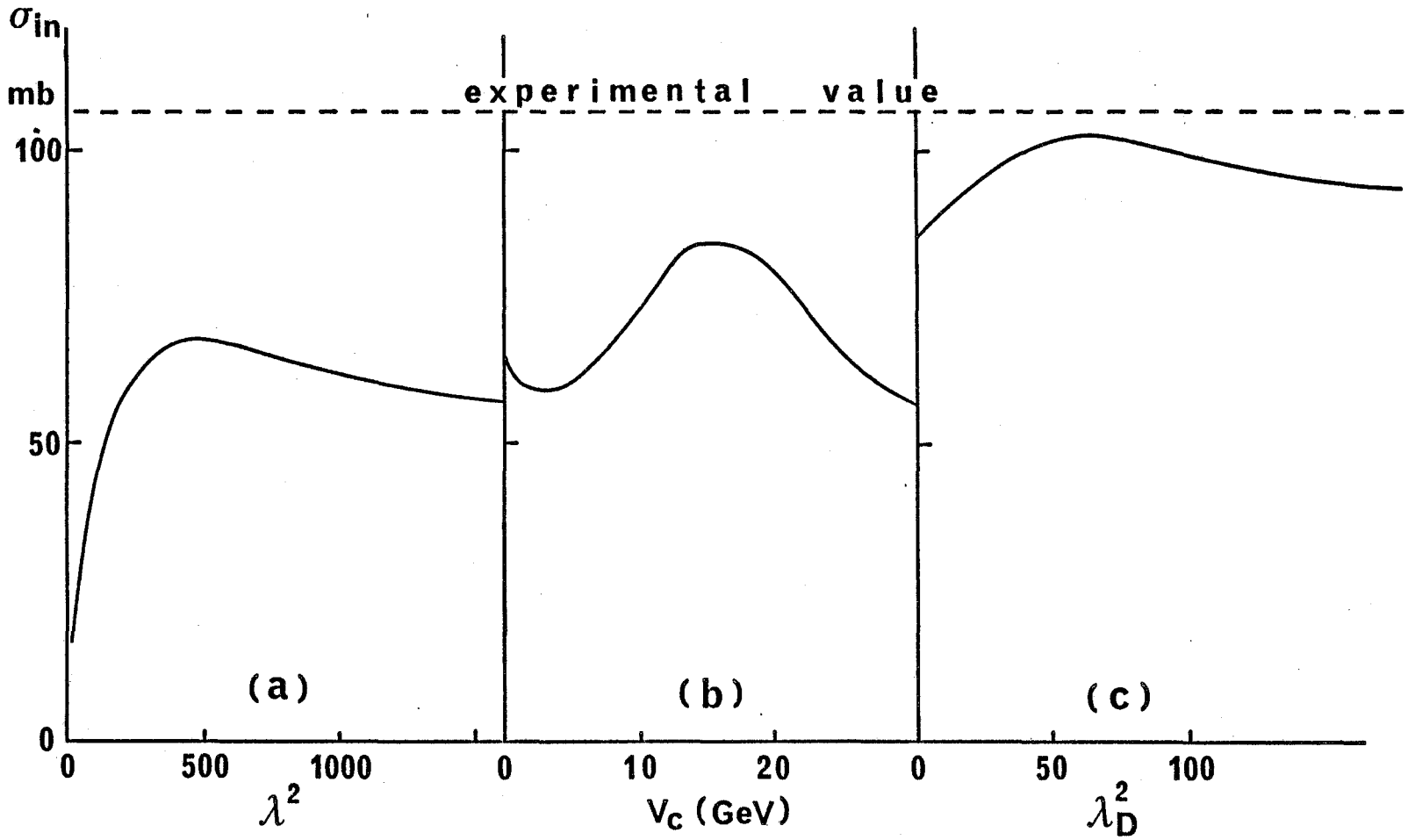
σ_{in}
mb
experimental value
100
50
0
(a)
(b)
(c)
0
500
1000
0
10
20
0
50
100
λ^2
V_c (GeV)
λ_D^2

fig. 20

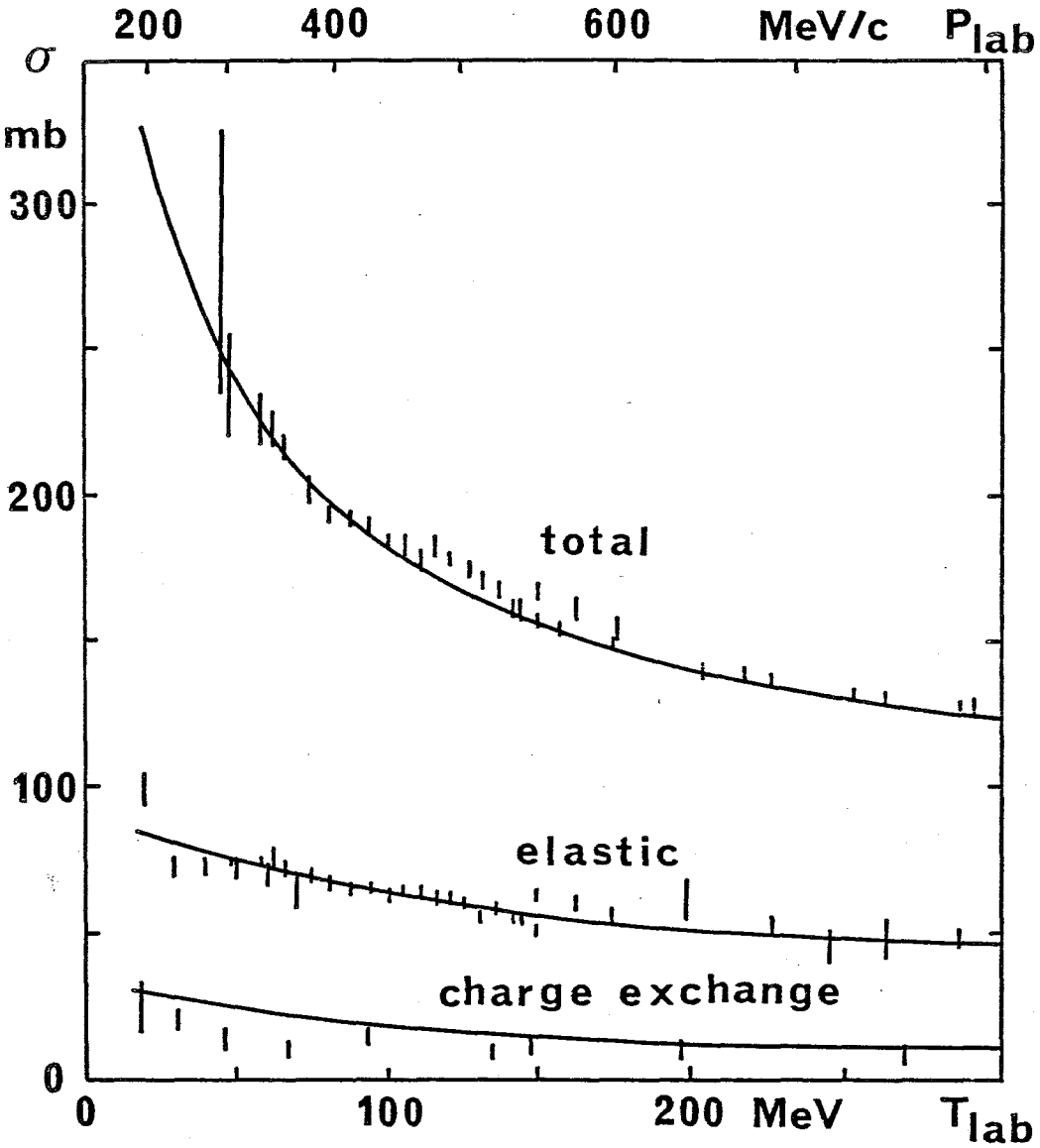
200
400
600
MeV/c
P_{lab}
σ
mb
300
200
100
0
total
elastic
charge exchange
0
100
200 MeV
T_{lab}

fig. 21

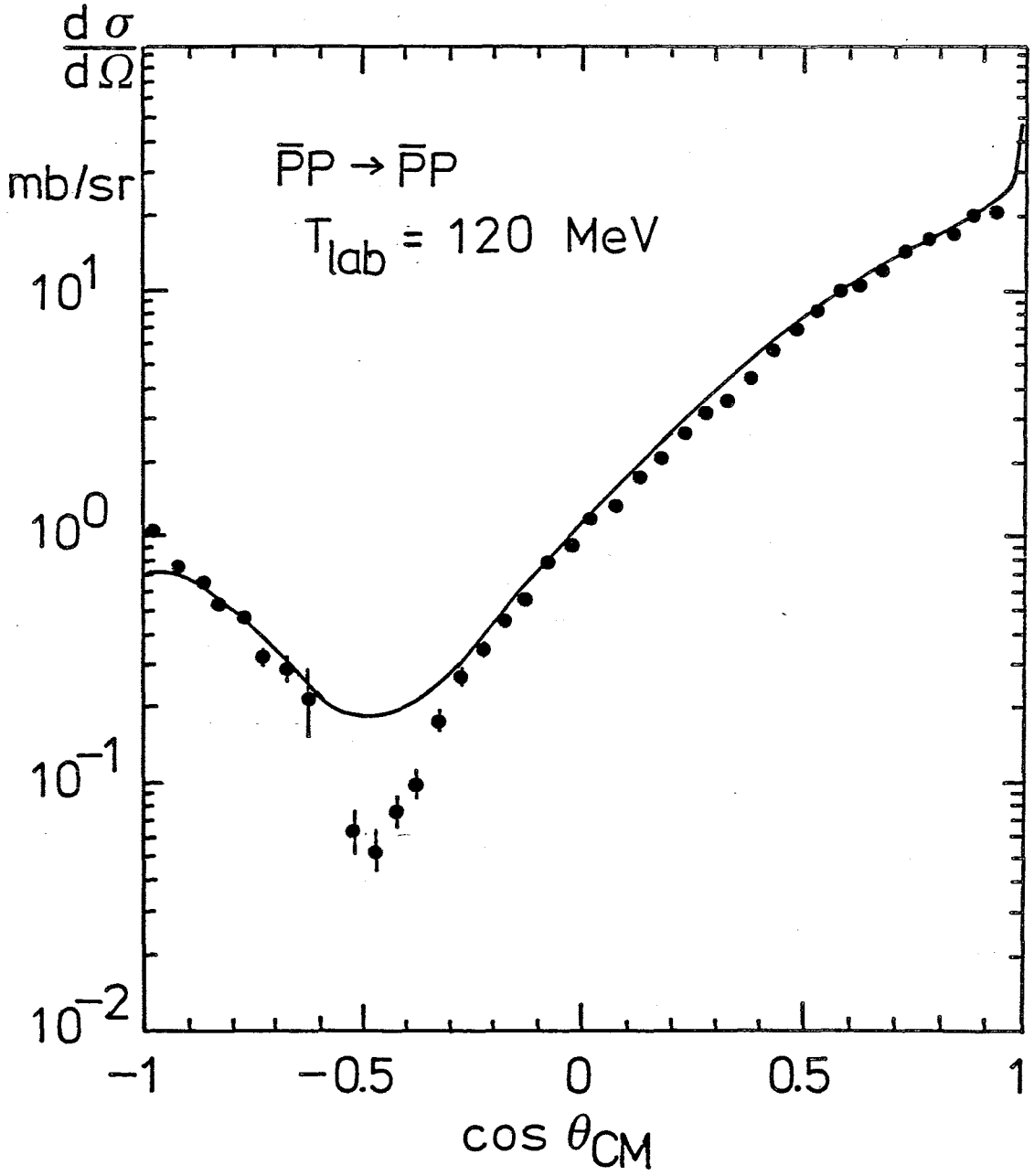
d σ / d Ω
mb/sr
$\bar{P}P \rightarrow \bar{P}P$
T_{lab} = 120 MeV
10^1
10^0
10^{-1}
10^{-2}
−1
−0.5
0
0.5
1
cos θ_{CM}

fig. 22

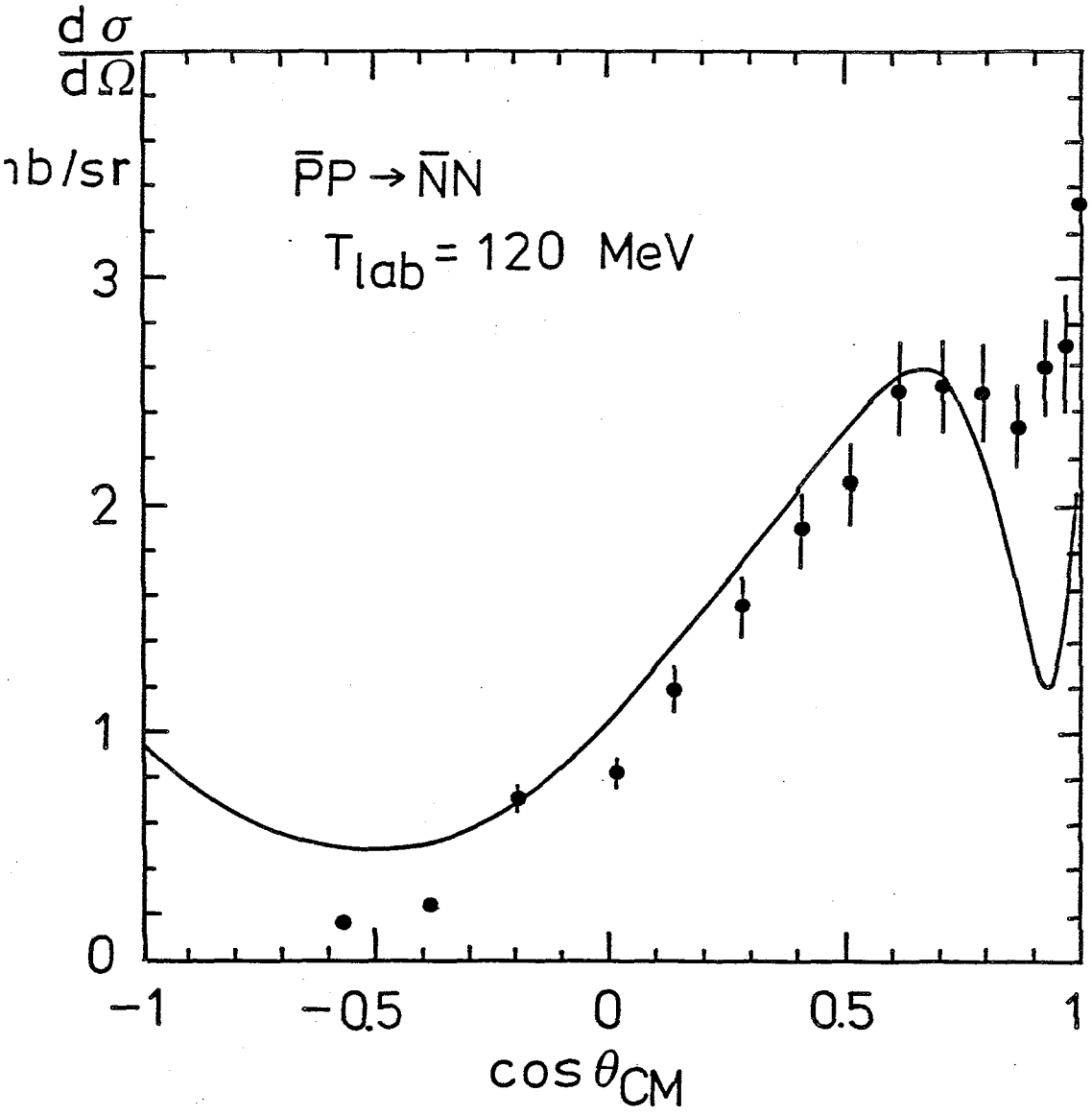
dσ/dΩ
nb/sr
$\bar{P}P \rightarrow \bar{N}N$
T_{lab} = 120 MeV
3
2
1
0
−1
−0.5
0
0.5
1
cos θ_{CM}

fig. 23

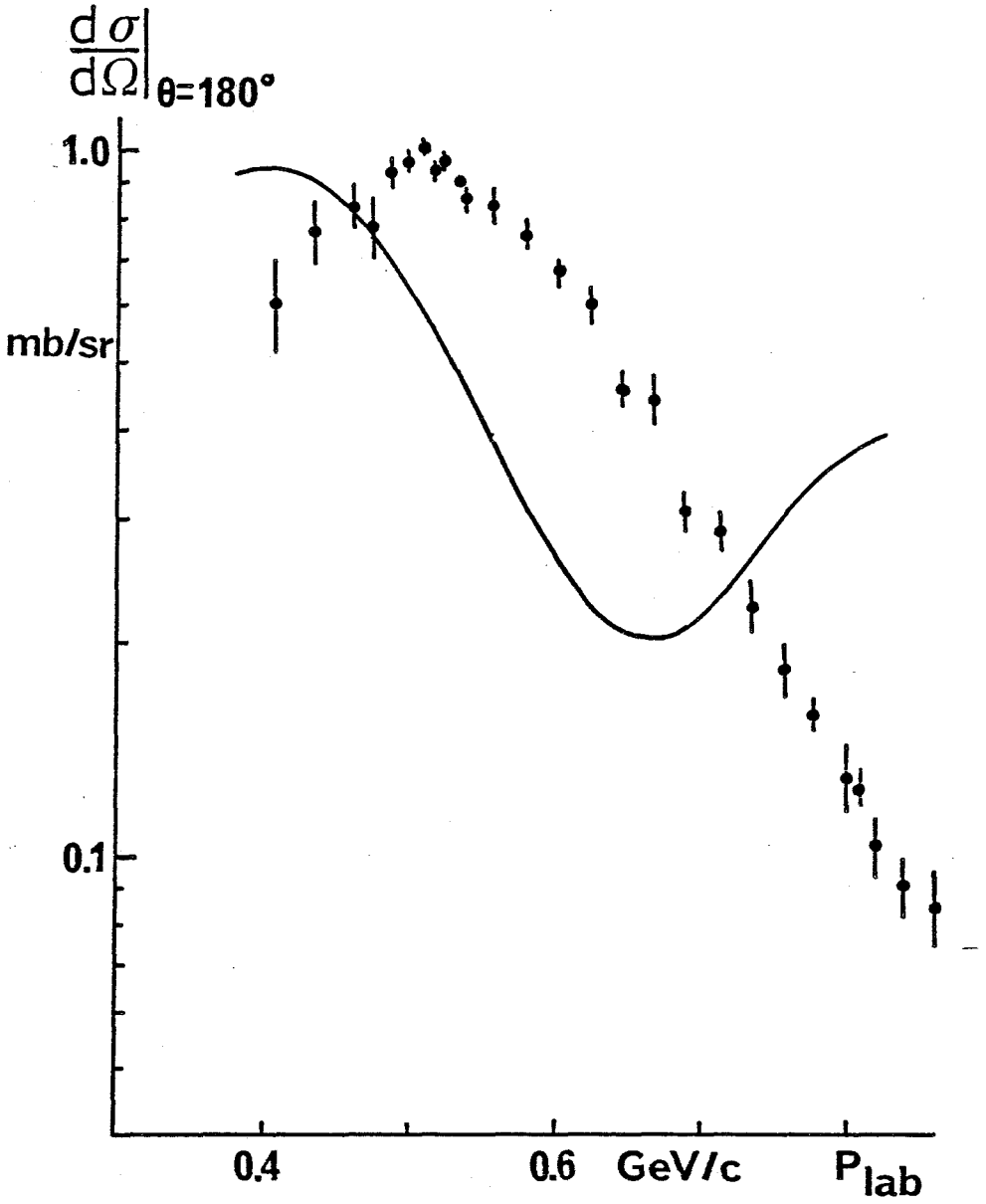

fig. 24

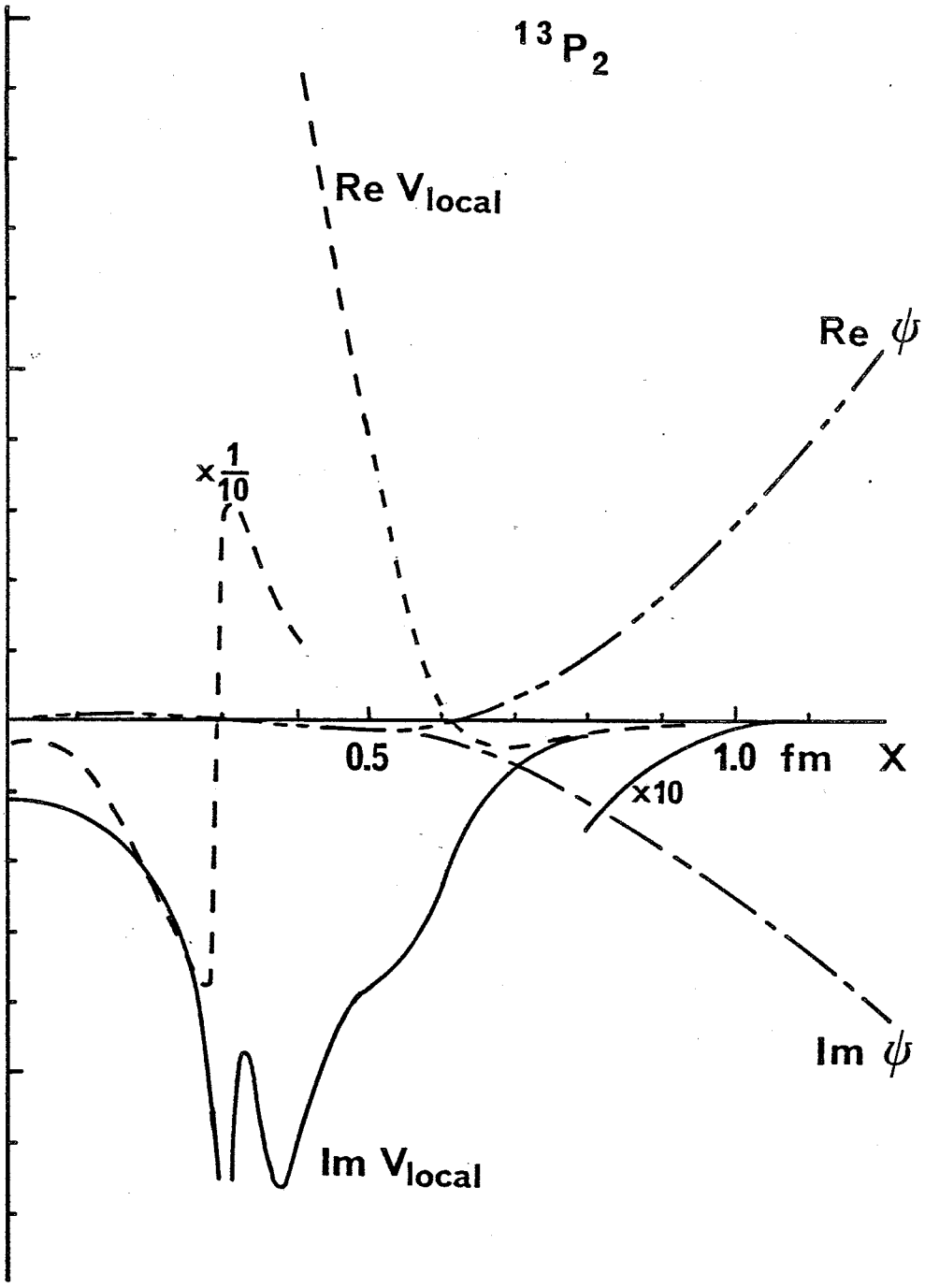
$^{13}P_2$
Re V_{local}
Re ψ
$\times\frac{1}{10}$
0.5
1.0 fm
X
$\times 10$
Im ψ
Im V_{local}

fig. 25